UNIVERSITY OF SOUTHAMPTON

FACULTY OF ENGINEERING, SCIENCE AND MATHEMATICS

School of Geography

Per-pixel uncertainty in change detection using airborne remote sensing

Volume 2 of 2

Kyle Mackenzie Brown

Thesis for the degree of Doctor of Philosophy

April 2005

6 Combining thematic and misregistration uncertainty using airborne-sensor data

6.1 Introduction

In Chapter 5 the misregistration and thematic uncertainty models were combined in a probabilistic change detection model using synthetic data. In this chapter, the model used in Chapter 5 (Figure 5.2) was applied to CASI and LiDAR data of the Ainsdale Sand Dunes test site (Figure 2.2; Appendix D).

In the previous chapter the use of both misregistration and thematic uncertainty resulted in an increased level of change detection accuracy compared to ignoring uncertainty. However, the synthetic data that were used in the testing stage may not accurately represent an actual CASI classification dataset. The synthetic data did not account for orthometric effects as elevation data were not incorporated in the geometric uncertainty model.

The geometric uncertainty model accounts for errors that can arise due to the interaction of instrument error and misalignment with the surface terrain. This will be particularly useful where geometric errors due to terrain misalignment have the potential to be large. In an imager such as the CASI the edge of imagery is where the greatest orthometric errors tend to occur. Orthometric errors are also likely to occur where the terrain height varies a great deal, as it is more likely that the elevation used in orthocorrection will be incorrect.

As well as orthometric effects there were other differences between the synthetic and remotely sensed data. The thematic errors in the synthetic data occurred randomly but in environmental remotely sensed data errors are also likely to occur in clumps, for example due to areas of shadowing or an area of vegetation that was not represented in the training data. The assumption was made in generating the synthetic data that the PNN accurately modelled multiple class membership, as well as uncertainty, which may not have been the case. The spatial distribution and number of classes in the synthetic data was very simple, with only two classes and a square representing one of those classes.

6.2 Method

The change detection models were tested using CASI and LiDAR data from the Ainsdale Sand Dunes test site from 28th August 2001 and 11th September 2002 (Section 2.6.1; Appendix C;

Table C.2; Table C.4; Appendix D). CASI and LiDAR images were processed following the methods described in Section 2.3.1. A 1.5 km by 1.5 km section of the data was used for the final change analysis.

The CASI data were classified using a PNN with a smoothing function (h) of 0.02, as this value produced the largest overall thematic accuracy and the most accurate measure of class specific thematic uncertainty in the 2002 test stage (Table 4.5). Training data were 1000 pixels per-class for the eight classes as in Chapter 4. For the 2002 data these pixels were reselected randomly, so that the training data were not the same as those used in Chapter 4.

Using the same 60 m grid stratified random sampling method described in Section 2.6.2, but with different random points, points on the 2001 CASI data were interpreted to estimate a prior probability for each class (Table 6.1). This was used for input in the 2001 PNN classification.

Table 6.1 Estimated prior probabilities of 2001 classes for PNN classification, derived from interpretation of CASI data.

Water	Sand	Marram	Grass	Reeds	Creep	Buckthorn	Woodland
0.05242	0.09274	0.04435	0.37500	0.02419	0.10081	0.00806	0.30242

For the 2001 survey the only ground data were in polygon format. This meant that accuracy assessment data were not selected using the stratified random sampling method used in 2002. For this reason, the following procedure was used to select training and accuracy assessment data for 2001:

1. Polygons were evenly allocated to either training or accuracy assessment.
2. Training data were selected randomly. For each class, an equal number of pixels per training polygon were selected.
3. Using the same 60 m grid stratified random sampling method described in Chapter 4, but different random points, points on the 2001 CASI data were interpreted to produce an estimated prior probability for each class (Table 6.2). These points were different from those derived for input to the PNN so that the accuracy assessment was not biased.
4. Assuming a maximum number of five pixels per polygon to minimise autocorrelation, the estimated prior probabilities (Table 6.2) were used to determine the number of pixels that were randomly selected from the accuracy assessment polygon data. This resulted in 207 accuracy assessment pixels for the 2001 data.

Table 6.2 Estimated prior probability of 2001 classes for derivation of accuracy assessment data, derived from interpretation of CASI data.

Water	Sand	Marram	Grass	Reeds	Creep	Buckthorn	Woodland
0.05598	0.10687	0.06234	0.35751	0.02417	0.09415	0.01018	0.28880

The outputs from the 2001 and 2002 PNN classification stages were per-pixel posterior probability data for each of the eight classes. The geometric uncertainty model was derived as described in Chapter 5. Using the PNN classification input, the four change models used in Chapter 5 were again tested: Combined uncertainty, Thematic uncertainty, Misregistration uncertainty and No Uncertainty. The accuracy of the different change models were tested using the areas identified as having undergone no change and the transect data (Section 2.6.2).

To determine which pixels were predicted as having undergone change the thematic change vector was determined. If the class with the maximum probability at t_1 is e and the class with the maximum probability at t_2 is s then thematic change vector (δg) is calculated using:

$$\delta g = \frac{(\rho_{e_{t_1}} - \rho_{s_{t_1}}) + (\rho_{s_{t_2}} - \rho_{e_{t_2}})}{2} \qquad 6.1$$

where $\rho_{e_{t_1}}$ is the posterior probability of class e at t_1.

Change was predicted to occur when $\delta g >= 0.5$

Differences between the change detection results using uncertainty and not using uncertainty were tested for significance using the Wilcoxon matched pairs test (Fowler and Cohen, 1990). This is a non-parametric test for comparing matched samples.

6.3 Results

6.3.1 PNN classification accuracy

P_o for the 2001 classification (Figure 6.1) was 0.865. The 2001 Producer's and User's accuracy values were greater than 70% for all classes apart from the Reed class (Table 6.3). For the Reed class, both class accuracy measures were 20% (Table 6.3).

Table 6.3 **Confusion matrix for 2001 PNN classification used for change detection.**

	Water	Sand	Marram	Grass	Reeds	Creep	Buckthorn	Woodland	Correct	Total	User's accuracy
Water	8	0	0	0	2	0	0	0	8	10	0.80
Sand	0	22	0	0	0	0	0	0	22	22	1.00
Marram	0	0	10	3	0	0	0	0	10	13	0.77
Grass	0	0	3	62	1	0	0	1	62	67	0.93
Reeds	0	0	0	2	1	1	0	1	1	5	0.20
Creep	0	0	0	5	0	16	0	0	16	21	0.76
Buckthorn	0	0	0	0	0	0	2	0	2	2	1.00
Woodland	3	0	0	2	1	3	0	58	58	67	0.87
Correct	8	22	10	62	1	16	2	58	179		
Total	11	22	13	74	5	20	2	60		207	
Producer's accuracy	0.73	1.00	0.77	0.84	0.20	0.80	1.00	0.97			0.865

P_o for the 2002 classification (Figure 6.2) was 0.810. The Water, Sand and Woodland classes were all classified accurately with Producer's and User's accuracy values of greater than 89% (Table 6.4). The smallest User's accuracies were 43% for the Reed class and 54% for the creep class, though these results were based on very small samples (Table 6.4).

Table 6.4 **Confusion matrix for 2002 PNN classification using for change detection.**

	Water	Sand	Marram	Grass	Reeds	Creep	Buckthorn	Woodland	Correct	Total	User's Accuracy
Water	55	2	0	0	0	0	0	0	55	57	0.96
Sand	2	61	1	3	0	0	0	0	61	67	0.91
Marram	0	1	14	6	0	0	0	0	14	21	0.67
Grass	0	0	11	224	2	28	0	8	224	273	0.82
Reeds	0	0	0	7	10	3	0	3	10	23	0.43
Creep	0	0	2	34	4	50	0	2	50	92	0.54
Buckthorn	0	0	0	0	0	0	5	3	5	8	0.63
Woodland	0	0	2	22	0	1	2	218	218	245	0.89
Correct	55	61	14	224	10	50	5	218	637		
Total	57	64	30	296	16	82	7	234		786	
Producer's accuracy	0.96	0.95	0.47	0.76	0.63	0.61	0.71	0.93			0.810

Though the overall accuracy of the 2002 PNN used in Chapter 2 (P_o = 0.827) was within 2% of the value obtained in this chapter, the class accuracy values were very different and generally smaller for the PNN used in this chapter (Table 6.4). The Water, Sand and Woodland class accuracy values were within 5%, but the Reeds and Buckthorn classes had a User's accuracy that was 20% smaller for the PNN in this chapter (Table 4.3; Table 6.4). The difference in training data for the 2002 PNN classifications in this chapter and Chapter 4 appear to result in very different outputs in terms of class accuracy, indicating that PNNs are very dependent on input data.

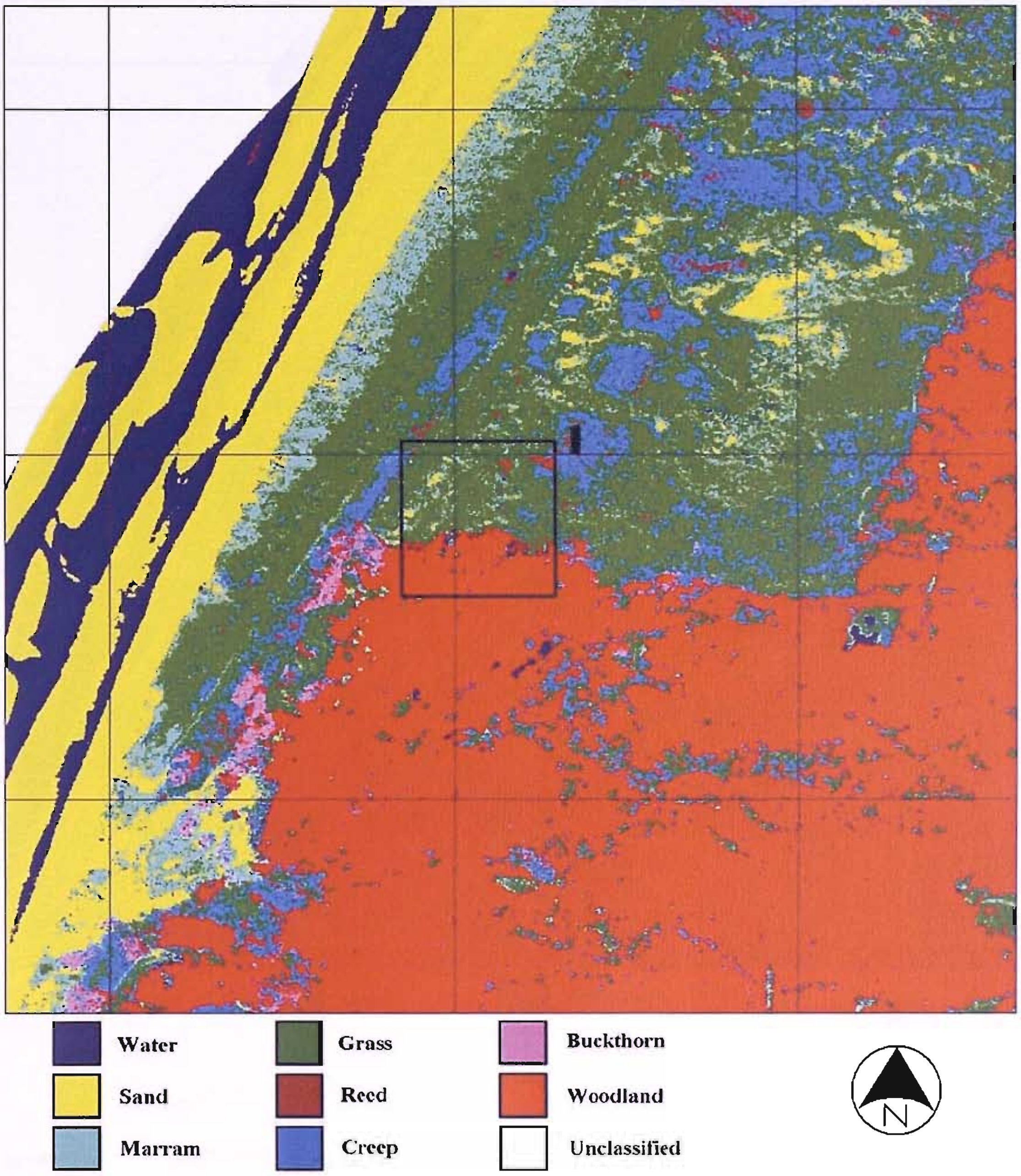

Figure 6.1 **2001 PNN classification of Ainsdale study area. Grid is 500 m. Area 1 is the extent of Figure 6.3.**

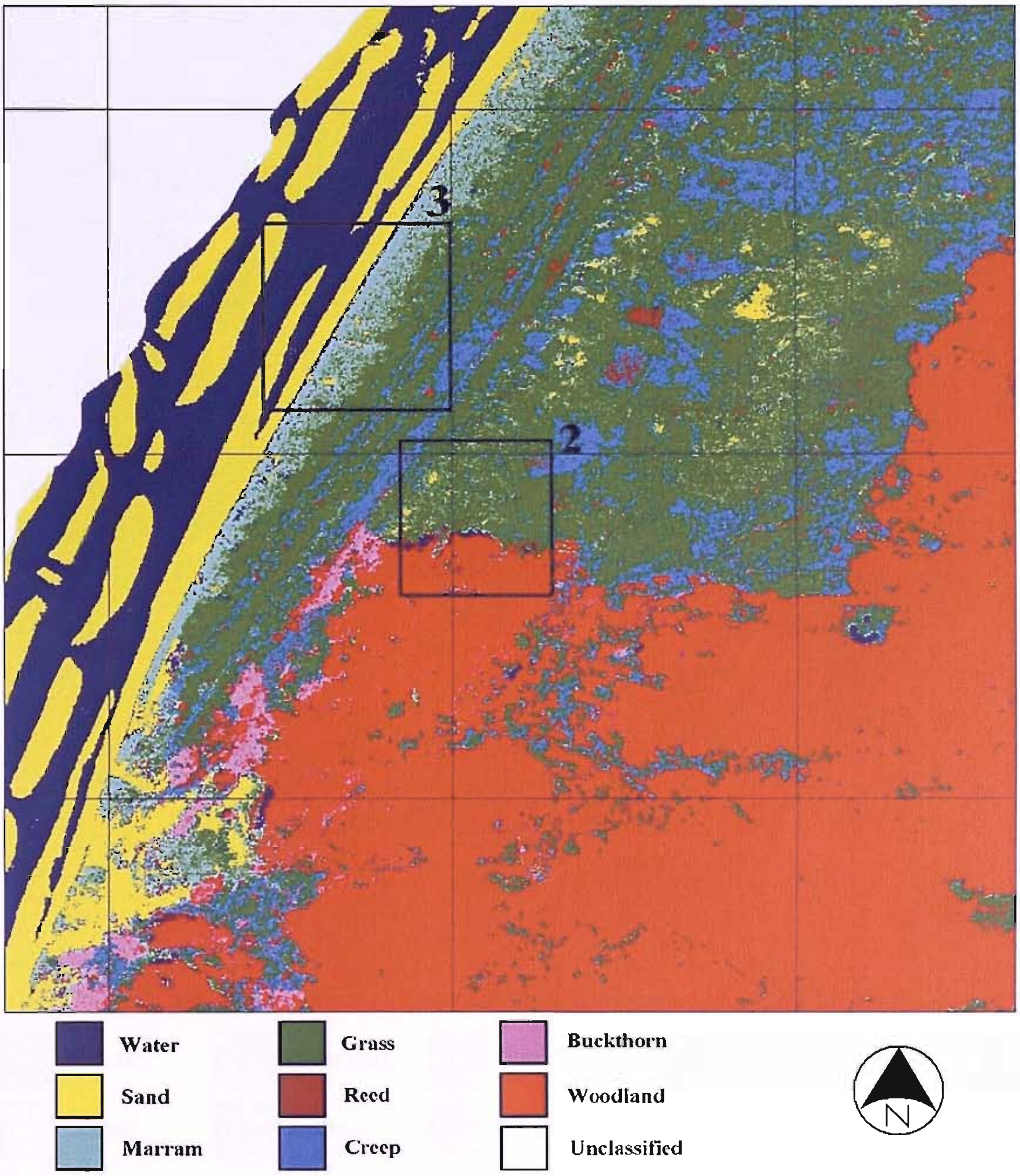

Figure 6.2 2002 PNN classification of Ainsdale study area. Grid is 500 m. Areas 2 and 3 are the extent of Figure 6.4 and Figure 6.5 respectively.

Many of the errors within both the classifications were due to shadowing. There was shadowing due to the tree canopy in both the 2001 and 2002 data that was misclassified as Water when it should have been either Grass or Creep (Area 1, Figure 6.1, Figure 6.3; Area 2, Figure 6.2, Figure 6.4). There was also shadowing due to the frontal dune system that was misclassified as Water when it should have been Sand (Area 3; Figure 6.2, Figure 6.5).

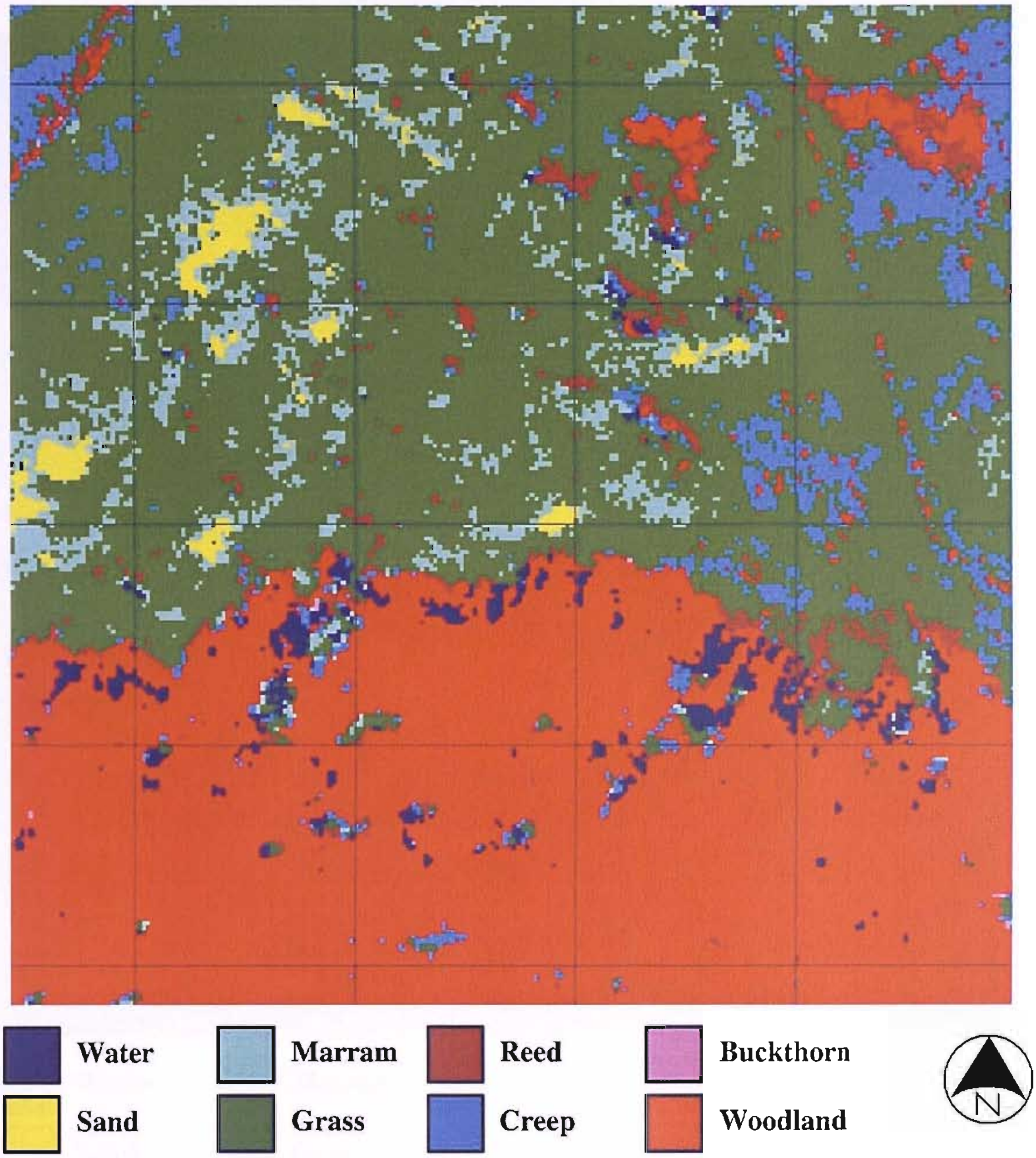

Figure 6.3 2001 PNN classification of subsection of Ainsdale study area showing shadowed areas in Woodland misclassified as Water. Region shown is that defined as Area 1 in Figure 6.1. Grid is 50 m.

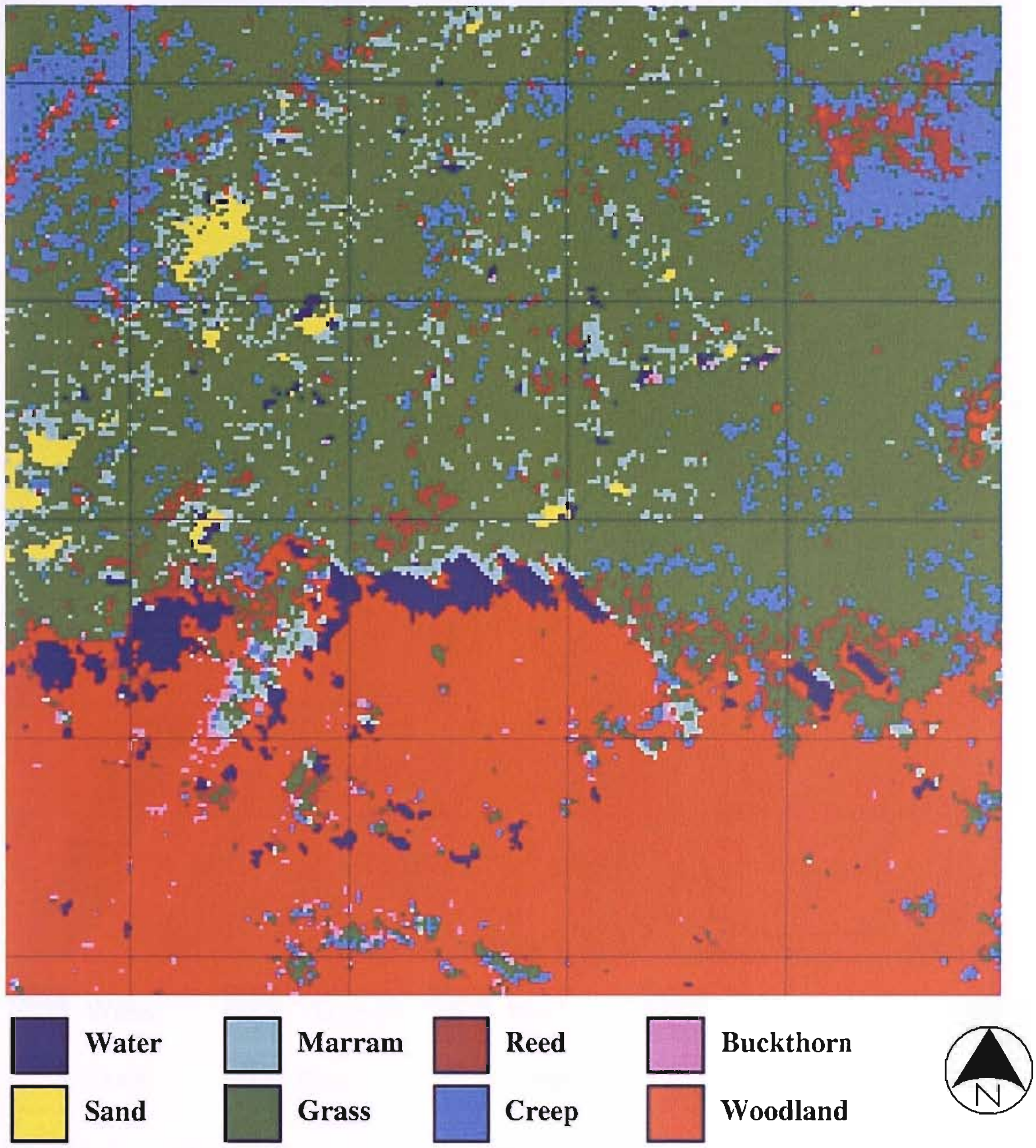

Figure 6.4 2002 PNN classification of subsection of Ainsdale study area showing shadowed areas at edge of woodland misclassified as Water. Region shown is that defined as Area 2 in Figure 6.2. Grid is 50 m.

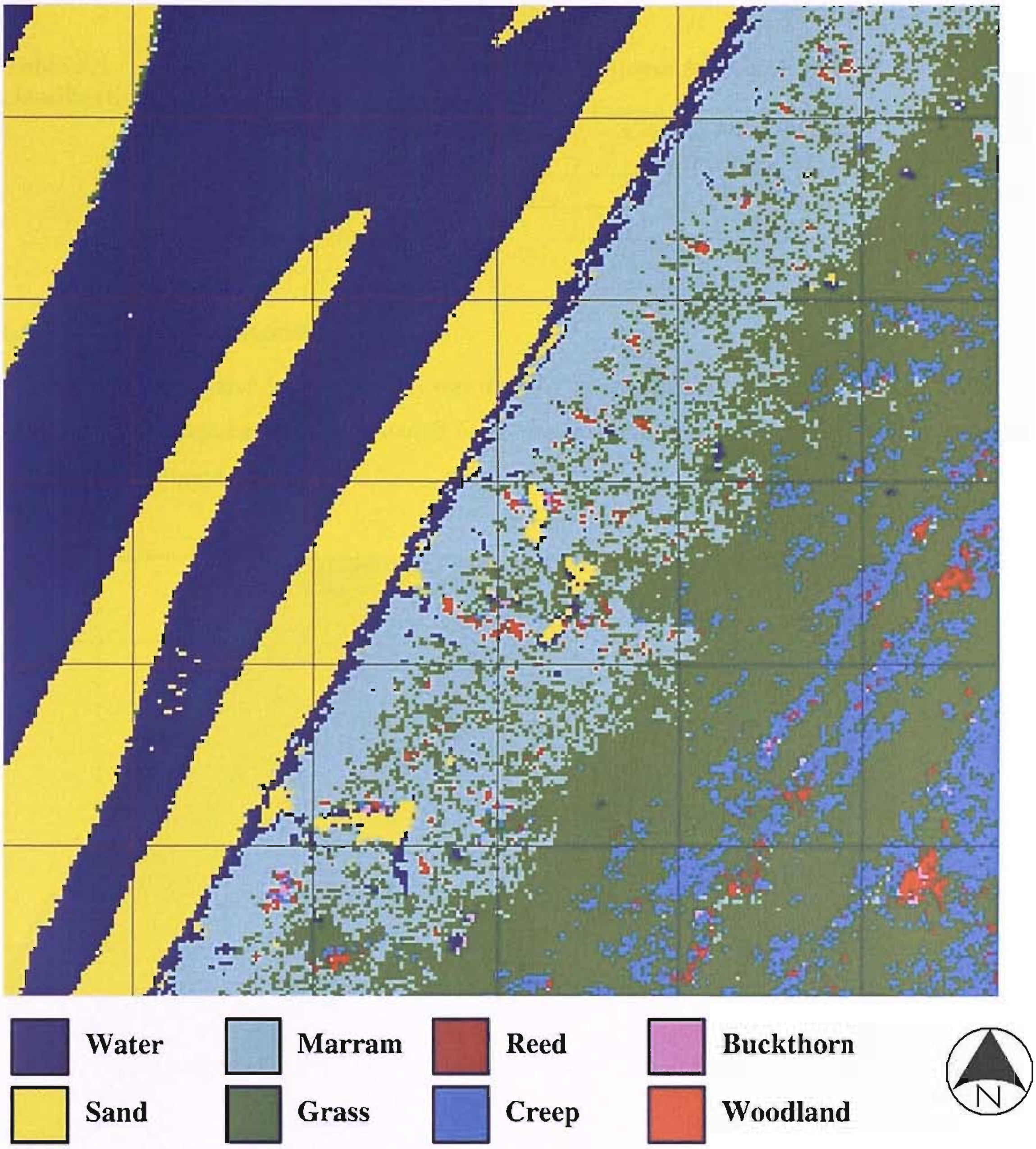

Figure 6.5 2002 PNN classification of subsection of Ainsdale study area showing areas shadowed by frontal dunes misclassified as Water. This is the narrow strip of water next to Marram class. Region shown is that defined as Area 3 in Figure 6.2. Grid is 50 m.

6.3.2 Thematic uncertainty

There were large differences in the accuracy of the thematic uncertainty measures derived from PNN classifications for 2001 and 2002 (Table 6.5). The class independent thematic uncertainty RMSE for 2001 was more than twice the value for 2002 (Table 6.5). The class specific thematic uncertainty RMSE for 2001 was almost three times the value for 2002 (Table 6.5). The thematic uncertainty accuracies were of a similar order for the testing stage of the PNN in Chapter 4 and the final classification for 2002 (Table 4.5; Table 6.5).

Table 6.5 Accuracy of thematic uncertainty measures for Ainsdale PNN classifications.

Year	Class independent thematic uncertainty RMSE	Class specific thematic uncertainty RMSE
2001	0.145	0.221
2002	0.071	0.082

6.3.3 Geometric uncertainty

A geometric error value for every pixel was derived by multiplying the predicted error vector with the probability that the vector would occur and summing the value derived for all predicted error vectors (Figure 6.6; Figure 6.7).

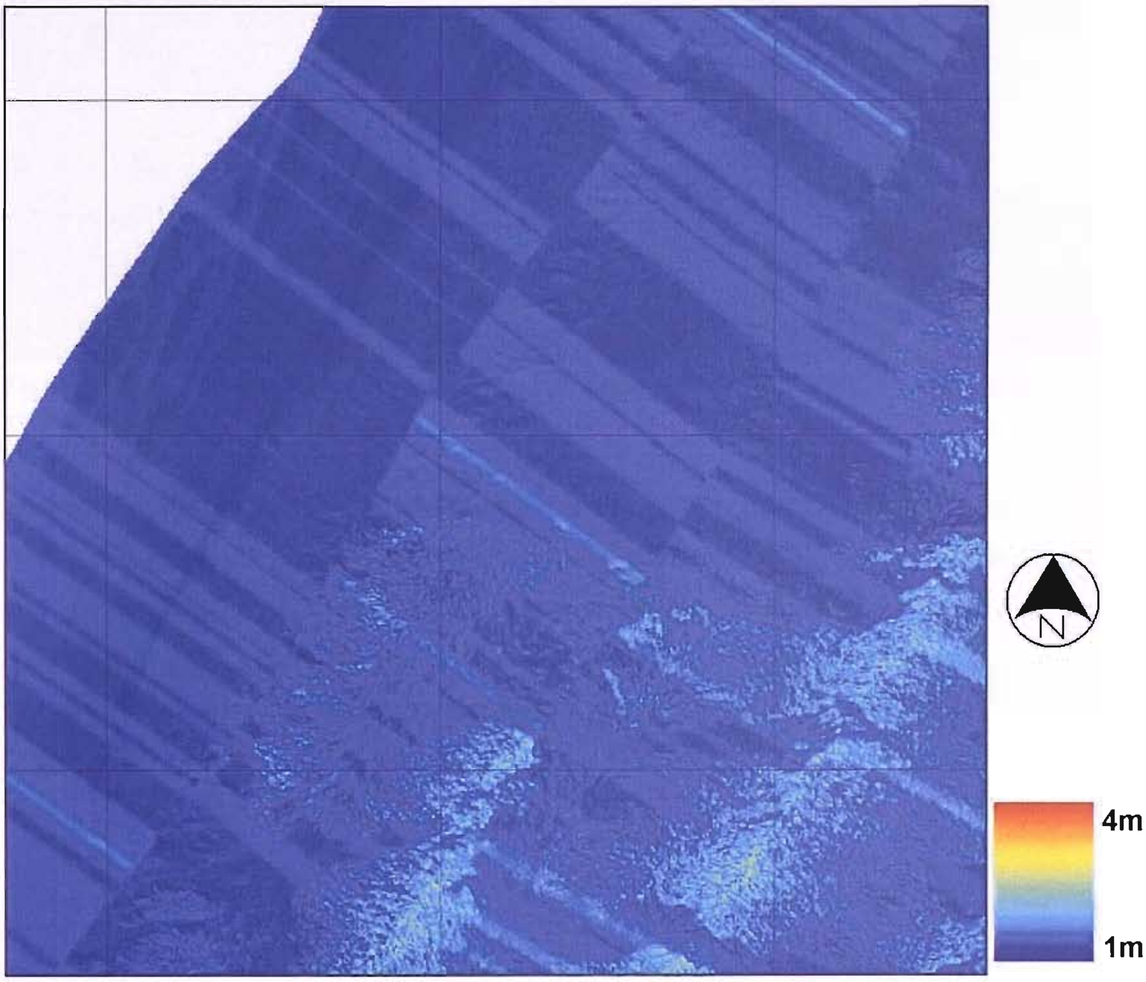

Figure 6.6 Predicted geometric error for Ainsdale test site 2001. The error is an averaged value. Grid is 500 m.

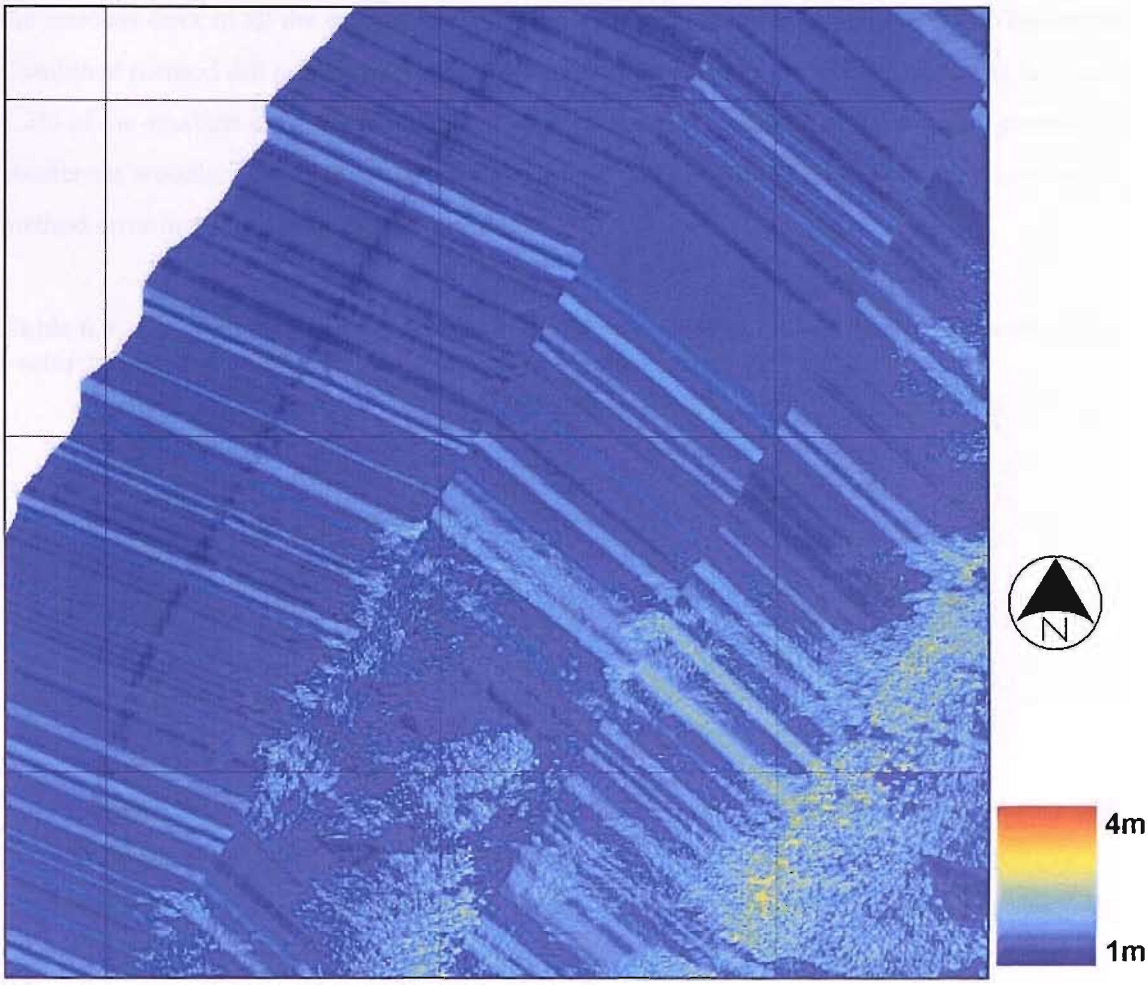

Figure 6.7 Predicted geometric error for Ainsdale test site 2002. The error is an averaged value. Grid is 500 m.

As would be expected, predicted geometric error was greatest over the wooded areas, as these areas had the greatest variation in surface elevation. At the edges of images the probability of orthometric effects are increased (Figure 3.2) and these areas did have an increased predicted error (Figure 6.6; Figure 6.7). The large predicted geometric errors that occur in stripes perpendicular to the flight path (approximately 45°) are due to large angular acceleration (Figure 6.6; Figure 6.7).

6.3.4 Change detection

6.3.4.1 Identifying areas of change using the magnitude of thematic change vector

Testing the areas of no change showed that the No Uncertainty method of determining change was the least accurate, with the largest error in all of the areas, apart from CW1 and CW3 where it had the equal largest error with the Thematic method (Table 6.6). The Combined method had the smallest error in all the deciduous woodland and scrub and the fixed dune areas. Where the Combined method did not have the smallest error, in the coniferous woodland, it was within 1.2% of the smallest error (Table 6.6). The Misregistration method had the smallest error in the coniferous woodland areas, but had an error of between 1.6% and 8.7% above the Combined method error in the other areas (Table 6.6).

Table 6.6 Proportion of pixels incorrectly classified as change using thematic change vector in areas of no change. Bold indicates smallest error for that area.

Area	Combined	Thematic	Misregistration	No Uncertainty
CW1	0.007	0.028	**0.006**	0.028
CW2	0.049	0.076	**0.041**	0.078
CW3	0.036	0.034	**0.024**	0.034
DS1	**0.103**	0.278	0.119	0.286
DS2	**0.122**	0.463	0.179	0.511
DS3	**0.101**	0.349	0.124	0.363
FD1	**0.090**	0.344	0.130	0.387
FD2	**0.140**	0.396	0.227	0.483
FD3	**0.064**	0.328	0.125	0.415

The Wilcoxon matched pairs test for the proportion of pixels classified as change showed that the Combined and Misregistration methods were both significantly more accurate (at 95% confidence) in areas of no change than the Thematic and No Uncertainty methods (Table 6.7). The Thematic method was significantly more accurate (at 95% confidence) than the No Uncertainty method, but there was no significant difference between Combined and the Misregistration methods (Table 6.7).

Table 6.7 Wilcoxon matched pairs test *p*-values comparing change detection methods for proportion of pixels incorrectly classified as change using thematic change vector and assuming change occurs at vector with a magnitude greater than 0.5. Bold values indicate significance at 95% confidence.

	Thematic	Misregistration	No Uncertainty
Combined	**0.008**	0.055	**0.008**
Thematic	/	**0.004**	**0.004**
Misregistration	/	/	**0.004**

The Combined method was significantly more accurate than the Misregistration method (at 95% confidence) when comparisons were made using the RMSE values of the thematic change vector and the resulting Wilcoxon tests (Table 6.8; Table 6.9). The Misregistration method was significantly more accurate than the Thematic method, which was significantly more accurate than the No Uncertainty method (Table 6.8; Table 6.9).

Table 6.8 RMSE of thematic change vector in areas of no change. Bold indicates the smallest error for that area.

Area	Combined	Thematic	Misregistration	No Uncertainty
CW1	**0.055**	0.134	**0.055**	0.167
CW2	0.155	0.217	**0.148**	0.279
CW3	0.134	0.141	**0.114**	0.184
DS1	**0.232**	0.444	0.253	0.535
DS2	**0.286**	0.558	0.327	0.715
DS3	**0.235**	0.505	0.257	0.602
FD1	**0.245**	0.480	0.276	0.622
FD2	**0.298**	0.497	0.365	0.695
FD3	**0.212**	0.443	0.272	0.644

Table 6.9 Wilcoxon matched pairs test *p*-values comparing change detection methods using thematic change vector RMSE, assuming the actual vector = 0. Bold values indicate significance at 95% confidence.

	Thematic	Misregistration	No Uncertainty
Combined	**0.004**	**0.039**	**0.004**
Thematic	/	**0.004**	**0.004**
Misregistration	/	/	**0.004**

From the transect results for the proportion of correct pixels the No Uncertainty method was the least accurate, with the smallest accuracy for Transects 1, 3 and 4 and the equal smallest accuracy with the Thematic method for Transects 2, 5 and 6 (Table 6.10). The Combined method had the largest accuracy in Transects 1, 2, 4 and 6 (Table 6.10). The Misregistration method had the largest accuracy in Transect 5 and the equal largest accuracy in Transect 3 (Table 6.10). The Combined method was significantly more accurate than the No Uncertainty method (at 95% confidence) using the Wilcoxon matched pairs test (Table 6.11). There were no significant differences between the other methods (Table 6.11).

Table 6.10 Proportion of correct transect pixels using thematic change vector threshold 0.5. Bold indicates largest accuracy for that transect.

Transect no.	Combined	Thematic	Misregistration	No Uncertainty
1	**0.968**	0.839	0.839	0.710
2	**1.000**	0.818	0.955	0.818
3	**1.000**	0.360	**1.000**	0.320
4	**0.903**	**0.903**	0.871	0.871
5	0.816	0.789	**0.842**	0.789
6	**0.895**	0.789	0.789	0.789

Table 6.11 Transect Wilcoxon matched pairs test p-values comparing change detection methods. Bold values indicate significance at 95% confidence.

	Thematic	Misregistration	No Uncertainty
Combined	0.063	0.125	**0.031**
Thematic	/	0.250	0.250
Misregistration	/	/	0.125

The proportion of correct pixels for the transects where no change occurred were examined. The Combined method was the most accurate for Transects 1, 2, and 4 (Table 6.12). The Combined and Misregistration methods were the most accurate for Transects 3, 5 and 6 (Table 6.12). The No Uncertainty method was the least accurate for Transects 1, 3, and 4 (Table 6.12). The No Uncertainty and Thematic methods were the least accurate for Transects 2, 5 and 6 (Table 6.12).

The Combined method was found to be significantly more accurate than the No Uncertainty and Thematic methods (at 95% confidence) using a Wilcoxon matched pairs test (Table 6.13). The Misregistration method was significantly more accurate than the No Uncertainty method (at 95% confidence) (Table 6.13).

Table 6.12 Proportion of correct transect pixels for pixels where no change occurred using thematic change vector threshold 0.5. Bold indicates largest accuracy for that transect.

Transect no.	Combined	Thematic	Misregistration	No Uncertainty
1	**0.968**	0.839	0.839	0.710
2	**1.000**	0.818	0.955	0.818
3	**1.000**	0.360	**1.000**	0.320
4	**0.960**	0.920	0.920	0.880
5	**1.000**	0.706	**1.000**	0.706
6	**1.000**	0.500	**1.000**	0.500

Table 6.13 Transect pixels where no change occurred Wilcoxon matched pairs test p-values. Bold p values indicate significance at 95% confidence.

	Thematic	Misregistration	No Uncertainty
Combined	**0.031**	0.250	**0.031**
Thematic	/	0.125	0.250
Misregistration	/	/	**0.031**

For the transect pixels where change had occurred the No Uncertainty and Thematic methods had the largest overall accuracy for Transects 4 and 5 (Table 6.14). On transect 6, the No Uncertainty, Thematic and Combined methods had the same overall accuracy for the points where change occurred (Table 6.14). The Combined method had the smallest overall accuracy in Transect 5, the Misregistration method in Transects 4 and 6 (Table 6.14).

Table 6.14 Proportion of correct transect pixels for pixels where change had occurred using thematic change vector threshold 0.5. Bold indicates largest accuracy for that transect.

Transect no.	Combined	Thematic	Misregistration	No Uncertainty
4	0.667	**0.833**	0.667	**0.833**
5	0.667	**0.857**	0.714	**0.857**
6	**0.867**	**0.867**	0.733	**0.867**

The confusion matrices for the different models derived from the change transects show the general effects of using misregistration and thematic uncertainty on change detection (Table 6.15). The confusion matrices were calculated using the transects in which change occurred using every pixel on the transect. This means that autocorrelation was likely and so care has to be taken when interpreting the matrices. The Thematic model has very similar results to the No Uncertainty models. They show similar overall, Producer's and User's accuracies (Table 6.15). The Misregistration and the Combined models have similar results, with both these models having larger User's accuracies for the Change class and Producer's accuracies for the Change class (Table 6.15). These results indicate that the No Uncertainty and Thematic models tend to overestimate change and the Misregistration and Combined models tend to underestimate change.

Table 6.15 Confusion matrices for Ainsdale transects in which change occurred. Care has to be taken when interpreting these matrices, as all pixels on transects were used and so autocorrelation will occur.

a) No Uncertainty model

Predicted change	Actual change: No change	Change	User's accuracy
No change	36	6	0.86
Change	10	36	0.78
Producer's accuracy	0.78	0.86	0.818

b) Misregistration model

Predicted change	Actual change: No change	Change	User's accuracy
No change	44	12	0.79
Change	2	30	0.94
Producer's accuracy	0.96	0.71	0.841

c) Thematic model

Predicted change	Actual change: No change	Change	User's accuracy
No change	37	6	0.86
Change	9	36	0.80
Producer's accuracy	0.80	0.86	0.830

d) Combined model

Predicted change	Actual change: No change	Change	User's accuracy
No change	45	11	0.80
Change	1	31	0.97
Producer's accuracy	0.98	0.74	0.864

6.3.4.2 Predicting the direction of the thematic change vector

The effect of using thematic and geometric uncertainty for predicting the direction of the thematic change vector was also examined. The direction of the thematic change vector describes the class at t_1 and t_2. Testing how accurately the change vector direction was predicted involved testing the accuracy of the different methods using an eight by eight class change scenario. This potentially involved all combinations of change between 2001 and 2002, which was 64 change classes. When the overall accuracy transect results are examined for the 64-class problem there did not appear to be one method that was most accurate (Table 6.16). The Thematic and No Uncertainty methods were the most accurate in Transects 1 and 6 and least accurate in all other transects (Table 6.16). The Misregistration method had the equal largest accuracy with the Combined method in Transects 2 and 3 (Table 6.16). The Combined method was most accurate in Transects 4 and 5 (Table 6.16). None of the methods was significantly more accurate (at 95% confidence) than the others using a Wilcoxon matched pairs test (Table 6.17).

Table 6.16 Proportion of transect pixels in which thematic change vector direction was correctly predicted. This involved 64 change classes. Bold indicates largest accuracy for that transect.

Transect no.	Combined	Thematic	Misregistration	No Uncertainty
1	0.548	**0.645**	0.484	**0.645**
2	**0.500**	0.455	**0.500**	0.455
3	**0.640**	0.200	**0.640**	0.200
4	**0.723**	0.583	0.702	0.583
5	**0.605**	0.368	0.579	0.368
6	0.440	**0.544**	0.398	**0.544**

Table 6.17 Transect Wilcoxon matched pairs test p-values comparing change detection methods using 64 change classes.

	Thematic	Misregistration	No Uncertainty
Combined	0.313	0.125	0.313
Thematic	/	0.563	1.000
Misregistration	/	/	0.563

6.3.4.3 Visualising change detection

Using the No Uncertainty model the deciduous woodland area to the south and east of the study site appeared to have the least change predicted (Figure 2.4; Figure 6.8). This was likely to be as a result of the homogeneous land cover type and large class accuracy. The area identified as undergoing greatest change using the No Uncertainty model was the beach area (Figure 2.4; Figure 6.8). This was expected, as the data were flown at different states of the tide and there are sand banks that move a great deal from year to year (Wolstenholme, personal communication). Though there were large areas where change was identified on the beach, there were also large homogeneous areas where little change was predicted (Figure 6.8). As the Sand and Water classes were classified accurately for both years (Table 6.3; Table 6.4) it was likely that the change identified in this area was an accurate representation of actual change.

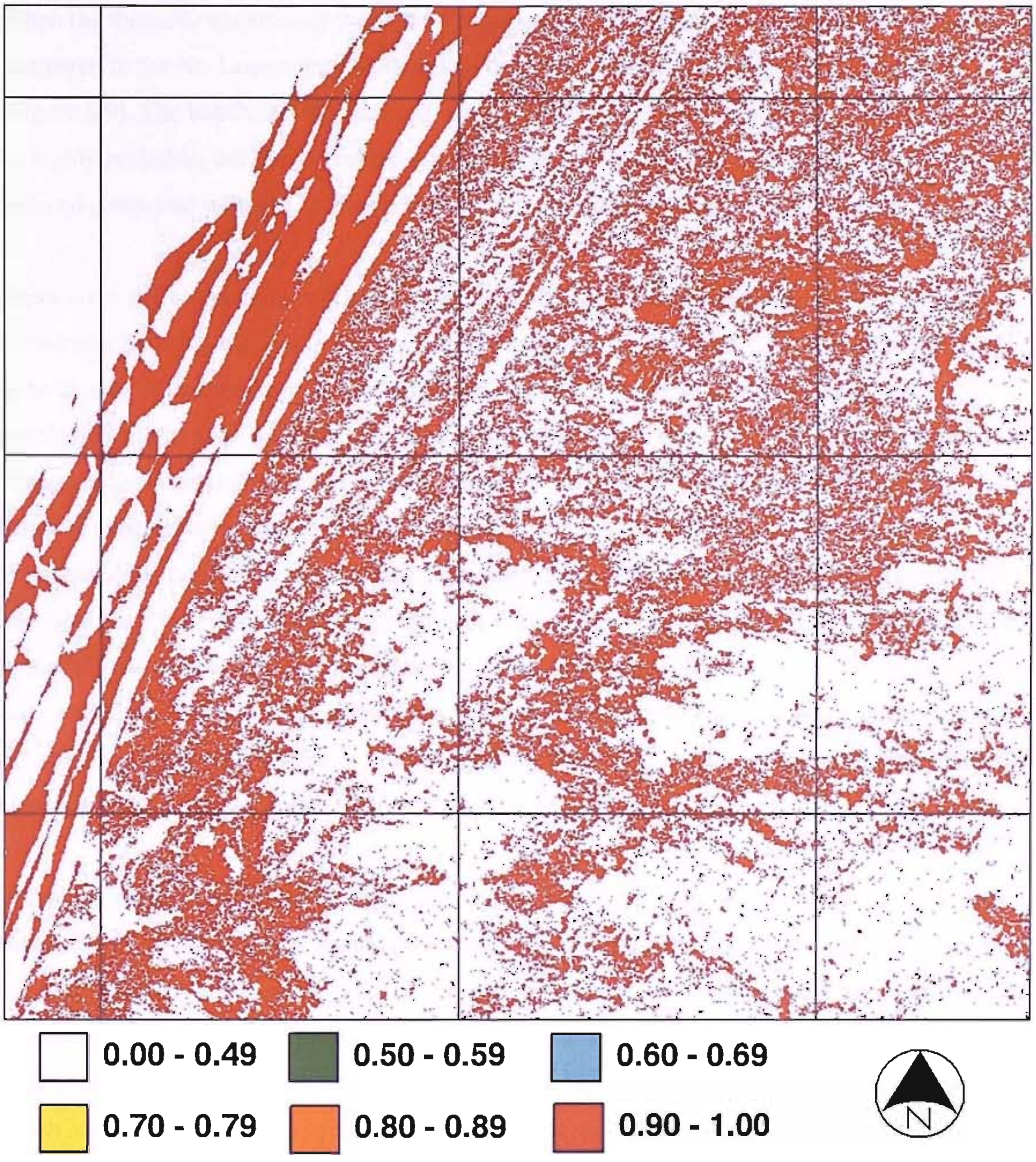

Figure 6.8 Thematic change vector between classifications of 2001 and 2002 data using No Uncertainty change model. Grid is 500 m.

LiDAR and photogrammetric data have been used to show large changes in the mobile dune system (Brown *et al.*, 2003a), with areas of erosion to the south of the study site and accretion in the north. The No Uncertainty model predicted a great deal of both scattered and clumped change areas in the mobile dune and fixed dune systems (Figure 2.4; Figure 6.8). Change was likely to occur in the mobile dune system, with the movement of sand and changes in Marram grass distribution (Rodwell *et al.*, 2000). However, the fixed dune was made up mainly of perennial species (Rodwell *et al.*, 2000) and therefore change was less likely.

When the thematic uncertainty was added to the change detection model, the main difference compared to the No Uncertainty method was that in many areas the change vector was reduced (Figure 6.9). The beach and the seaward edge of the mobile dunes area still showed change to be highly probable, but for a great deal of the fixed dune system the thematic change vector was reduced compared with the No Uncertainty method (Figure 2.4; Figure 6.8; Figure 6.9).

There were still some clumps where change was predicted in the fixed dune area and at the boundaries between the woodland and fixed dune (Figure 2.4; Figure 6.9). The areas predicted to be change at the boundary of the woodland were likely to be due to shadowing induced misclassifications such as those identified in Figure 6.3 and Figure 6.4. The clumped areas of change in the fixed dune system (Area 4, Figure 6.9, Figure 6.10) may have been partially the result of establishment of grasses. This area was woodland until 1992 (WS Atkins, 2004; Wolstenholme, personal communication) and may be undergoing succession. In this area there may also have been problems due to errors in the classification and the inability of the classifier to model mixed pixels in the uncertainty outputs (Figure 6.10). The area is a mixture of Marram, Sand and Grass classes. Small changes in the boundary of the classes in feature space may have resulted in large changes in the predicted distribution of those classes when pixels were mixed classes and the classifier failed to account for the mixing.

When misregistration uncertainty was used in the change detection model, the main difference compared to the No Uncertainty method was that in many areas the thematic change vector was reduced (Figure 6.8; Figure 6.11). This was also the case in comparison to the Thematic method (Figure 6.9; Figure 6.11). The main difference compared with the Thematic method was that there appeared to be fewer areas in which large thematic change vectors were predicted. The beach and the seaward edge of the mobile dunes area still showed the change to be highly probable, but for a great deal of the fixed dune, mobile dune and deciduous woodland and scrub the thematic change vector was reduced compared with the Thematic method (Figure 2.4; Figure 6.9; Figure 6.11). There were still some clumps where change was predicted in the fixed dune area and at the boundary between woodland and fixed dune (Figure 2.4; Figure 6.11).

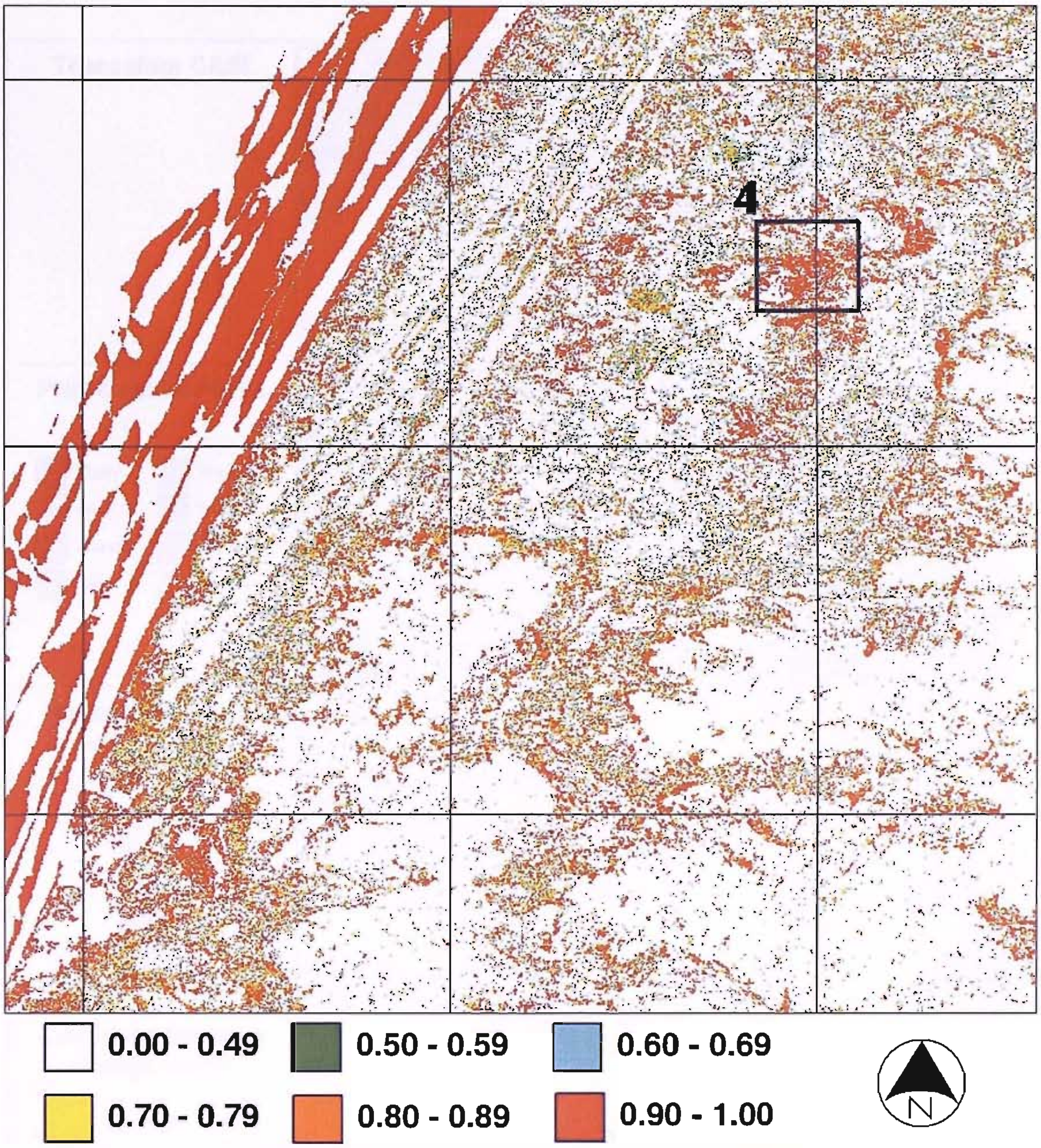

Figure 6.9 Thematic change vector between classifications of 2001 and 2002 data using Thematic change model. Grid is 500 m. Area 4 is the extent of Figure 6.10.

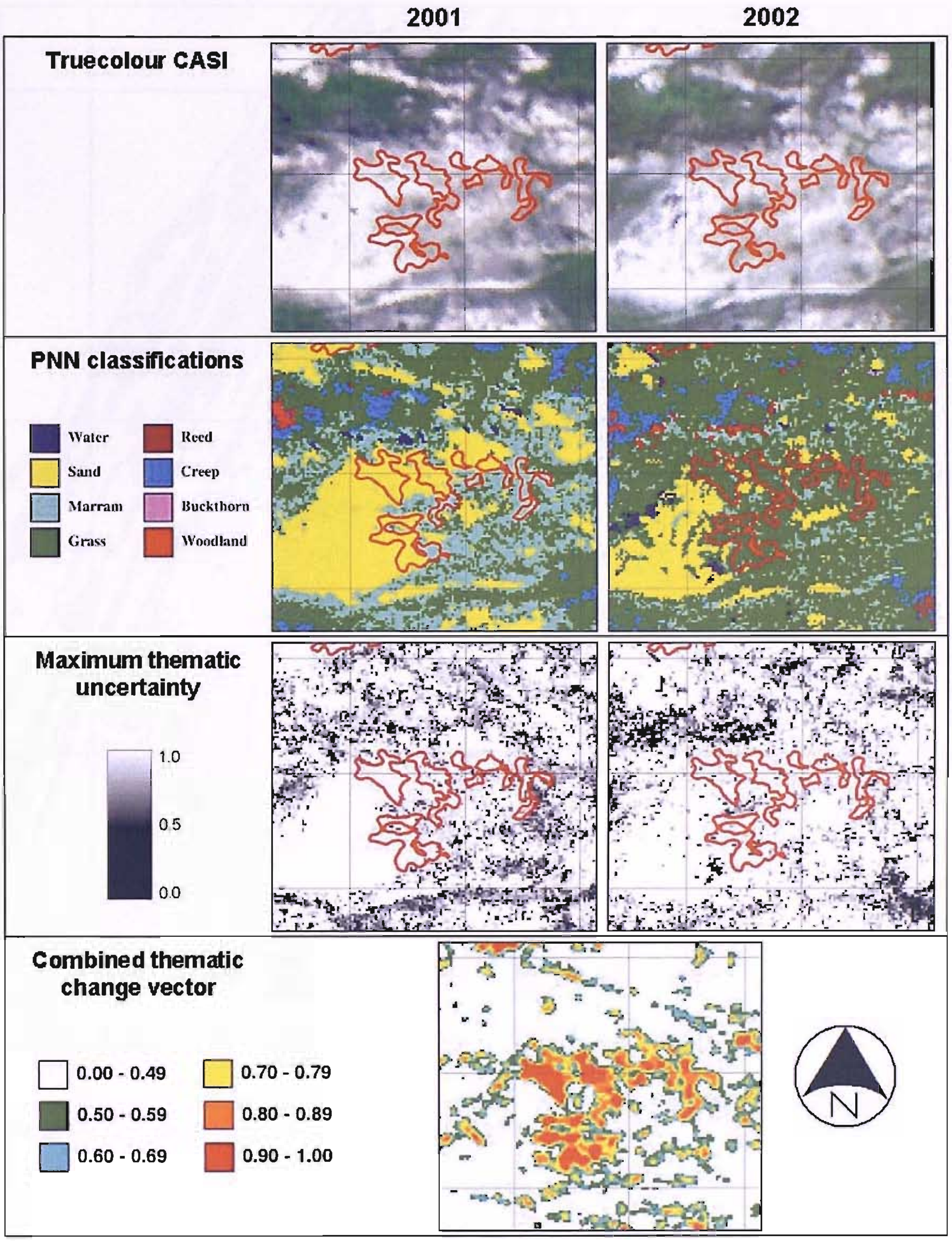

Figure 6.10 Differences in 2001 and 2002 for area of fixed dune and change predicted using Combined method. Red polygons are areas where predicted thematic change vector is greater than 0.8 using the Combined method. Region shown is that defined as Area 4 in Figure 6.9. Grid is 50 m.

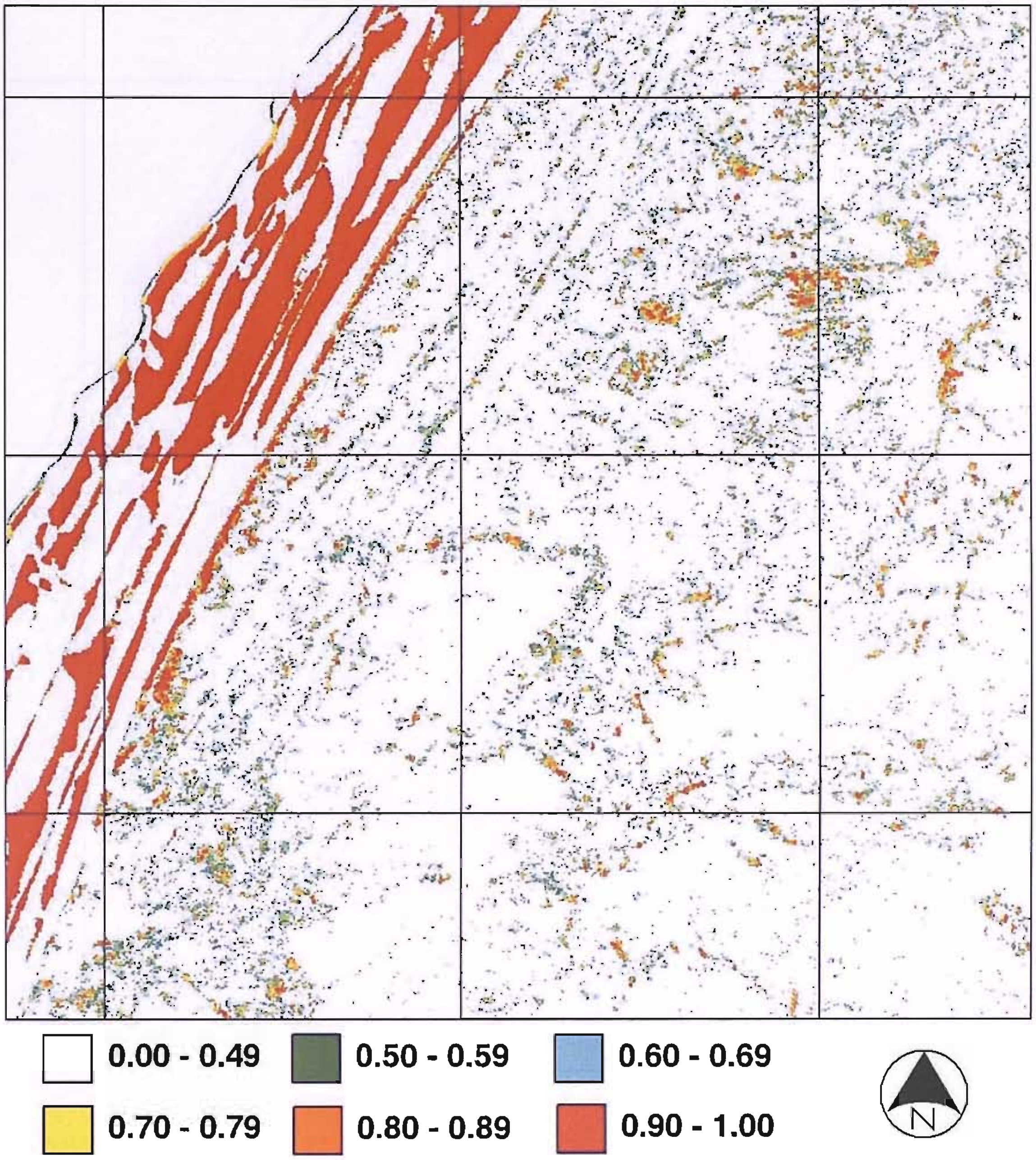

Figure 6.11 Thematic change vector between classifications of 2001 and 2002 data using Misregistration change model. Grid is 500 m.

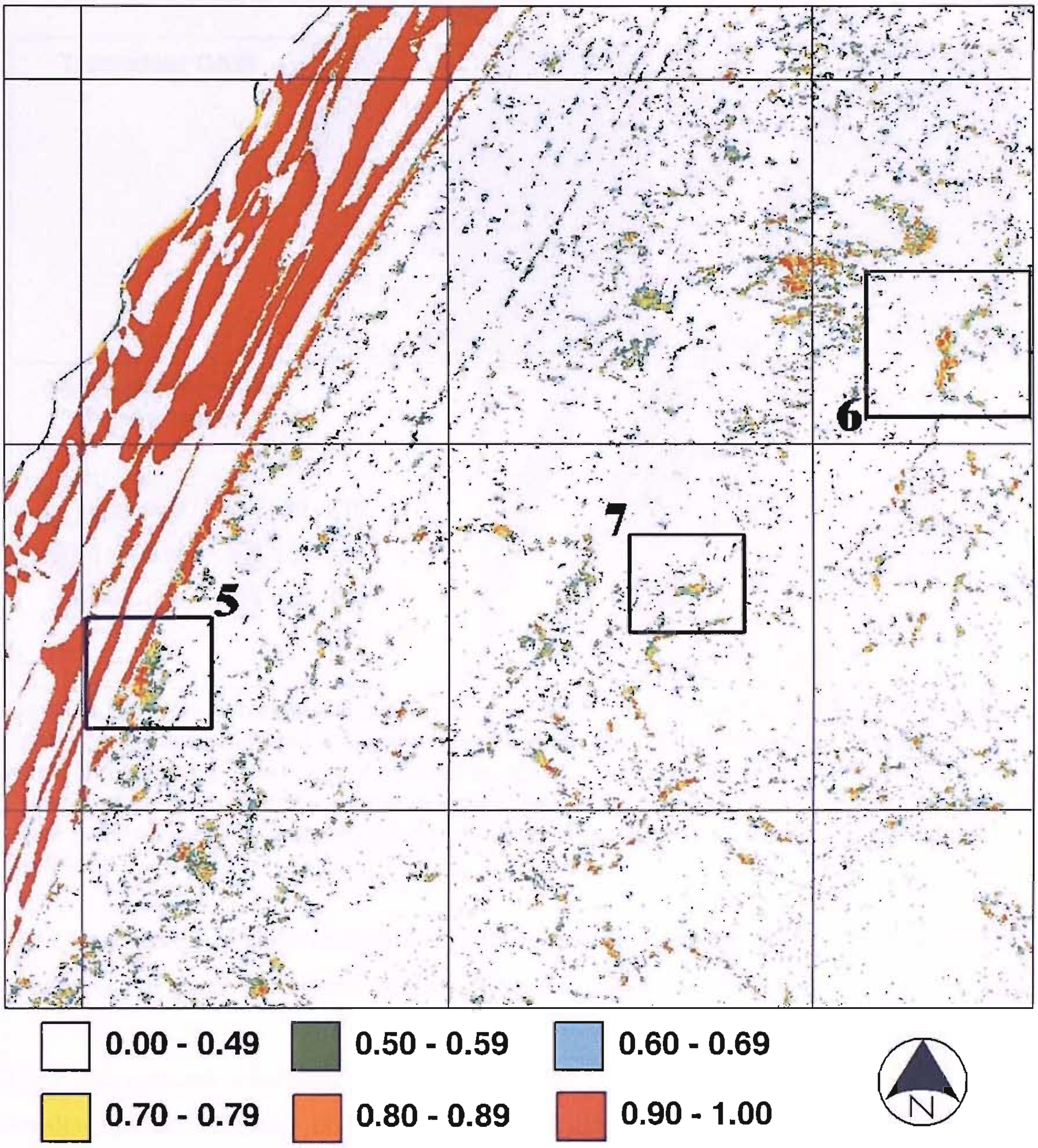

Figure 6.12 Thematic change vector between classifications of 2001 and 2002 data using Combined change model. Grid is 500 m. Areas 5, 6 and 7 are the extent of Figure 6.13, Figure 6.14 and Figure 6.15 respectively.

The strip of change along much of the mobile dune system using the Combined change image was likely to be due to errors from shadowing in the 2002 data (Figure 6.5). The shadowed area was misclassified as Water in 2002 data, but was Sand in the 2001 data.

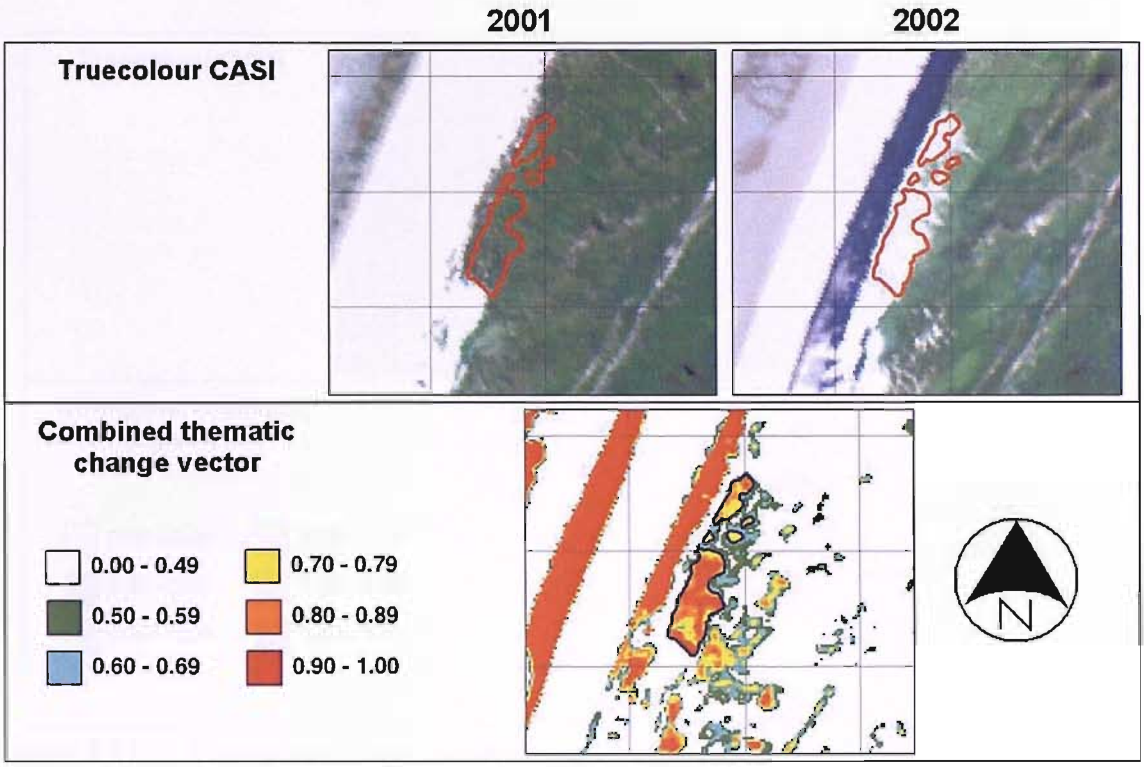

Figure 6.13 Overtopping of grasses by sand between 2001 and 2002 for area of mobile dune and change predicted using the Combined method. The red polygon is the area where overtopping occurs and predicted thematic change vector is greater than 0.7 using Combined method. Overtopping areas identified as red polygons on CASI imagery and black polygon on change image. Region shown is that defined as Area 5 in Figure 6.12. Grid is 50 m.

The change identified at the southern end of the mobile dune system appeared to be erosion or overtopping of vegetation by sand (Area 5; Figure 6.12, Figure 6.13).

There still appeared to be areas where change was incorrectly predicted due to shadowing from woodland (Area 6, Figure 6.12, Figure 6.14). The shadowing occurred in data from both years and resulted in areas of vegetation being misclassified as Water. However, the positioning of the shadow was different due to the data being flown at different times of day (Appendix C; Table C.2; Table C.4).

The change detection uncertainty output could be used to identify whether change has taken place or predict what change has occurred. For example, Figure 6.16 shows the areas predicted as changing to the Sand class in 2002. Large areas of the beach have changed to Sand in 2002. This is likely to be due to sand banks shifting between 2001 and 2002. There are also areas where overtopping by sand is likely to have occurred in and around the frontal dunes to the south west of the study area (Figure 6.16), as in Figure 6.13.

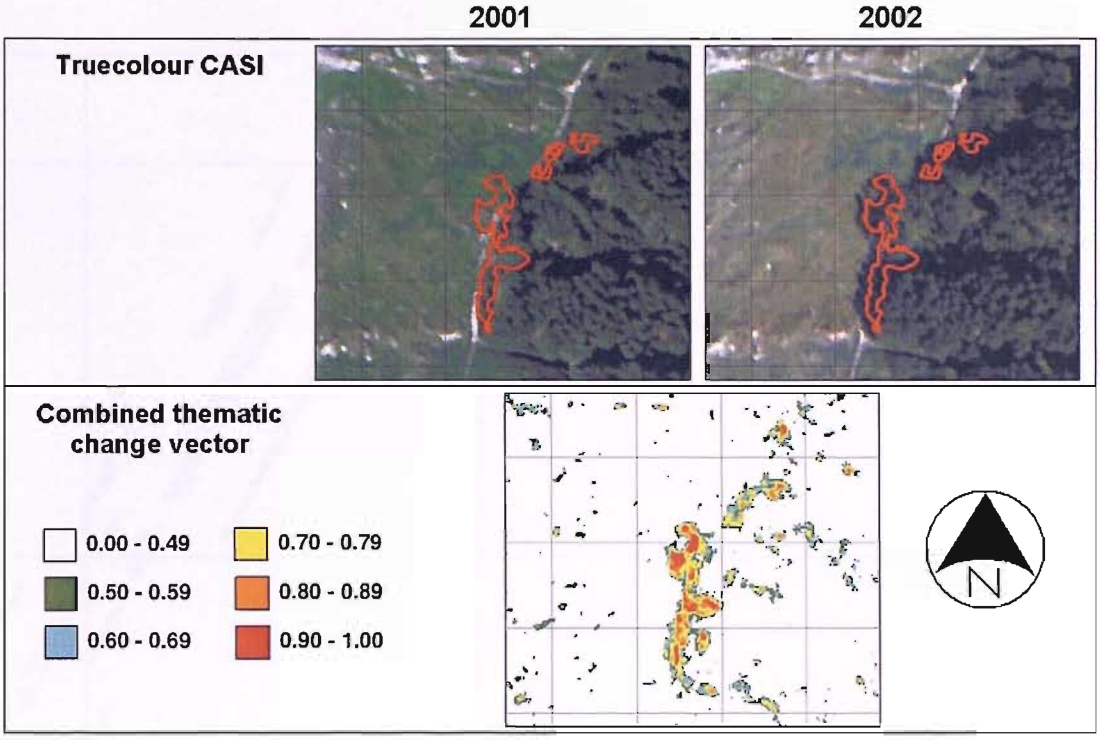

Figure 6.14 Change error due to shadowing at edge of woodland and change predicted using the Combined method. Red polygons are areas where predicted thematic change vector is greater than 0.7 using Combined method. Region shown is that defined as Area 6 in Figure 6.12. Grid is 50 m.

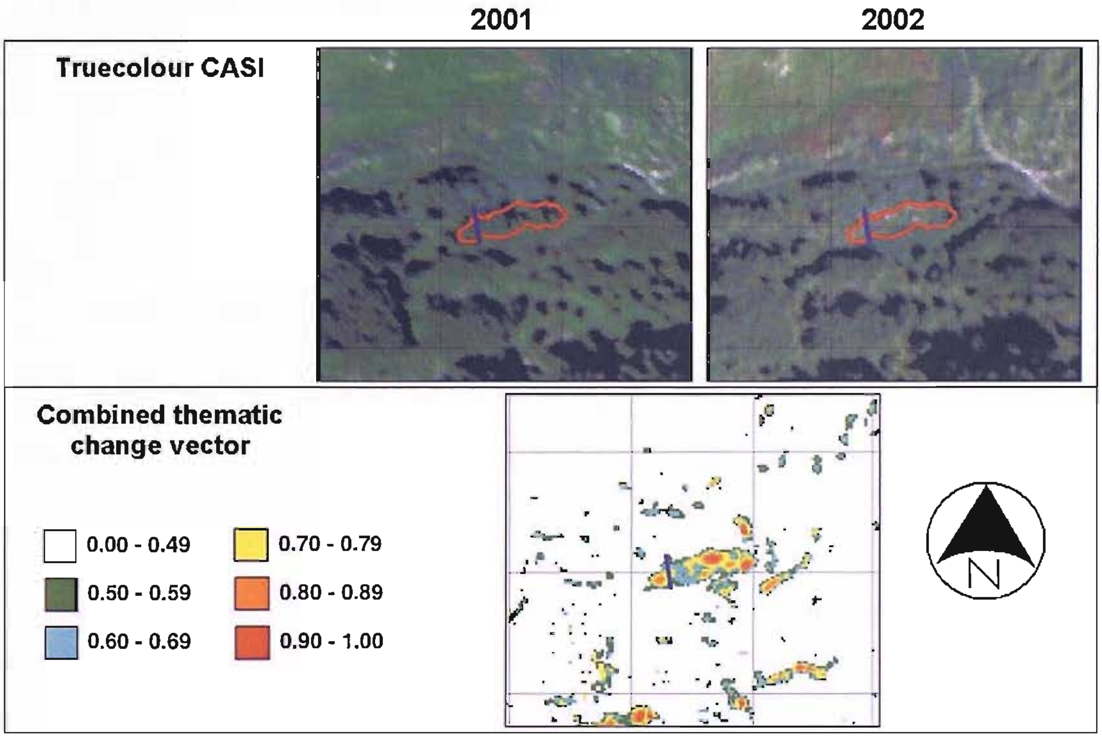

Figure 6.15 Area of woodland removed between 2001 and 2002 and change predicted using Combined method. The red polygon is the area believed to be felled where the predicted thematic change vector is greater than 0.6 using Combined method. The blue line is section of transect 6 where ground data show that trees have been removed. Region shown is that defined as Area 7 in Figure 6.12. Grid is 50 m.

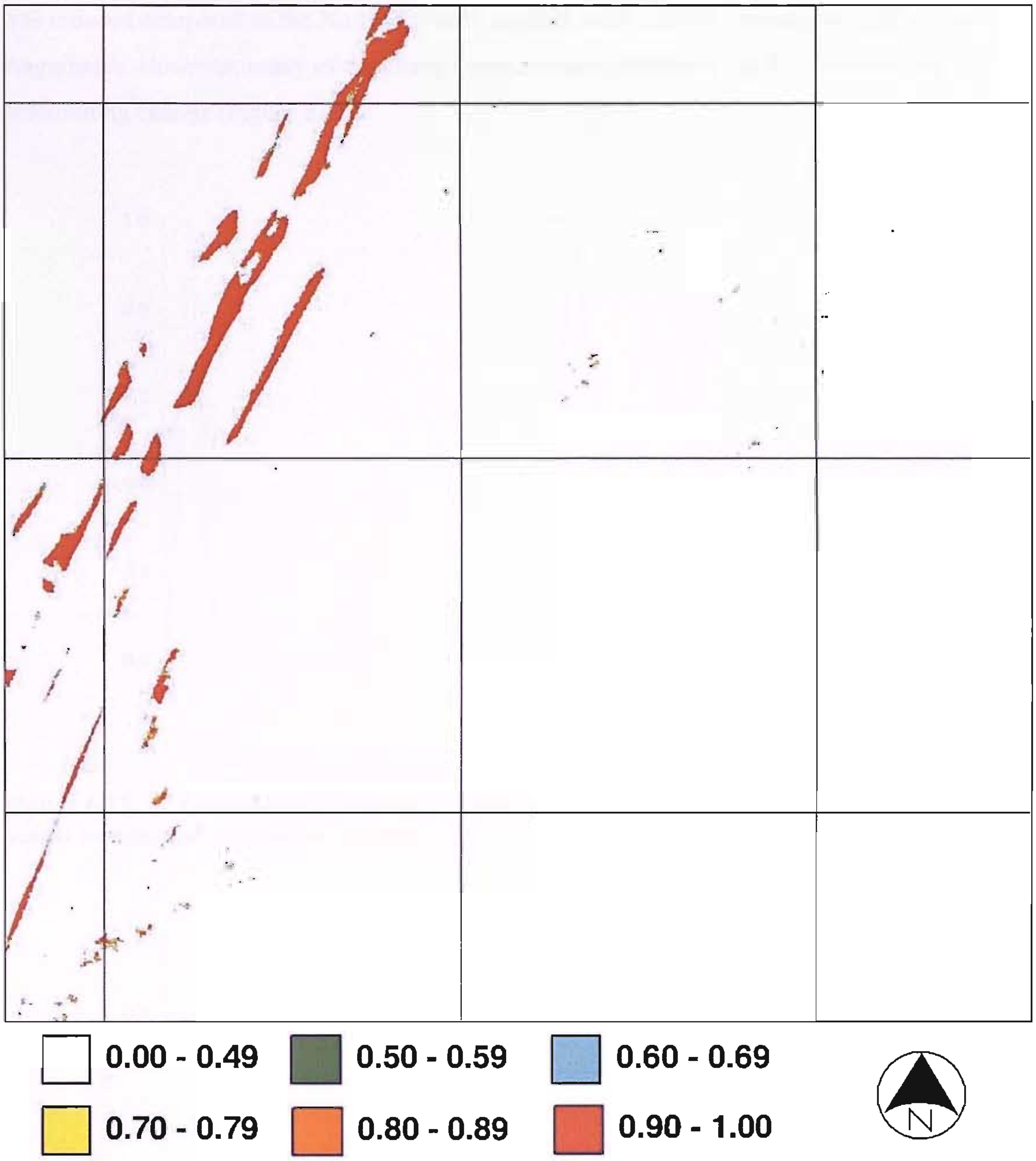

Figure 6.16 Areas predicted as changing to Sand in 2002 using Combined change model. This is the predicted thematic change vector from 2001 to 2002 from all classes apart from Sand in 2001 to Sand in 2002. Grid is 500 m.

When the transect thematic change vectors were examined, several trends relating to the change detection could be seen (Figure 6.17 to Figure 6.22). In all transects the largest overall errors were obtained using the No Uncertainty method (Table 6.10), and these errors were greatest where there was no change (Table 6.12). Thematic errors appear to result in change being predicted where none occurred. This was particularly the case in Transect 3 where 68% of the transect was predicted as change, but the ground data predicted minimal change between 2001 and 2002 (Table 6.10; Figure 6.19). The Thematic method resulted in a similar effect, but this was reduced compared to the No Uncertainty method, with smaller thematic change vector magnitudes. However, many of the change vectors were still above the 0.5 threshold for determining change (Figure 6.19).

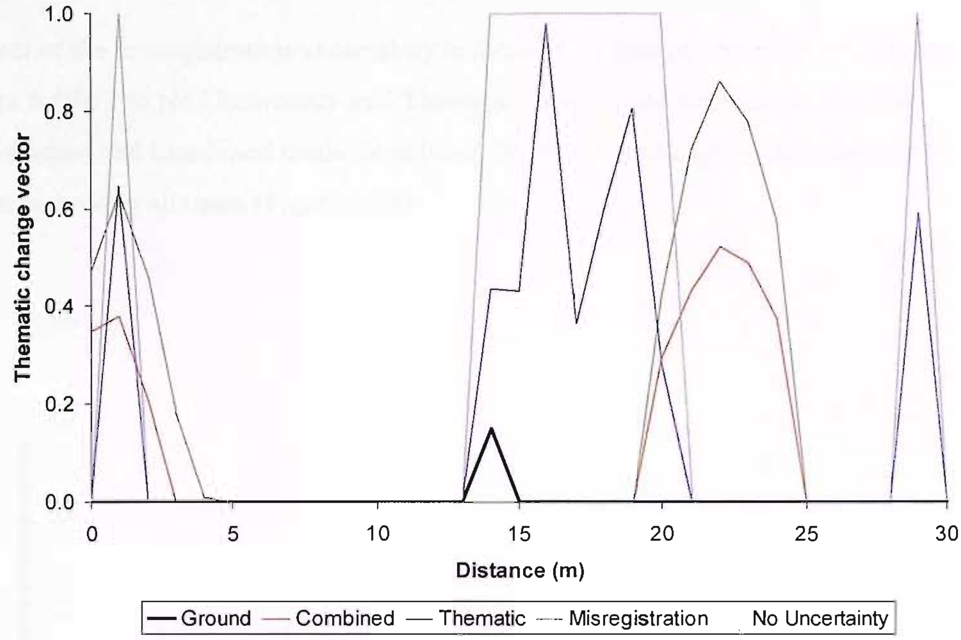

Figure 6.17 Ainsdale data transect 1 thematic change vector. Pixels are plotted as points to minimise confusion between change models.

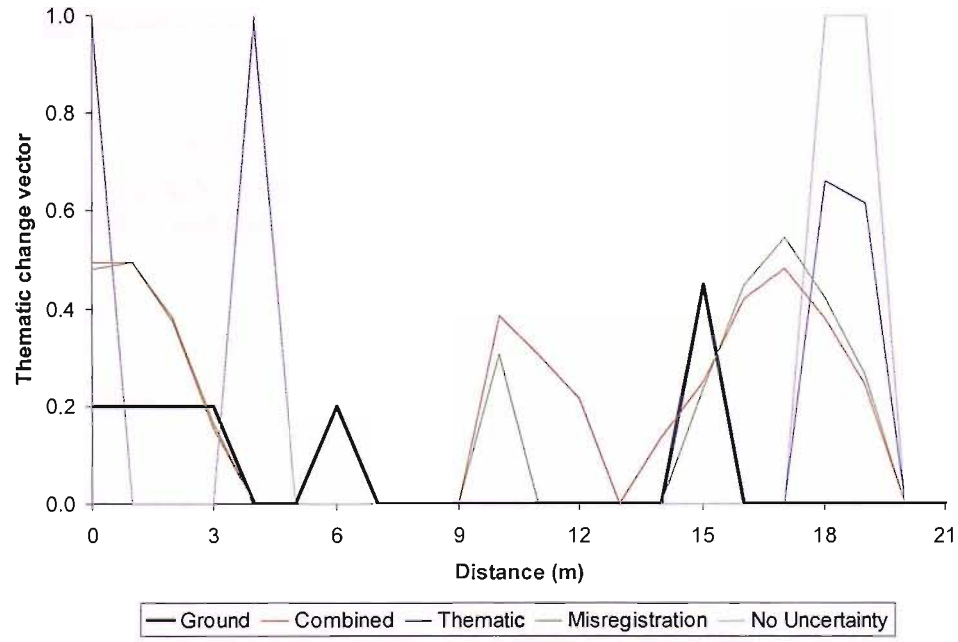

Figure 6.18 Ainsdale data transect 2 thematic change vectors. Pixels are plotted as points to minimise confusion between change models.

The Misregistration method reduced the overestimation of change in areas of no change, but did not completely remove this effect as may be seen in Transects 1 and 2 (Figure 6.17; Figure 6.18). The Combined method showed similar results in areas of no change to the Misregistration method, but the thematic change vector magnitudes were reduced, in many cases below the 0.5 threshold (Figure 6.17; Figure 6.18).

The effect of the misregistration uncertainty in areas of no change was most obvious in Transect 3 (Figure 6.19). The No Uncertainty and Thematic methods had large errors, but the Misregistration and Combined methods reduced the thematic change vector magnitudes below the 0.5 threshold in all cases (Figure 6.19).

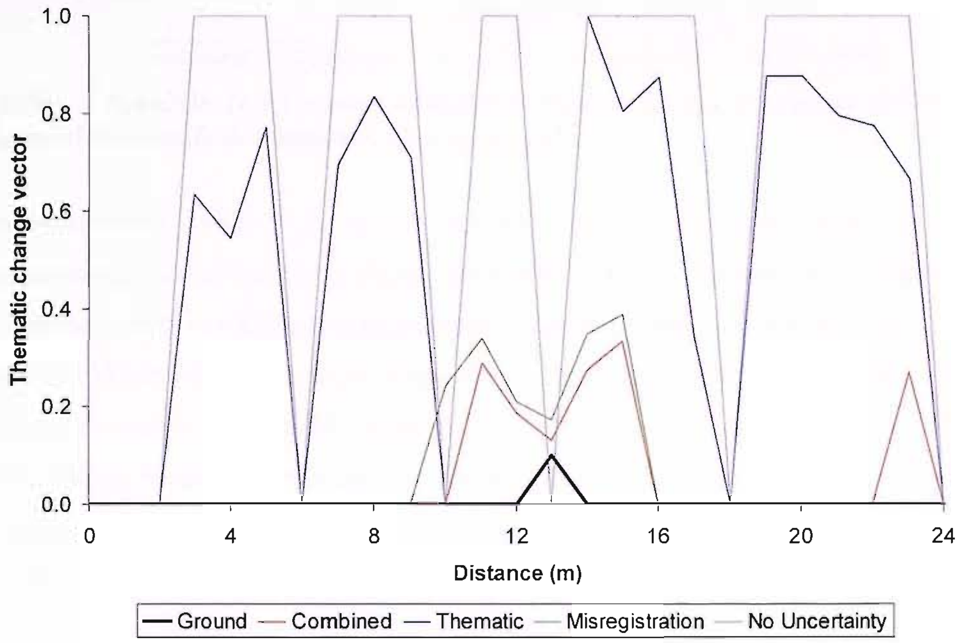

Figure 6.19 Ainsdale data transect 3 thematic change vectors. Pixels are plotted as points to minimise confusion between change models.

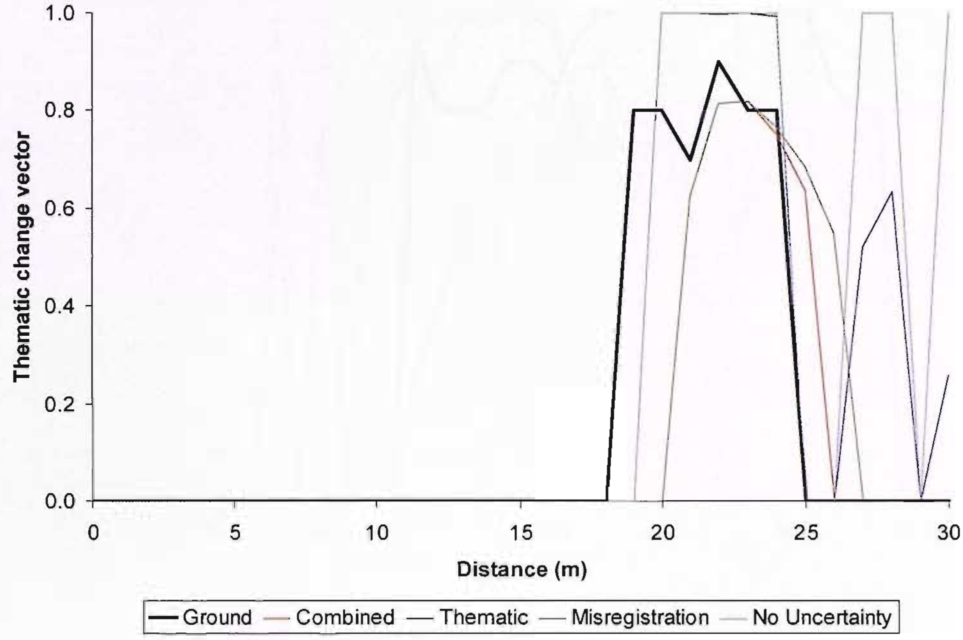

Figure 6.20 Ainsdale data transect 4 thematic change vectors. Pixels are plotted as points to minimise confusion between change models.

In the transects where change occurred, the No Uncertainty and Thematic change vectors generally accurately identified where change occurred (Figure 6.20; Figure 6.21; Figure 6.22) but these methods both overestimated and underestimated the thematic change vector. The Combined and Misregistration methods generally underestimated the thematic change vector where change occurred (Figure 6.20; Figure 6.21; Figure 6.22). In the data there were five Change/No change boundaries, two each in transects 4 and 5, and one in transect 6. If the 0.5 threshold was used to identify where change occurred, then the position of the Change/No change boundary predicted using the Combined method was within the change area in the Transect 4, Transect 5 (twice) and Transect 6 data (Figure 6.20; Figure 6.21; Figure 6.22). One of the predicted boundary positions was within the no change area in the Transect 4. Though no definite conclusions may be drawn from this, it tended to indicate that smoothing using the misregistration uncertainty methods resulted in the Change/No change boundary being shifted to within the area of change. This would result in change being underestimated if misregistration uncertainty was used, which agreed with the synthetic data in Table 5.9 and Table 5.10.

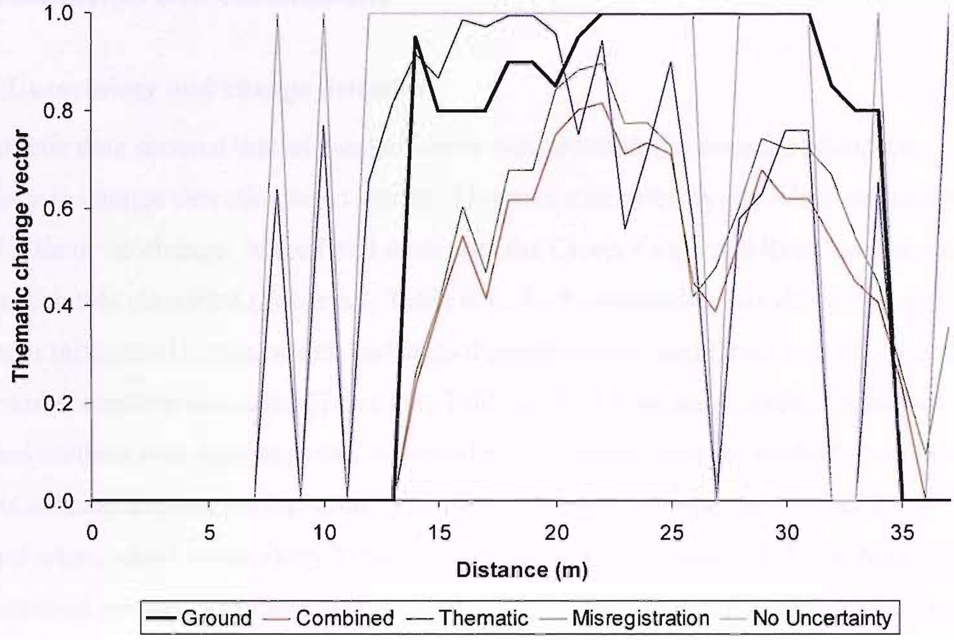

Figure 6.21 Ainsdale data transect 5 thematic change vectors. Pixels are plotted as points to minimise confusion between change models.

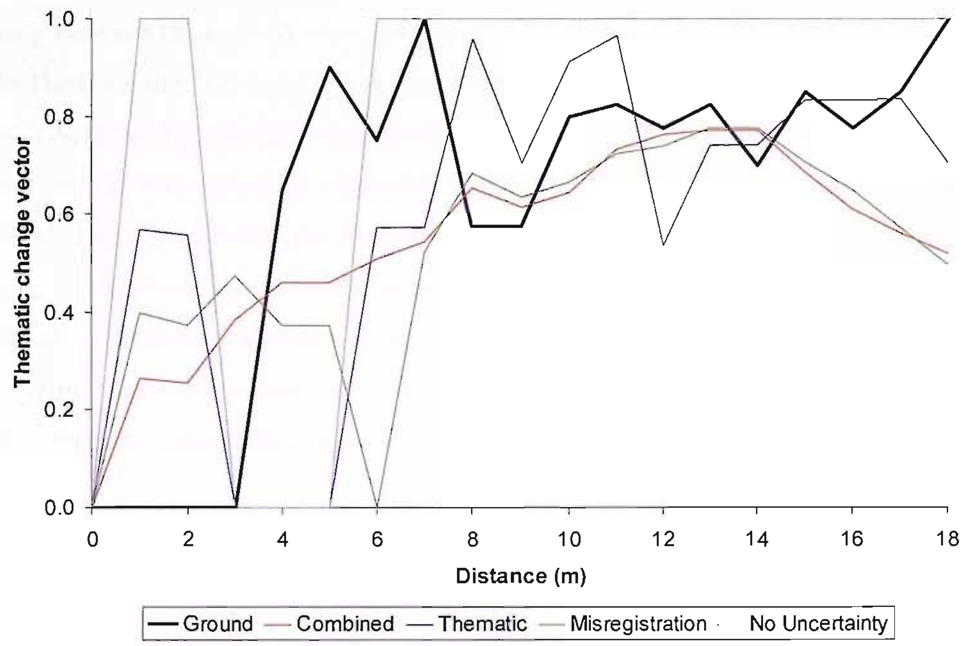

Figure 6.22 Ainsdale data transect 6 thematic change vectors. Pixels are plotted as points to minimise confusion between change models.

6.4 Discussion and Conclusions

6.4.1 Uncertainty and change detection

The synthetic data showed that as thematic error was reduced, the impact of thematic uncertainty in change detection was reduced. This was supported by the Ainsdale results in the areas of little or no change. In the fixed dune area the Creep, Grass and Reed classes were likely to be inaccurately classified (Table 6.3; Table 6.4). In the deciduous woodland and scrub areas there was a mixture of Creep, which had large thematic errors, and Grass and Woodland classes which were accurately classified (Table 6.3; Table 6.4). In both these types of area the Combined method was most accurate, followed by the Misregistration method, then the Thematic method and the No Uncertainty method was least accurate. In the coniferous woodland areas, which were likely to be classified accurately (Table 6.3; Table 6.4), the Misregistration method was more accurate than the Combined method, and the No Uncertainty method had similar accuracy values to the Thematic method (Table 6.6).

When the Combined method was more accurate than the Misregistration method, the difference in accuracy between the methods was as large as 8.7% (Table 6.6). This result was also seen when the Thematic method was more accurate than the No Uncertainty method (Table 6.6). However, where the Misregistration method was more accurate than the Combined, the Combined method was within 2% of the Misregistration (Table 6.6). Where the No Uncertainty method was more accurate than the Thematic, the Thematic method was within 0.5% of the No Uncertainty (Table 6.6). This indicates that even when class and overall accuracy values were large, the use of thematic uncertainty only resulted in a small decrease in change detection accuracy. When class and overall accuracy values were small, use of thematic uncertainty in per-pixel change detection reduced overestimation of change.

As thematic accuracy increased, use of thematic uncertainty appeared to become less appropriate. This was likely to be due to uncertainty resulting in errors, as the uncertainty model contained errors and was therefore uncertain itself. If an output is 100% accurate in positional or thematic terms then the probability of having a correct output will be 100%. If an uncertainty measure is used in this situation then errors in the estimation of uncertainty will potentially result in errors in estimation of change. Though it is important to model uncertainty, as uncertainty levels increase, the ability to detect change will decrease (Edwards and Lowell, 1996) and so any model of uncertainty should be as accurate as possible.

When the impact of just misregistration uncertainty and just thematic uncertainty were compared in the areas of little or no change it was seen that the Misregistration method was more accurate in all cases (Table 6.6). It was shown above that the relative importance of thematic uncertainty was increased in the fixed dune and the deciduous woodland and scrub areas where thematic error was large. Despite this, the difference in accuracy between the Misregistration and Thematic methods was greater in these areas than for the coniferous woodland areas (Table 6.6). Some of the increase in relative accuracy using misregistration uncertainty may have been due to smoothing of small areas containing thematic errors. However, it was also probable that in fragmented areas where misregistration had a greater impact (Serra *et al.*, 2003), the use of misregistration uncertainty was likely to produce greater accuracy.

Misregistration generally results in the incorrect prediction of change at the boundaries of classes (Verbyla and Boles, 2000; Stow and Chen, 2002). By accounting for misregistration, errors in change detection will be reduced. Stow and Chen (2002) found that compensating for misregistration reduced incorrect prediction of change, which agrees with the results in this study.

In areas of change the No Uncertainty method was as accurate as the other methods for identifying the change (Table 6.14; Table 6.15). The most likely reason for this was that the No Uncertainty method overestimated change more than the other methods, identifying areas of change through error. This was supported by both the Ainsdale and synthetic results (Table 5.9; Table 5.10; Table 6.6). The Combined method smoothed change, and, particularly at boundaries, it reduced the sensitivity to change by over-compensating for misregistration. This may be seen in the transect data of the Ainsdale and the synthetic imagery. The Combined and Misregistration methods generally positioned the boundary between change and no change within the area of change (Figure 6.20; Figure 6.21; Figure 6.22), therefore underestimating change. The Thematic and No Uncertainty methods generally placed the boundary within the area of no change, therefore overestimating change (Figure 6.20; Figure 6.21; Figure 6.22).

The change detection model that combined per-pixel thematic and geometric uncertainty measures was significantly more accurate (at 95% confidence) than a change detection model that did not use geometric or thematic uncertainty under the following conditions:

1. When determining whether Change or No change had taken place (Table 6.10; Table 6.11 p=0.031)

2. When identifying whether change had taken place in areas of no change (Table 6.6, Table 6.7, p=0.008; Table 6.12, Table 6.13, p=0.031).

The change detection model that combined per-pixel thematic and geometric uncertainty measures was not significantly more accurate (at 95% confidence) than a change detection model that did not use geometric or thematic uncertainty under the following conditions:

3. When identifying whether change had taken place in areas of change (Table 6.14).
4. When identifying what change had taken place (the sixty-four class problem) (Table 6.16, Table 6.17, p=0.313).

Results indicated that the use of thematic and geometric uncertainty increased change prediction accuracy for areas of no change (Table 6.6; Table 6.7; Table 6.12; Table 6.13), but decreased accuracy for areas of change (Table 6.14). Though the use of thematic and geometric uncertainty was significantly more accurate in this study for condition 1 above, this would partially depend on the ratio of change to no change pixels. An increase in the proportion of area where change was taking place would potentially reduce the relative accuracy of the Combined method compared to the No Uncertainty method.

The use of uncertainty models did not significantly increase the accuracy of predicting what change had occurred (Table 6.16; Table 6.17). This would be likely to occur if the use of uncertainty did not result in an increase in the thematic accuracy of the classification data from either year. The effect of uncertainty was likely to be complex, with increases in accuracy due to smoothing in some areas, and a reduction in others.

6.4.2 Fragmentation and class error

When class heterogeneity was examined as a function of change detection error, spatial heterogeneity or fragmentation resulted in large errors compared to areas that were spatially homogeneous or clumped (Table 6.6). The coniferous woodland areas showed much less change incorrectly predicted than the deciduous woodland and scrub and the fixed dune areas, though this difference could not be tested for significance due to too small a sample size. This result agreed with the studies by Verbyla and Boles (2000) and Carmel *et al.* (2001) who found that when land cover classes were heterogeneous or classes were fragmented, change detection errors were greater than when classes were homogenous or clumped. This was due to increased class boundary length compared with un-fragmented landscapes and so the effects of misregistration were greater (Serra *et al.*, 2003).

However, care has to be taken when interpreting the results for the areas of little or no change, as they were likely to be a function of class accuracy, as well as fragmentation. The Woodland class was more accurate than most of the other vegetation classes in terms of Producer's and User's accuracy in both the 2001 and 2002 classifications. The only class measures that were more accurate than the Woodland class were the User's accuracy of the Grass class and both class measures for the Buckthorn in the 2001 data (Table 6.3; Table 6.4). This would result in fewer errors in the change layer when compared to the fixed dune areas where the classes generally had smaller accuracy values (Table 6.3; Table 6.4).

6.4.3 Impact of shadows on change detection

Much of the error in change detection was due to the effect of shadows resulting in misclassification in the 2001 and 2002 imagery (Figure 6.3, Figure 6.4, Figure 6.5). Though the imagery was acquired at similar times of year (28^{th} August 2001 and 11^{th} September 2002) they were acquired at different times of day (between 1330 and 1400 in 2001 and 0940 and 1010 in 2002). This resulted in the direction that shadows lay being markedly different in either year and so misclassifications being in different areas in either year. If the imagery had been acquired at the same time of the day some of these errors would not have occurred as shadows were generally misclassified as Water in either year (Figure 6.3, Figure 6.4, Figure 6.5). But in operational remote sensing specifying exact times for multiple flights is not practical as there may be the requirement to acquire data at multiple sites. This combined with weather and tidal restrictions may mean that specific times for data acquisition are difficult to achieve.

6.4.4 Impact of imagery errors on thematic uncertainty

The methodology developed did not compensate fully for thematic errors using uncertainty. Classification errors that were due to shadowing and other bi-directional effects did not necessarily result in smaller posterior probabilities output by the PNN. For this reason the thematic uncertainty method requires further development in order to compensate for variations in lighting. Operational methodologies are also required that can reduce the impact of bi-directional effects, as the variations in lighting resulted in errors, particularly in those areas where there were large amounts of shadowing, such as at the edge of woodland (Figure 6.3; Figure 6.4) and near the steep-sided mobile dune system (Figure 6.5).

6.4.5 Defining change

Within this study, change was defined in terms of land cover conversion (Jansen and Gregorio, 2002). In a data model that does not use measures of uncertainty, change is defined easily, though not necessarily accurately. The use of uncertainty complicates this, as change may be defined at any arbitrary level of probability, as well as using various methods to define that change. This definition is complicated further if a fuzzy data model is used, as change then has to be defined in terms of probability as well as partial changes in cover.

6.4.6 Fuzziness and change detection

The results for Area 4 (Figure 6.9; Figure 6.10) suggested that the PNN did not accurately model the fuzziness associated with a pixel's membership to multiple classes. If fuzziness was modelled accurately then this area, consisting of mixed pixels, would have had small thematic change vectors, as pixels were a relatively even mixture of three class types. As the PNNs used did not model fuzziness, the areas where mixed pixels occurred were not modelled accurately in the change detection layer.

There are three main alternatives that could explain this:

1. PNNs cannot be used to model multiple class membership.
2. PNNs cannot be used to model thematic uncertainty and multiple class membership simultaneously.
3. The PNN used in this study was optimised for overall and thematic uncertainty accuracy, but it would be possible to select a network that provided an accurate fuzzy output or fuzzy data could be used in the training process.

As identified by Ricotta (2004), fuzziness and uncertainty are two separate concepts and the PNN may be unable to accurately output fuzzy measures, as its outputs are inherently probabilistic. However, other classifiers that output posterior probabilities such as the ML have successfully been used to model fuzziness (Foody *et al.*, 1992; Bastin, 1997) making it likely that the PNN can provide an output that incorporates multiple class membership.

Though PNNs can output indicators of multiple class membership or accurate posterior probabilities, they may not be able to do both simultaneously, as the optimum smoothing function will be different for each output. In this case, PNN output could be optimised for either uncertainty or fuzziness, but which output would have to be determined prior to classification. Alternatively PNNs are capable of outputting a probabilistic measure that can incorporate fuzziness, but the PNNs used in this study were not optimised for producing both measures. This would require a stage in which PNNs were tested to maximise thematic accuracy, thematic uncertainty accuracy and fuzzy output accuracy. This would reduce errors in the final change layer by incorporating the effects of mixed pixels, which appear to be reducing accuracy in the final change detection map (Figure 6.9; Figure 6.10).

6.4.7 Thematic change vector direction

Using the Ainsdale data, the direction of the thematic change vector was used to determine what change had occurred. Using 64 change classes, no method is significantly (at 95% confidence) more accurate than another (Table 6.16). This may be expected, as the use of uncertainty will not necessarily increase the overall thematic accuracy and may reduce the thematic accuracy in certain places. In areas where spatially random thematic errors occur, the use of misregistration uncertainty will smooth errors. However, at the boundary between classes, where the misregistration error is small, the use of misregistration uncertainty may result in increased thematic errors due to over smoothing. As thematic accuracy of the input layers for the change process (the combined thematic and misregistration uncertainty for a given year) will not necessarily be increased then the accuracy of the change vector direction will not be increased.

6.4.8 Limitations in ground data

There are a number of limitations in the ground data acquired that restricted the outputs of this study. One limitation was that there were insufficient transect ground data. The limited number of transects meant that though one methodology was more accurate for the majority of the transects, significant differences were unlikely to be found. Another limitation was that there were no ground data for testing the impacts of mixed pixels on thematic uncertainty measures. This was due to the study being set up for hard classification and consideration was not given to the impacts of mixed pixels. Future studies should consider this and acquire ground data that incorporate multiple class membership.

6.4.9 Satellite based change detection using per-pixel uncertainty

The land cover change model was specifically derived for a CASI airborne sensor. The complete method is directly transferable to other airborne systems, as long as the geometric uncertainty associated with the various navigational parameters can be determined. However, it also has potential for application using satellite-based systems. The methods of deriving thematic uncertainty are directly transferable to imagery from satellite systems. If the geometric error model can be adapted for satellite navigation systems then it may be used to predict geometric error, even if the geometric model uses a global measure of instrument navigational geometric uncertainty combined with a terrain model to determine potential orthometric errors.

6.4.10 Accuracy and change detection

Though the study by Wright and Morrice (1997) quoted a required overall accuracy for change detection of 85%, there is also a requirement for class accuracy values to be large as well.

Even though per-pixel uncertainty may be used to increase change detection accuracy, accuracy of the input data needs to be maximised in order to minimise errors in change detection. The ability to detect change is partially a function of the errors within the input data layers (Edwards and Lowell, 1996; Carmel and Dean, 2004). As those errors are decreased, the potential to detect change increases. Though methods of estimating uncertainty are important to determine potential errors, future work needs to continue examining methods for reducing thematic and geometric errors. In terms of thematic accuracy, this will be a function of the quality of ground and remotely sensed data, as well as classification methods used.

Errors in the spectral data used can result from instrument noise or errors during radiometric correction. These errors and bi-directional effects are likely to result in uncertainty in the classification process during the training stage due to the spectral characteristics of each class being less precisely represented. During the allocation process, errors in spectra may result in incorrect allocation of classes. Spectral variability may also result in thematic uncertainty being less accurately predicted.

Instrument errors or errors due to bi-directional effects may result in the spectra of a given pixel appearing to be that of a different class. If this occurs then the classifier will not be able to determine that the class allocation is uncertain and so predicted thematic uncertainty will be small. This occurred in the 2002 data due to bi-directional effects. In the areas of shadow, pixels were incorrectly allocated to the Water class rather than Grass, but the predicted probability of the pixel being allocated Water was close to 1.

Some of these problems may be overcome by operational methods, such as minimising shadowing and bi-directional effects by acquiring data as close to solar midday as possible. In a multitemporal survey lines should be flown in the same direction and as closely as possible to up or down Sun (at the solar azimuth angle or a reciprocal bearing). However, this reduces the scope for remote sensing data acquisition, reducing the possibility of applying these techniques over large areas, particularly in the UK, where weather constraints already restrict data acquiring a great deal. For sites that are orientated east-west, it may be impractical to acquire data with consistent orientation.

Geometric and therefore misregistration accuracy using an automated georeferencing system are a function of the accuracy of the positional, attitude and elevation data. Increases in the accuracy of these data are mainly a function of technological fixes. These include the potential increase in positional accuracy when the European Galileo satellite navigation constellation comes online in 2008 (ESA, 2005). The use of additional satellites offered by this system has the potential to increase positional accuracy, particularly errors due to restricted satellite numbers or geometries that may occur with the current GPS system (ESA, 2005).

7 Conclusions

7.1 Introduction

In previous chapters the errors that occur in change detection were discussed. Methodologies were developed that could be used to model those errors, increasing the accuracy of change detection. In this chapter the research carried out in this study is summarised, further areas of study are suggested and conclusions are drawn about the suitability of the approaches taken in this study for operational land cover change detection in natural and semi-natural habitats.

7.2 Summary

Methods of land cover change detection using remote sensing are not sufficiently accurate that UK governmental organisations such as the Environment Agency and English Nature use them operationally for legislative reporting or input for management plans. This study identified that misregistration and thematic errors within remotely sensed datasets were likely to be major factors causing change detection errors (Section 1.4). The study also identified that the prediction of the spatial variability of misregistration and thematic errors or the uncertainty associated with these errors could be used to increase change detection accuracy (Section 1.4.3). Previous studies examining change detection have derived per-pixel measures of thematic uncertainty using a variety of classifiers (Shi and Ehlers, 1996; Ediriwickrema, and Khorram, 1997; de Bruin and Gorte, 2000; Gong *et al.*, 1996; McIver and Friedl, 2001) and derived methods of accounting for the variation in misregistration error on a per-pixel basis (Stow, 1999), but had not combined the two in a per-pixel model of change detection. Within this study it was shown that it was possible to derive local thematic and geometric uncertainty measures and combine these to provide a local uncertainty measure of thematic change in post-classification change analysis. Figure 7.1 shows the model of uncertainty propagation used in this study. It combines geometric and thematic errors in the form of probabilities or uncertainties and propagates them through the change detection process.

The study examined the derivation of a local geometric uncertainty model using a model of instrument error based on a general model of geometric uncertainty combined with a local measure of geometric error based on angular acceleration derived from the IMU (Section 3.6.4). The instrument geometric uncertainty model was combined with an orthometric error model that accounted for errors due to incorrect elevation values being used in the geometric correction process (Section 3.6.5). This resulted in per-pixel measures of geometric uncertainty. The geometric uncertainty models for two images were merged to provide per-pixel measures of misregistration that was found to be significantly correlated with the actual misregistration measured on the images (Section 3.6.6).

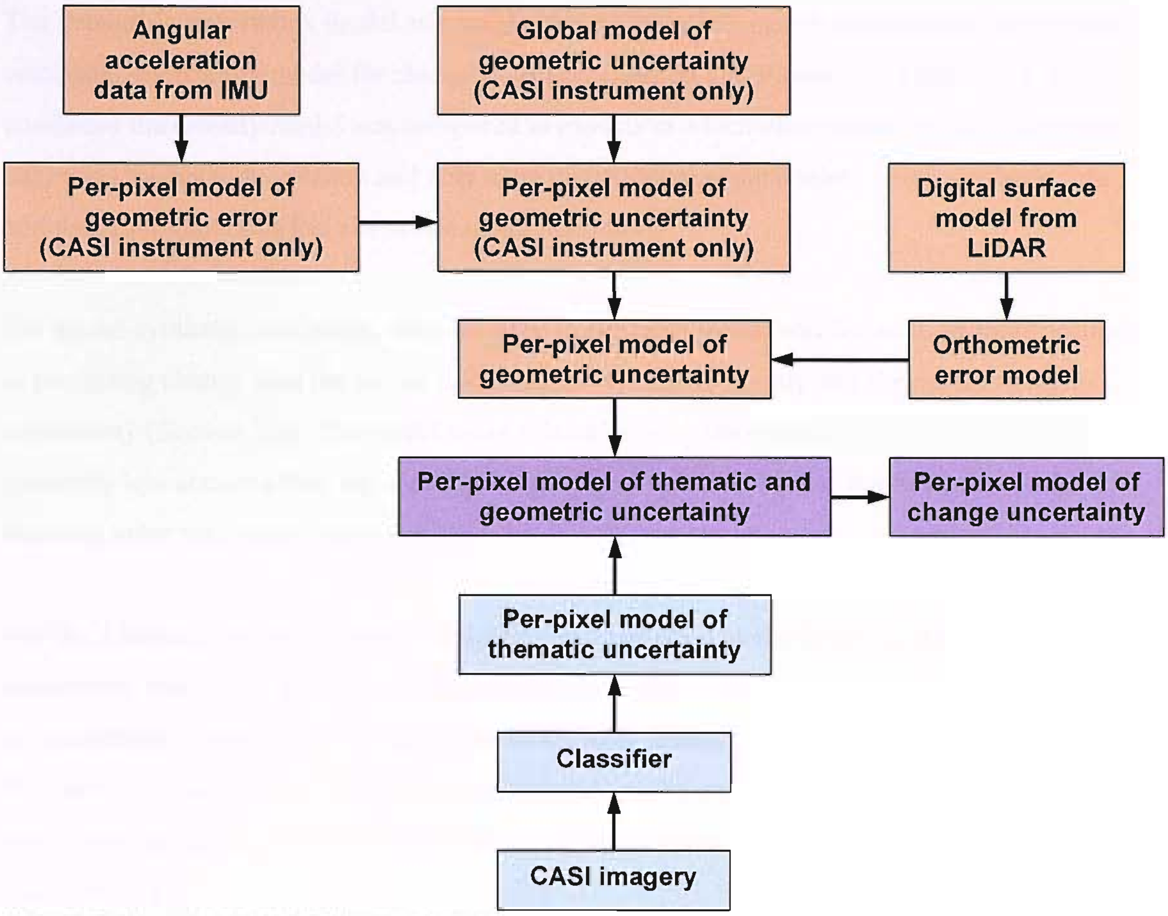

Figure 7.1 Model of change detection uncertainty propagation used in this study. Orange indicates geometric uncertainty, blue indicates thematic uncertainty and purple indicates combination of geometric and thematic uncertainty.

The study showed that both PNN and MLP neural networks could produce outputs that were significantly correlated with thematic uncertainty (Section 4.7.1.2; Section 4.7.2.2). The study also examined the relationship between heuristics and accuracy of thematic uncertainty measures for both types of network (Section 4.7.1.2; Section 4.7.2.2). It was shown that the classifier that had the largest overall accuracy was not necessarily the classifier that would produce the most accurate measure of thematic uncertainty (Table 4.2; Table 4.5). For this reason it is essential that the final use of a classification is considered. An accurate measure of thematic uncertainty may be of use in determining where thematic errors are likely to occur. However, if the classification is inaccurate the accuracy of the final change detection will be reduced. To maximise the accuracy of the change detection may involve compromise between the overall accuracy of the classifications and the accuracy of the thematic uncertainty measures. Further studies are required to examine the relationship between overall, class and thematic uncertainty accuracy with the precision and accuracy of change detection.

The geometric uncertainty model and the thematic uncertainty model were merged to provide a combined uncertainty model for change detection (Section 5.4; Figure 5.2; Figure 7.1). This combined uncertainty model was compared to models in which uncertainty was not predicted, only used thematic uncertainty and only used misregistration uncertainty using synthetic data and data of a sand dune test site at Ainsdale, Southport.

For all the synthetic data tested, the combined uncertainty model was found to be more accurate at predicting change than the model using thematic uncertainty only and the model using no uncertainty (Section 5.6). The model using misregistration uncertainty only was found to be generally less accurate than the combined uncertainty model using the synthetic data, unless the thematic error was small (Section 5.6).

For the Ainsdale test site the model that combined per-pixel misregistration and thematic uncertainty resulted in significantly larger change detection accuracy than the method that used no uncertainty (Section 6.3). When the methods were tested in areas where change took place, the model that did not use uncertainty was generally more accurate than the model that combined uncertainty, but only three transects where change had taken place were tested (Section 6.3).

This study indicates that as thematic accuracy increases, the use of thematic uncertainty in predictions of land cover change detection becomes less relevant. This is likely to be the case for misregistration as well. From this it may be concluded that there is likely to be a level of misregistration error at which the use of uncertainty results in increases in the error of change detection, though studies have shown that even small levels of misregistration may result in large change detection errors (Dai and Khorram, 1998; Stow and Chen, 2002). No conclusions on the use of thematic uncertainty in change detection can be drawn from this study, but the point at which using both misregistration and thematic uncertainty results in increases in change error is likely to vary according to the accuracy of the uncertainty models, the distribution of errors, the amount and distribution of change and the level of fragmentation of the surface being surveyed.

7.3 Future work

7.3.1 Use of synthetic data for modelling change detection

The synthetic data generated in this study were unlikely to be an accurate model of data generated using actual airborne data. The random nature of the thematic error introduced was not an accurate representation of error within the data, as may be seen from the actual CASI classification change detection (Figure 6.8). In the CASI data, errors due to effects such as shadowing are not spatially random and so future work with synthetic data should more accurately model the data in terms in the spatial distribution of thematic and geometric errors.

Future work should also compare smoothing as a method of reducing errors with the methods derived in this study. It is likely that simple smoothing will be able to reduce certain errors, particularly spatially random errors. However, systematic or clumped errors are less likely to be reduced using this method and it would not account for the spatial variability in misregistration.

7.3.2 Fuzziness and uncertainty

Studies should be carried out that test whether the classification outputs used in this study simultaneously provide indications of fuzziness (the presence of more than one land cover class in a pixel) and thematic uncertainty (the probability that a given pixel has been allocated the incorrect class). Though the data in this study indicated that fuzziness was not modelled using the PNN, this should be tested further (Figure 6.10; Section 6.4.6). Posterior probabilities in the form of output from ML classifiers have been used to provide measures of fuzziness (Foody *et al.*, 1992; Bastin, 1997), indicating that the PNN has the potential to output a soft classification. Previous work on the ML and MLP has shown that these classifiers can provide measures of fuzziness and uncertainty (Foody *et al.*, 1992; Gong *et al.*, 1996; Shi and Ehlers, 1996; Bastin, 1997; Ediriwickrema, and Khorram, 1997; Foody, 1997; de Bruin and Gorte, 2000; Zhang *et al.*, 2004), but this work has not focused on testing both measures simultaneously. As previously discussed (Section 5.3) it is likely that there is some correlation between fuzziness and uncertainty, as increased fuzziness will result in increased probability of confusion between classes. Even though fuzziness and uncertainty are completely separate models (Ricotta, 2004), it is also likely that fuzzy measures will automatically incorporate some uncertainty, for example, due to training data that do not completely represent a class, or classes that are not spectrally separate. It may be difficult to establish an accurate measure of thematic uncertainty that does not partially incorporate fuzziness and *vice versa*. Other classification methods may need to be developed that provide separate measures of fuzziness and thematic uncertainty.

One approach to predicting fuzziness would be to use fuzzy training data. By using fuzzy training data it is possible to derive a classification that more accurately models multiple class membership than if training data were made up of single classes (Foody, 1997; Foody, 1999). However, this is likely to have an impact on how accurately errors are modelled using the thematic uncertainty measures and different approaches to deriving these measures may be required.

7.3.3 Geometric uncertainty and post-processing

The automated geocorrection and, therefore, the geometric uncertainty model used separate navigational data from an IMU and post processed GPS. By combining the IMU and GPS it is possible to obtain a more precise positional and attitude data (Mostafa and Hutton, 2001; Toth, 2002). The geometric error study should be extended to examine whether the similar relationships between geometric error and angular acceleration exist when IMU attitude data and GPS positional data are post processed together. Studies with more samples need to be carried out to determine whether other navigational parameters such as angular velocity are correlated with geometric error.

7.3.4 Local uncertainty

As thematic and geometric errors vary spatially (Lanter and Veregin, 1992; Stow, 1999), it may be seen that the effect of using global uncertainty measures for modelling change is dependent on the spatial distribution of errors within the input data layers. Where the global uncertainty measure is greater than the actual error, the sensitivity of change detection will be below the maximum potential value. Where the global uncertainty measure is smaller than actual error, the error of change detection will be increased compared to a larger uncertainty measure. From this it may be seen that the use of per-pixel uncertainty measures has the potential to maximise the sensitivity of change detection and minimise the error, by varying uncertainty measures according to the probable error. However, the effects of using global and local measures of uncertainty in change detection were not compared in this study so further work is required to test the relative accuracies of these methods.

7.4 Conclusions

This study aimed to derive an accurate method of change detection using airborne sensor data that would be suitable for use by organisations such as English Nature or the Environment Agency that have to manage or report on the status and extent of coastal habitats. To increase the accuracy of land cover change detection, models of thematic and geometric per-pixel uncertainty were derived. The geometric uncertainty model provided measures of the magnitude and probability of geometric errors on a per-pixel basis. Thematic uncertainty models were derived from the output of neural network classifiers and provided measures of the probability of correct classification for every class on a per-pixel basis. These thematic and geometric uncertainty models were combined in change detection modelling to provide more accurate change detection outputs than could be achieved using traditional methods that do not account for uncertainty. Though the use of per-pixel uncertainty can be used to increase the accuracy of change detection for coastal habitats, further study needs to be carried out before these techniques can be applied in an operational context for regular monitoring.

The work on per-pixel thematic uncertainty needs to be expanded to determine the effects of mixed pixels on uncertainty and examine methods of predicting thematic uncertainty in fuzzy classification. Airborne sensor geometric uncertainty models need to be expanded to account for the effect of navigational variables other than angular acceleration on geometric error. The work on per-pixel uncertainty should not be carried out in isolation, as other areas such as instrument noise, remote sensing data collection, ground data collection, radiometric normalisation, bi-directional effects and classifier accuracy are all essential if the goal of operational land cover change detection for a variety of habitats is to be achieved.

Appendix A Remotely sensed data for coastal mapping

A.1 Multispectral imagery

There are three main factors to be considered when selecting a multispectral sensor to monitor coastal vegetation; spatial resolution, waveband availability (wavelength and width) and monitoring opportunities.

Much of the variation in land cover type within UK coastal habitats occurs at scales of a few metres (Rodwell *et al.*, 2000) and so coarse spatial resolution data would be inappropriate for monitoring the diversity of species even if sub-pixel classifications are carried out. Of the medium resolution satellite sensor data that are readily available, Systeme Pour l'Observation de la Terre (SPOT) High Resolution Visible (HRV) and Landsat Thematic Mapper (TM) are therefore inappropriate as they have a finest multispectral spatial resolution of 10 m (SPOT 5), and 30 m respectively (NASA, 2002; SPOT, 2005).

The combination of a narrow seasonal window, possible tidal limitations and weather mean that frequent return time is very important, especially in the UK. Obtaining imagery when there are no clouds and tidal conditions are correct may be difficult (Smith *et al.*, 1998).

Table A.1 Specifications of Current Multispectral Sensors readily available to acquire data in UK (Digital Globe, 2005; ITRES, 2005; NASA, 2002; Space Imaging, 2005; SPOT, 2005; USGS, 2005).

Sensor/ Platform	Spatial Resolution (m)	No. wavebands	Spectral Range (μm)	Return Cycle (days)
Landsat TM and Enhanced TM (ETM+)	30	7	0.45-2.35	16 5-6 (using all satellites)
SPOT HRV	20 10 (SPOT 5)	3 4 (SPOT 4)	0.50-0.89 0.50-1.75 (SPOT 4)	26 at nadir 1-4 off nadir 9 at nadir using all SPOT satellites 1 off nadir using all SPOT satellites
IKONOS	4	4	0.45-0.9	1.5 off nadir
Quickbird	2.4	4	0.45-0.9	1.5 off nadir
CASI (Airborne)	1-10	8-288	0.40-1	Mission dependant
Aerial Photography	0.075-0.5	3 or 4	0.45-0.90	Mission dependant

IKONOS and Quickbird have the most suitable spatial resolution of satellite sensor data currently available, with a multispectral pixel size of 4 m and 2.4 m, respectively, and a return time of approximately 1.5 days (Table A.1; Digital Globe, 2005; Space Imaging 2005). The Quickbird satellite was launched in October 2001 (Digital Globe, 2005), after the start of this study. There are limitations even with a return time as short as IKONOS and Quickbird. Cloud free conditions may be limited even when data may be acquired every few days. Another limitation of both systems is that they only provide four broad wavebands in the blue, green, red and near-infrared wavelengths. This may not provide the number of narrow wavebands required for an accurate classification of coastal habitats (Thomson *et al.*, 1998).

Airborne sensor systems generally provide fine spatial resolution data and the ability to target specific weather and tidal conditions. However, geocorrection of airborne imagery may be difficult and radiometric normalisation may be required if multiple image lines are acquired.

Airborne sensors are less limited by the time constraints, as data may be acquired at any time when light levels are high enough. Missions may be targeted for a particular stage of the tide and weather conditions. Data may also be acquired under clouds, though there may be large variation in lighting levels.

The CASI 2 system currently in operation at the Environment Agency provides standard 1 m to 4 m spatial resolution data in up to 18 wavebands (Brown *et al.*, 2003b; Itres, 2005). CASI imagery is automatically geocorrected using high precision attribute data and post-processed differential GPS to locate the CASI sensor head and its viewing geometry accurately (Brown *et al.*, 2003b).

Using aerial photography, the spatial resolution can be much finer than CASI, with systems currently available that can be flown operationally with a resolution of less than 5cm, though a resolution of 15 cm to 25 cm is more common. Even though there are now four waveband digital cameras that can provide high spatial resolution data in visible and near infrared, these wavebands are relatively wide (Strawbridge *et al.*, 2000).

Of the sensors mentioned above, IKONOS and aerial photography do not offer the number or the narrow wavelength wavebands that may be necessary to discriminate accurately between coastal vegetation classes (Thomson *et al.*, 1998). Though the CASI sensor does not have the fine spatial resolution of aerial photography, it does have the capability to provide up to 18 narrow targeted wavebands. This capability is important when automated classifications are to be carried out for the coastal zone.

A.2 Digital elevation model data

If airborne multispectral imagery is to be automatically georeferenced a digital elevation model (DEM) or digital surface model (DSM) dataset must be used to account for terrain effects. For UK coastal habits DSMs or DEMs may be derived from three main sources; photogrammetry, laser terrain mappers and radar.

Laser terrain mappers operate using the principle of Light Detection and Ranging (LiDAR). A laser pulse is fired towards the ground, the pulse reflects off the ground and returns to the instrument, where the time of flight is measured. This is used to estimate the slant distance between the instrument and the point on the ground. This process is repeated at frequencies of 1 kHz to 100 kHz. A DEM may then be generated using the slant distances, the position of the instrument estimated using GPS and the attitude of the instrument estimated from an inertial motion unit (IMU). The points are then resampled to form a raster grid with a spatial resolution of between 0.5 m to 10 m. The UK Environment Agency has been acquiring LiDAR data since 1997 at 2 m or finer horizontal spatial resolution and has coverage of over 16% of England and Wales, much of it for the coastal region (Duncan, personal communication).

Generating DEMs using photogrammetry requires the use of overlapping aerial photographs and either ground control points (GCPs) or high precision aircraft GPS and attitude data. Stereoscopic analysis of points on two overlapping images is used to generate height data. The principles of photogrammetry are described in detail in Burnside (1985). This approach may be used to provide x, y, z points with a greater horizontal and similar vertical precision to LiDAR (NSL, 2001). However, there are a number of limitations with the photogrammetric approach. Though the points generated may be more precise than those generated with LiDAR, there may not be continuous coverage, as distinct points are not easy to identify in natural or semi-natural habitats. Photogrammetry also requires specialist experience, hardware and software and requires a large time and therefore cost investment to generate accurate DEMs. The financial cost of photogrammetric DEM generation is approximately 2.5 times that of LiDAR (NSL, 2001) and the accuracy and precision may be compromised if inexperienced personnel carry out the analysis.

Airborne radar interferometry is capable of providing high spatial resolution data under a variety of conditions, including during rain and through cloud, with similar vertical resolution to LiDAR (Sties *et al.*, 2000). Though airborne radar data may be acquired with a spatial resolution of approximately 2 m (NERC, 2002), to generate DEMs requires specialist knowledge and software. Airborne radar DEMs are available from commercial sources, but these have a ground spatial resolution of 5 m and a vertical root mean square error (RMSE) of 1 m (Intermap, 2005).

The requirement for specialist knowledge and the cost implications of photogrammetry make it an inappropriate approach of DEM generation for this study. Though airborne radar has similar specifications in terms of spatial resolution it is not as precise as LiDAR. For these reasons LiDAR was the most appropriate for this study as there is no requirement for specialist knowledge, it may be used in featureless regions and data are readily available for coastal regions from the EA. Also CASI and LiDAR data may be acquired simultaneously by the EA, as these instruments are mounted in same aircraft platform (Brown *et al.*, 2003b).

Appendix B Classification

In remote sensing classification is the process by which generally multispectral imagery data are converted to thematic data generally representing land cover or land use classes. There are two main approaches to classification: unsupervised and supervised.

During an unsupervised classification, an algorithm splits feature space into clusters of data (Schowengerdt, 1997). To provide an output map, clusters are allocated membership to a class determined by an operator. Though the unsupervised approach to classification can provide accurate results there are several limitations that make it unsuitable for change detection (Campbell, 2002). The clusters identified may contain large numbers of pixels of more than one of the classes of interest. As the clusters are not trained on predefined classes they may not match the classes of interest on the ground (Schowengerdt, 1997). Clustering from two different times can result in clusters that incorporate different positions in feature space (Schowengerdt, 1997; Campbell, 2002). This could result in changes being detected due to the clustering algorithm, rather than actual change occurring.

Supervised classification can be carried out by an analyst visually interpreting the boundaries of classes or can be achieved using automated computer-based methods. Though the visual interpretation approach is used in operational remote sensing, it is time consuming and requires specialist knowledge of the habitats being classified. Using this approach, it is also not possible to derive per-pixel measures of error. As was discussed in the Section 1.4, the inability to derive per-pixel measures made the visual interpretation method unsuitable for this study.

In computerised supervised classification, there are three main stages for all classifiers:

1. Training
2. Allocation
3. Accuracy assessment

B.1 Training

Training is the process by which the spectral characteristics of each of the classes of interest are determined from selected pixels. How the spectral characteristics are determined is dependent of the classifier used.

B.2 Allocation

These spectral characteristics are used in the allocation stage to determine the class of all pixels within an area of interest in an image. While the accuracy assessment stage does not have to be carried out to produce a map output, it is essential to determine the accuracy of that output.

There are many different approaches to supervised classification. Two commonly used methods are the Maximum Likelihood (ML) classifier (Benediktsson *et al.*, 1990; Schowengerdt, 1997; Campbell, 2002) and neural network classifiers, particularly the Multi Layer Perceptron (MLP) (Atkinson and Tatnall, 1997).

B.4 Accuracy assessment

Accuracy assessment is one of the most important stages in the classification process, as it provides a measure of the usefulness of the final classification in a particular application and may be used to compare the effectiveness of classifiers. Until the early 1980s, the accuracy assessment process was an afterthought in many studies (Congalton, 1991). Most of the techniques used were relatively simple and provided an overall accuracy statistic. In many cases, little effort was expended in acquiring reference data, resulting in too small a sample size for the number of classes generated. Interpretation of aerial photography or other remotely sensed imagery was commonly used to assess the accuracy of classifications (Congalton, 1991). The manual interpretation process was assumed to be error free, but this is highly unlikely, potentially introducing large errors when assessing classifiers.

Since the 1980s a variety of methods have been developed for remote sensing studies and as the importance of the accuracy assessment stage has been realised, these have become much more commonly used.

The aim of the accuracy assessment stage is to estimate thematic errors within the classification. This is achieved by comparing a pixel class as determined by ground sampling with the predicted class from the classification. However, the error value obtained is a function of positional, classification and reference dataset errors. The significance of these errors will be discussed in the Uncertainty section of this chapter.

B.4.1 Sampling design for accuracy assessment

The sampling design is the method by which pixels are selected from the study area for use in the accuracy assessment process. There are a variety of approaches that may be used at this stage, of which the following are most commonly considered in remote sensing studies: simple random, systematic, stratified random and clustered (Lo and Watson, 1998; Stehman, 1999).

B.4.1.1 Simple random sampling

In simple random sampling a predetermined number of units are selected randomly from the population. This approach meets the assumption that every pixel has an equal chance of being selected and is a very simple approach to implement (Lo and Watson, 1998). It has the advantage that the number of samples may be changed before, during or after the initial survey. As pixels have been selected randomly, reducing or increasing the number of pixels changes the sample size, but not the random nature of the sampling.

However there are limitations, as the random sample is less likely than other design approaches to meet the criteria that samples are spatially well distributed (Stehman, 1999).

B.4.1.2 Systematic sampling

Using the systematic approach, pixels are selected using a regular sampling pattern started at a random point. This approach is simple to carry out and results in a good spatial coverage (Stehman, 1992; Stehman, 1999). The approach results in every pixel having an equal probability of being selected (Stehman 1999) though some researchers disagree with this (Congalton, 1988; Lo and Watson, 1998). They claim that because the first point is the only one to be randomly selected, there is not an equal chance of the other pixels being selected. However, prior to the first pixel being randomly chosen, all pixels have an even chance of being selected.

The main disadvantage of the systematic approach is that if there is a strong spatial periodicity in the pattern of ground classes or the pattern of misclassification, it may be strongly biased, particularly if the frequency of sampling is similar to that of the ground data misclassification (Stehman, 1992; Stehman, 2000).

B.4.1.3 Stratified random sampling

In stratified sampling the population is split into strata and each of the strata is sampled equally (Lo and Watson, 1998). There are two main approaches to the stratification of the population in remote sensing. The strata may be based on thematic classes, such as the land cover classes used in a classification, or geographic units, such as a regular grid (Barber, 1988; Lo and Watson, 1998).

The advantage of the thematic approach is that all classes will be represented, as a fixed number of samples may be derived from each. However, the thematic classes have to be specified prior to ground data collection. This could be using the classification that is to be tested or by some other mapping. The requirement for prior mapping is likely to result in delays for ground data collection. This may be a potential problem, especially for areas that are dynamic, as change may occur between remote sensed data collection and ground data collection. Also the strata are likely to be different for different classifications. If a series of classifications are to be tested with large differences from the classification used to define the strata, then the sampling may be poorly distributed among classes that were represented differently in the different classifications (Stehman, 1999).

The use of geographic strata will result in data collection across complete population. It may result in small sample sizes for classes with small areas, but has advantages over the use of thematic strata, in that it does not require prior knowledge of the site and there is no requirement for potentially delaying and biased image interpretation or classification prior to sampling. It also provides spatially distributed data and will reduce the effects of spatial correlation (Lo and Watson, 1998; Stehman, 2000)

B.4.1.4 Cluster sampling

In cluster sampling the population are divided into mutually exclusive, exhaustive units. These may be thematic or geographic units as in stratified sampling. Individual units are selected at random and then these units are either randomly sampled, or a census is taken. This method generally reduces the time required for surveying, as sampling is restricted to a few areas rather than the whole of the study site (Barber, 1988; Stehman, 2001). This approach is generally only accurate if the units selected are representative of the population as a whole (Barber, 1988). If this is not the case the sample will be biased. Classification errors tend to be correlated spatially and so the cluster sampling is likely to result in imprecise sampling and therefore estimation errors (Stehman, 2000; Stehman, 2001).

B.4.2 The confusion matrix

In traditional accuracy assessment, the class allocated to a pixel is considered correct or incorrect. The overall accuracy (P_o) is calculated from the sum of the diagonal values divided by the total number of pixels (N):

$$P_o = \frac{1}{N}\sum_{i=1}^{M} X_{ii} \tag{B.1}$$

where M is the number of classes.

Table B.1 Confusion Matrix for three class classification.

		Reference Data			
		Class 1	Class 2	Class 3	Row Totals ($i+$)
Classified Data	Class 1	X_{11}	X_{12}	X_{13}	S_{1+}
	Class 2	X_{21}	X_{22}	X_{23}	S_{2+}
	Class 3	X_{31}	X_{32}	X_{33}	S_{3+}
	Column Totals ($+i$)	S_{+1}	S_{+2}	S_{+3}	

Error statistics may be generated using a confusion matrix (Table B.1) on a per-class basis to provide estimates of accuracy (Janssen and van der Wel, 1994, Campbell, 2002). The producer's accuracy (Storey and Congalton, 1986) is the proportion of reference pixels that are correctly classified and provides an estimate of the proportion of pixels incorrectly omitted from a class and classified as another class during the classification. For a given class, the producer's accuracy (PA) is the ratio of correctly allocated pixels (the yellow box in Table B.1) to the total number of reference pixels belonging to the class (column total), and in the case of Class 1 (Table B.1) would be:

$$PA = \frac{X_{11}}{S_{+1}} \tag{B.2}$$

The user's accuracy (Storey and Congalton, 1986) is an indication of how many pixels allocated to a particular class by the classification actually belong to that class and provides an estimate of the proportion of pixels from other classes that were incorrectly included or commissioned into a class during the classification. For a given class, the user's accuracy (UA) is the ratio of correctly allocated pixels (grey value) to the total number of pixels allocated to the class (row total) and in the case of Class 2 (Table B.1) the user's accuracy is:

$$UA = \frac{X_{22}}{S_{2+}} \qquad \text{B.3}$$

This approach provides overall and per-class error estimates.

B.4.3 Compensating for chance agreement

The overall accuracy fails to consider the possibility that there is chance agreement between the classified pixels and the classification. There are methods that attempt to account for chance agreement between classified pixels and reference data, including Kappa (Cohen, 1960; Stehman, 1996), modified Kappa (Foody, 1992) and Tau (Ma and Redmond, 1995) coefficients.

Though use of Kappa and other methods is common in remotely sensed studies there is an argument that there is no need to compensate for chance agreement (Foody, 2002; Turk, 2002). Measures of classification accuracy are derived by determining using a sampled set of ground points and determining for all sampled points whether the pixel representing a specific ground point has been allocated the correct class. Within this process there is no requirement to compensate for chance agreement, as a pixel that is correct due to chance is as representative of the final map as pixel that is correct without chance being a factor (Turk, 2002). Whether or not the overall accuracy of a map is due to chance or not is irrelevant, the factor that is important is the accuracy of the map and by removing chance agreement, kappa will underestimate the accuracy of the final map (Turk, 2002). As well as underestimating accuracy Kappa and Tau may incorrectly estimate chance agreement (Foody, 2002) and so in this study overall accuracy was used.

Appendix C Flight logs for airborne data acquisition

Images of all remotely sensed data are in Appendix D.

Table C.1 Coventry geocorrection test data acquisition 25/08/01.

Date	25/08/01	**Bandset**	EA Vegetation 1	**CASI mode**	Spatial
Site	Coventry	**Surveyor**	B Tarrant	**Aperture**	5
Weather comments	High cloud			**Instruments**	CASI

Image no.	Line no.	Start time (UT)	End Time	Heading (deg)
5136	4	1035	1037	317
5137	1	1040	1041	224
5138	5	1043	1044	317
5139	2	1047	1049	224
5140	5	1051	1053	317
5141	3	1055	1058	224
5142	4	1100	1102	317
5143	1	1105	1107	044

Table C.2 Ainsdale Sand Dunes data acquisition 28/08/01.

Date	28/08/01	**Bandset**	EA Vegetation 1	**CASI mode**	Spatial
Site	Ainsdale	**Surveyor**	C O'Dwyer	**Aperture**	5
Weather comments	High cirrus for later lines			**Instruments**	CASI LiDAR

Image no.	Line no.	Start time (UT)	End Time	Heading (deg)
5151	5	1331	1333	030
5153	4	1340	1342	030
5154	1	1344	1346	210
5155	3	1349	1351	030
5156	2	1358	1400	210

Table C.3 Coventry geocorrection test data acquisition 09/09/01.

Date	09/09/01	**Bandset**	EA Vegetation 1	**CASI mode**	Spatial
Site	Coventry	**Surveyor**	B Tarrant	**Aperture**	5
Weather comments	Cloud at 1300 m			**Instruments**	CASI

Image no.	Line no.	Start time (UT)	End Time	Heading (deg)
5162	4	1242	1244	317
5163	2	1248	1249	317
5164	7	1252	1254	225
5165	7	1257	1259	045
5166	8	1305	1307	225

Table C.4 Ainsdale Sand Dunes data acquisition 11/09/02.

Date	11/09/02	**Bandset**	EA Vegetation 1	**CASI mode**	Spatial
Site	Ainsdale	**Surveyors**	C O'Dwyer K Brown	**Aperture**	5
Weather comments	Sky clear over study site		**Instruments**	CASI LiDAR Digital photography	

Image no.	Line no.	Start time (UT)	End Time	Heading (deg)
5360	5	0941	0943	210
5361	2	0945	0948	030
5362	4	0951	0954	210
5363	3	0959	1002	030
5364	1	1005	1008	210

Appendix D Remotely sensed data

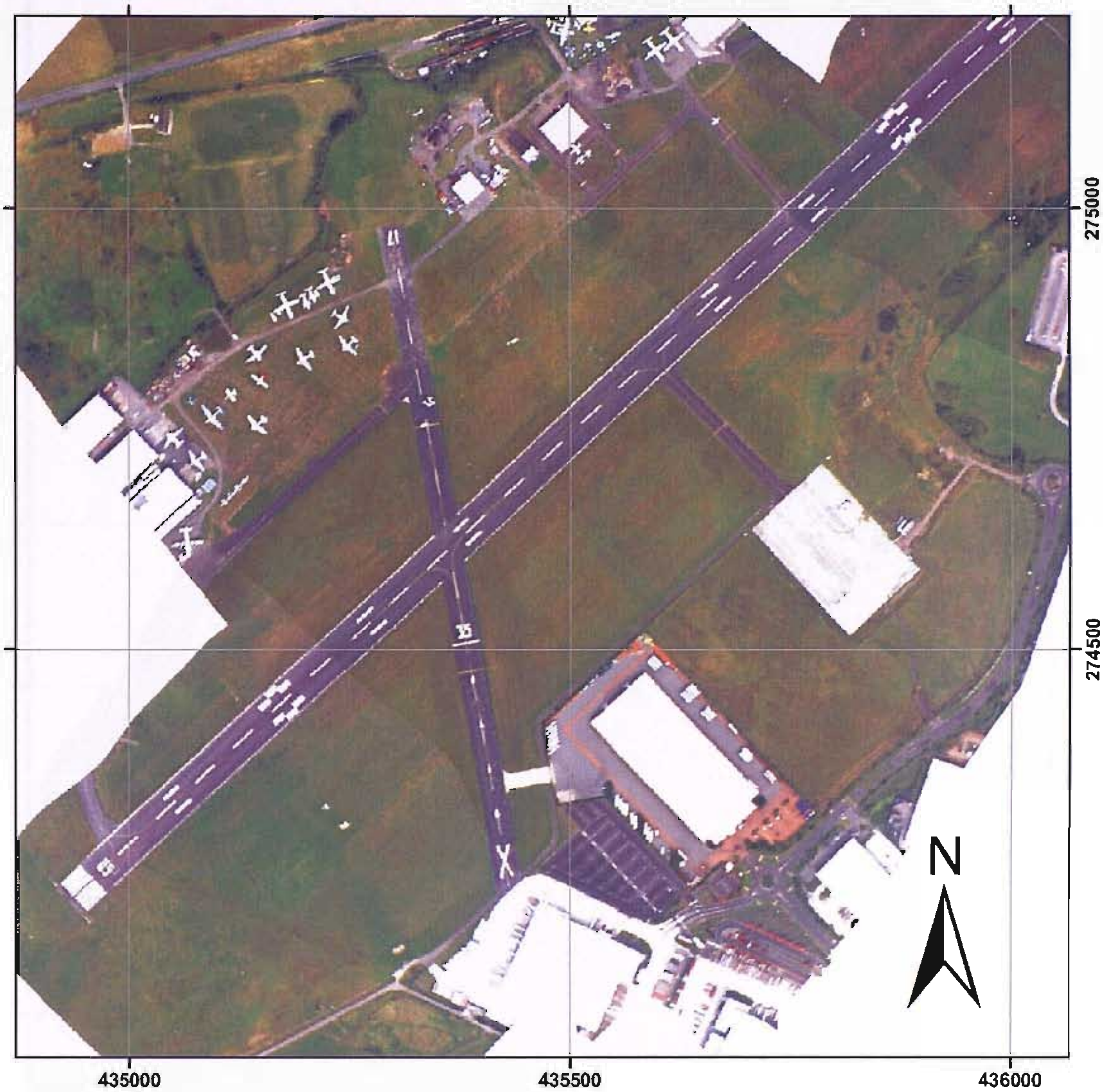

Figure D.1 Truecolour CASI data of Coventry test site acquired 25/08/01.

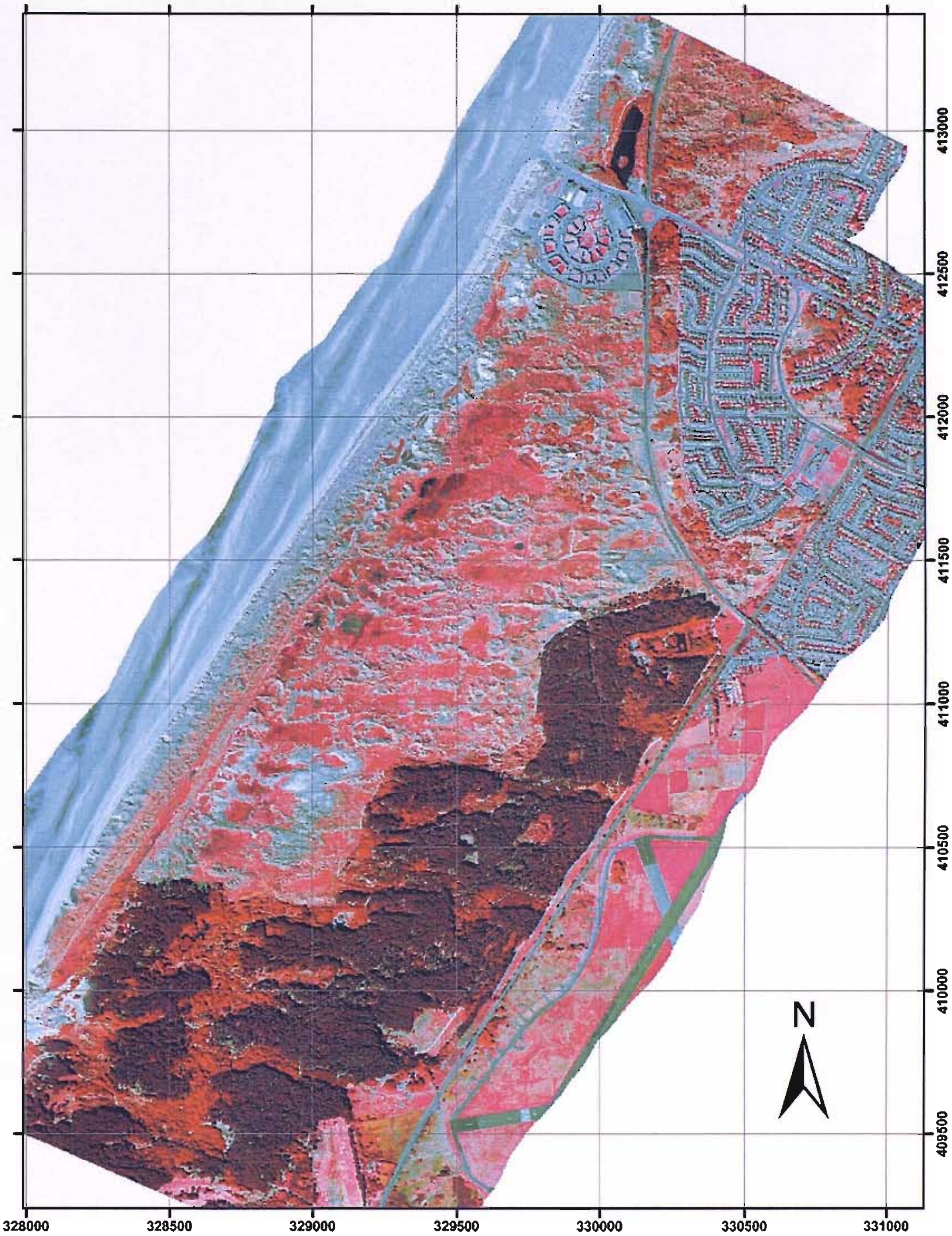

Figure D.2 Falsecolour CASI data of Ainsdale test site acquired 28/08/01.

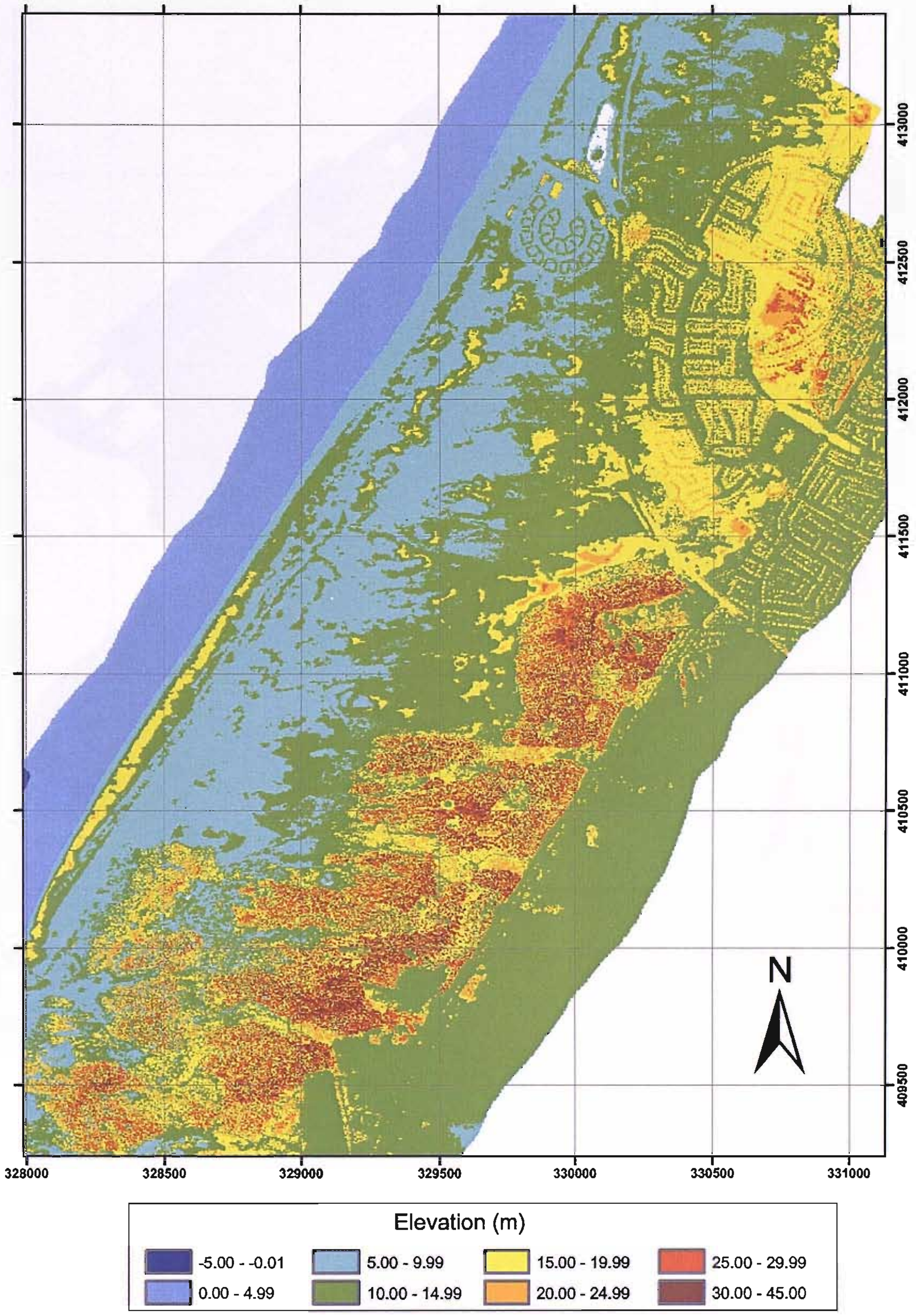

Figure D.3 LiDAR data of Ainsdale test site acquired 28/08/01.

Figure D.4 Truecolour CASI data of Coventry test site acquired 09/09/01.

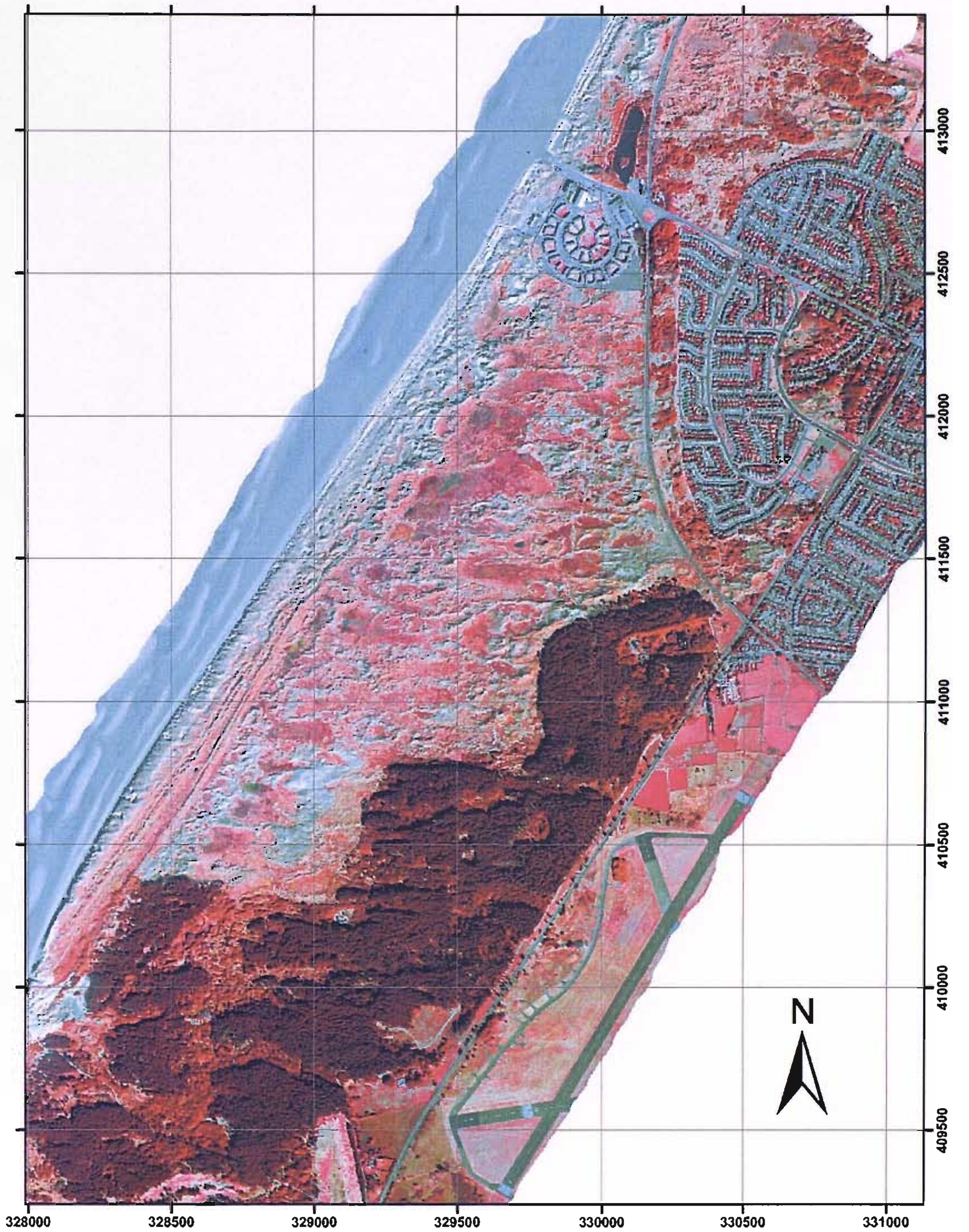

Figure D.5 Falsecolour CASI data of Ainsdale test site acquired 11/09/02.

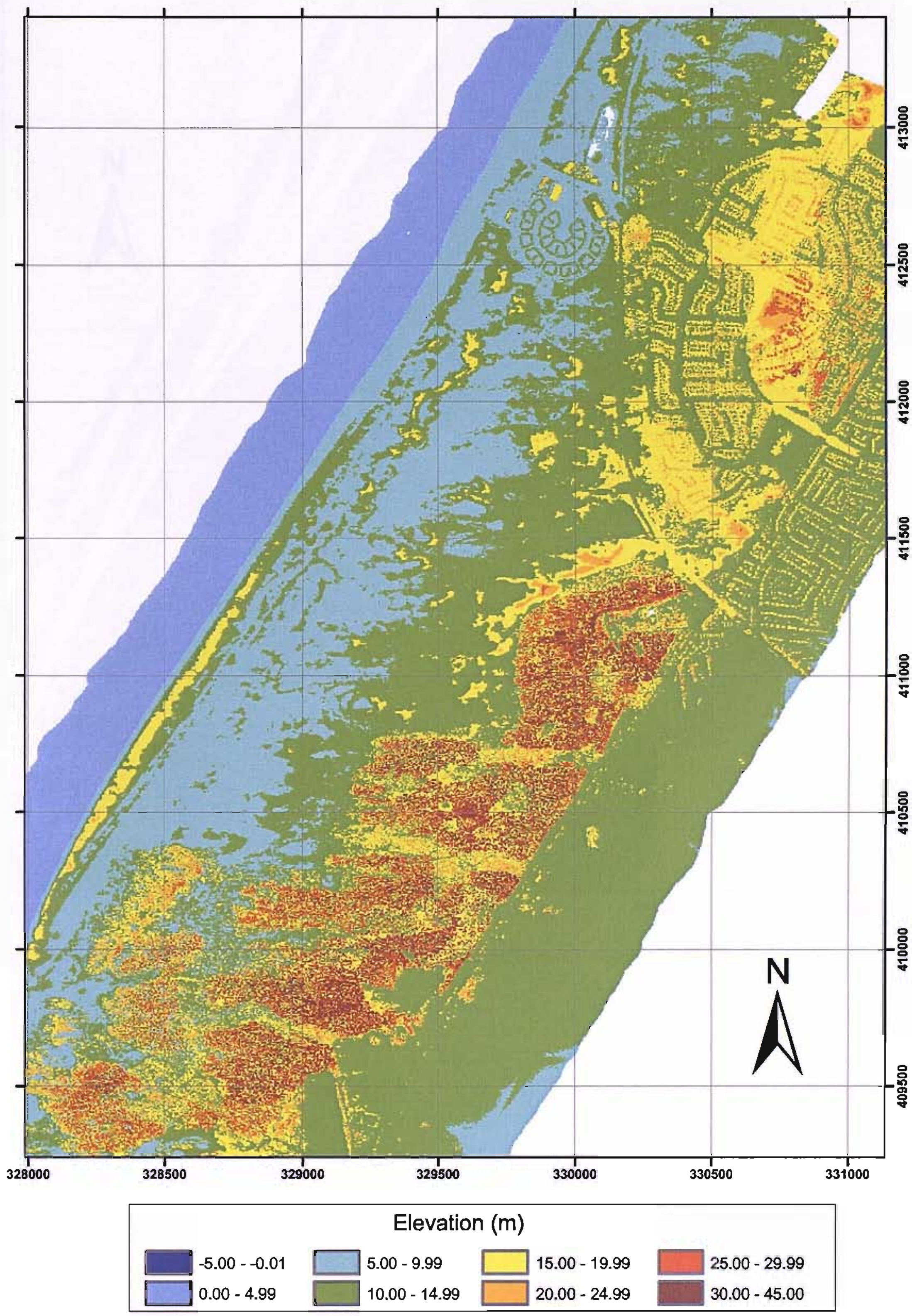

Figure D.6 LiDAR data of Ainsdale test site acquired 11/09/02.

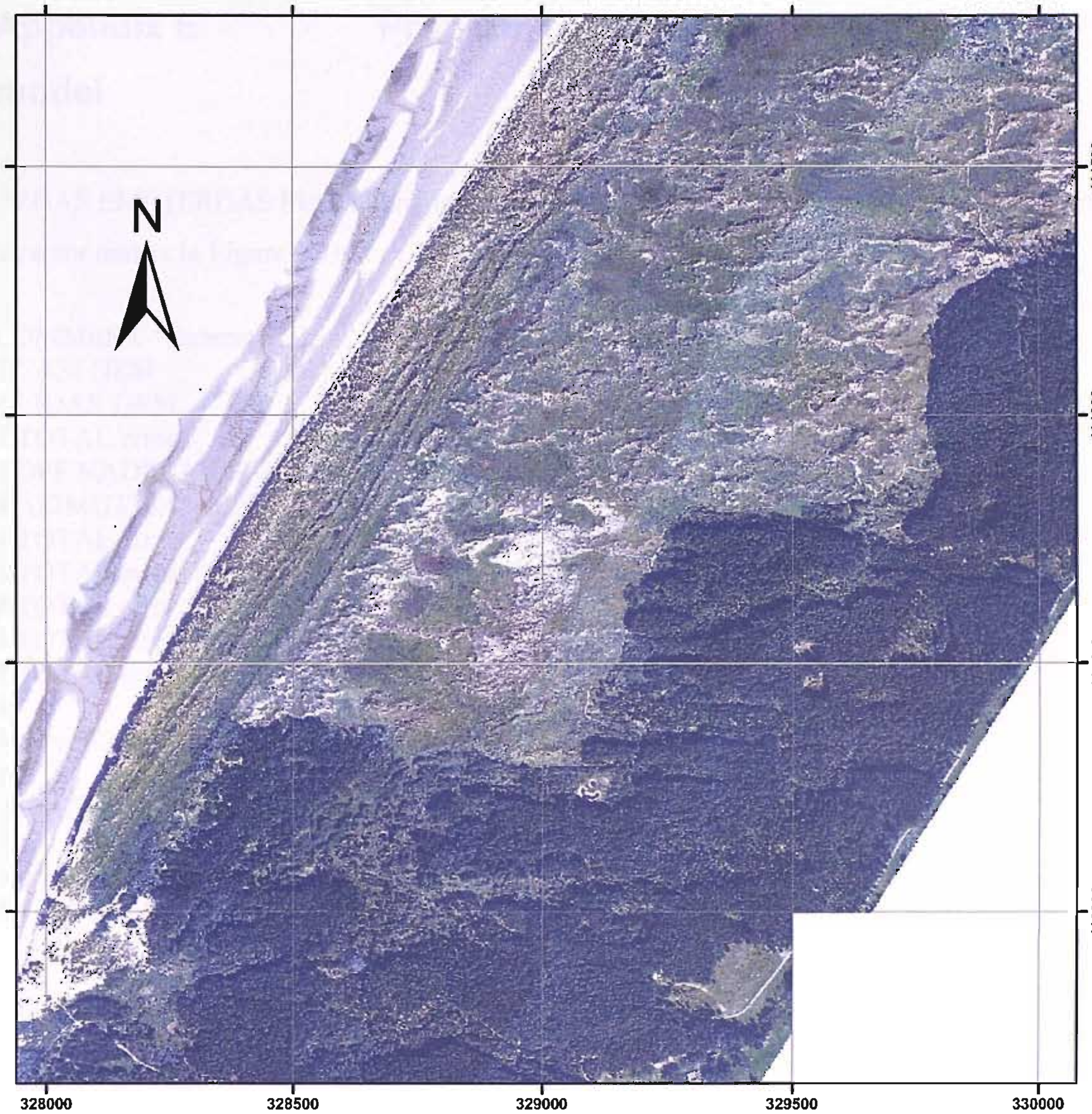

Figure D.7 Digital photography of Ainsdale test site acquired 11/09/02.

Appendix E Program to generate orthometric error model

ERDAS EML (ERDAS Macro Language) program to generate orthometric error vectors based on error matrix in Figure 3.21.

```
COMMENT "Generated from graphical model: c:/ainsdale/test.gmd";
# CASI DEM
# LIDAR DEM
# TOTAL error
# OFF NADIR ANGLE
# AZIMUTH ANGLE
# TOTAL error
# TOTAL error
# TOTAL error
# TOTAL error
# TOTAL error
#
# set cell size for the model
#
SET CELLSIZE MIN;
#
# set window for the model
#
SET WINDOW UNION;
#
# set area of interest for the model
#
SET AOI NONE;
#
# declarations
#
Float RASTER n1_off_nadir FILE OLD NEAREST NEIGHBOR AOI
"c:/ainsdale/demcutout.aoi" "c:/ainsdale/2001_off_nadir.img";

Float RASTER n5_lidar FILE OLD NEAREST NEIGHBOR AOI "c:/ainsdale/demcutout.aoi"
"c:/ainsdale/urban2001_lidar.img";

Float RASTER n12_azimuth FILE OLD NEAREST NEIGHBOR AOI
"c:/ainsdale/demcutout.aoi" "c:/ainsdale/2001_azimuth.img";

Integer RASTER n67_casi_dem FILE OLD NEAREST NEIGHBOR AOI
"c:/ainsdale/demcutout.aoi" "c:/ainsdale/urban2001_casidem_xyz.img";

Float RASTER n70_horizontal_errors FILE DELETE_IF_EXISTING USEALL ATHEMATIC
FLOAT SINGLE "c:/ainsdale//horizontal_errors2001_77.img";

FLOAT MATRIX n7_Custom_Float;
```

```
{
#####The following section was repeated 77 times for all combinations of position within the
matrix
##### to determine the potential orthometric error for each pixel in the matrix

#define n2_memory Float($n67_casi_dem(5))
############################################ Start 1
#
# load matrix n7_Custom_Float
#
n7_Custom_Float = MATRIX(9, 9:
        0, 1, 0, 0, 0, 0, 0, 0, 0,
        0, 0, 0, 0, 0, 0, 0, 0, 0,
        0, 0, 0, 0, 0, 0, 0, 0, 0,
        0, 0, 0, 0, 0, 0, 0, 0, 0,
        0, 0, 0, 0, 0, 0, 0, 0, 0,
        0, 0, 0, 0, 0, 0, 0, 0, 0,
        0, 0, 0, 0, 0, 0, 0, 0, 0,
        0, 0, 0, 0, 0, 0, 0, 0, 0,
        0, 0, 0, 0, 0, 0, 0, 0, 0);
#
# normalize matrix n7_Custom_Float
#
if (global sum ($n7_Custom_Float) NE 0)
        {n7_Custom_Float = $n7_Custom_Float / global sum ($n7_Custom_Float);}
#
# function definitions
# orthometric error is defined as positive towards the sensor

#define n201_memory Float((TAN($n1_off_nadir))*(\
 ( $n2_memory  )\
 -\
(FOCAL MAX ( $n5_lidar, $n7_Custom_Float ))\
))
#define n101_memory Float(STACKLAYERS(\
(-SIN($n12_azimuth)*$n201_memory),\
(-COS($n12_azimuth)*$n201_memory)\
)\
)

##########################################
## Merge data to provide an output layer that corresponds to
## x, y orthometric error for each pixel in 77 pixel matrix
##########################################
n70_horizontal_errors = STACKLAYERS(
$n101_memory(1), $n101_memory(2)
######Repeat for all 77 positions within the matrix###########
);
}
QUIT;
```

Appendix F Digital photography geometric accuracy assessment

Table F.1 Digital photography independent ground points error. Total RMSE 1.80 m

GCP	Error (m)			GCP	Error (m)		
no.	*x*	*y*	total	no.	*x*	*y*	total
1	-0.20	0.58	0.61	23	-0.82	1.58	1.78
2	-1.12	-0.92	1.45	24	-0.91	-2.20	2.38
3	0.33	1.55	1.58	25	-0.18	0.10	0.20
4	-0.01	-2.21	2.21	26	0.38	-0.39	0.55
5	-3.72	0.84	3.81	27	-3.20	-1.69	3.62
6	0.09	0.81	0.81	28	1.22	-0.59	1.35
7	1.20	-2.44	2.72	29	-1.00	0.57	1.15
8	-0.61	1.20	1.35	30	-0.21	-0.22	0.30
9	0.71	0.07	0.71	31	-2.39	-0.76	2.50
10	-0.46	-1.19	1.27	32	1.09	0.53	1.22
11	0.45	-0.24	0.51	33	-1.50	0.08	1.50
12	-0.94	-0.36	1.01	34	-0.09	-0.35	0.36
13	-0.48	0.44	0.65	35	-1.46	-0.26	1.48
14	1.21	0.02	1.21	36	0.72	-0.83	1.09
15	1.68	0.01	1.68	37	-2.35	0.00	2.35
16	0.96	0.80	1.25	38	0.64	1.11	1.28
17	0.35	-0.69	0.77	39	-0.48	2.01	2.07
18	0.94	-1.99	2.20	40	-0.51	0.94	1.07
19	0.42	-0.45	0.61	41	0.43	-0.92	1.02
20	2.32	0.43	2.36	42	2.35	0.13	2.36
21	1.13	2.16	2.44	43	-1.49	-3.05	3.40
22	-1.55	-2.94	3.33	44	0.36	-0.03	0.36

Appendix G MLP thematic uncertainty results

Table G.1 MLP P_o.

		Nodes							
		5	10	15	20	25	30	35	40
Iterations	250	0.726	0.766	0.770	0.804	0.798	0.796	0.779	0.776
	500	0.746	0.768	0.776	0.802	0.809	0.799	0.804	0.774
	750	0.747	0.781	0.779	0.805	0.807	0.808	0.800	0.777
	1000	0.747	0.791	0.775	0.809	0.810	0.813	0.805	0.776
	1250	0.746	0.785	0.777	0.808	0.818	0.817	0.816	0.781
	1500	0.742	0.793	0.776	0.816	0.817	0.814	0.819	0.793
	1750	0.746	0.798	0.781	0.816	0.824	0.813	0.817	0.795
	2000	0.746	0.793	0.781	0.816	0.827	0.814	0.817	0.785
	2250	0.744	0.791	0.781	0.814	0.827	0.814	0.818	0.793
	2500	0.744	0.799	0.788	0.808	0.821	0.816	0.813	0.798
	2750	0.746	0.798	0.795	0.804	0.818	0.813	0.812	0.799
	3000	0.744	0.802	0.800	0.804	0.819	0.814	0.809	0.800
	3500	0.754	0.794	0.798	0.802	0.804	0.813	0.817	0.817
	4000	0.747	0.798	0.805	0.805	0.807	0.816	0.817	0.809

Table G.2 MLP class independent thematic uncertainty RMSE.

		Nodes							
		5	10	15	20	25	30	35	40
Iterations	250	0.098	0.102	0.096	0.077	0.103	0.145	0.104	0.174
	500	0.108	0.107	0.102	0.093	0.115	0.136	0.144	0.168
	750	0.115	0.074	0.118	0.101	0.112	0.111	0.117	0.142
	1000	0.115	0.059	0.107	0.104	0.105	0.120	0.114	0.131
	1250	0.118	0.061	0.109	0.107	0.098	0.135	0.124	0.156
	1500	0.120	0.062	0.125	0.108	0.112	0.121	0.117	0.138
	1750	0.121	0.071	0.103	0.096	0.103	0.124	0.107	0.152
	2000	0.131	0.070	0.107	0.094	0.092	0.124	0.100	0.166
	2250	0.130	0.071	0.116	0.103	0.095	0.130	0.114	0.172
	2500	0.132	0.059	0.096	0.108	0.089	0.160	0.099	0.141
	2750	0.130	0.070	0.114	0.126	0.084	0.151	0.106	0.137
	3000	0.136	0.081	0.088	0.121	0.097	0.148	0.116	0.143
	3500	0.139	0.120	0.125	0.088	0.118	0.109	0.108	0.115
	4000	0.137	0.084	0.137	0.099	0.125	0.115	0.125	0.158

Table G.3 MLP class specific thematic uncertainty RMSE.

		Nodes							
		5	**10**	**15**	**20**	**25**	**30**	**35**	**40**
Iterations	**250**	0.053	0.036	0.072	0.075	0.084	0.070	0.101	0.069
	500	0.051	0.045	0.056	0.064	0.064	0.047	0.101	0.086
	750	0.047	0.054	0.055	0.052	0.056	0.048	0.079	0.077
	1000	0.044	0.054	0.050	0.047	0.056	0.046	0.066	0.079
	1250	0.044	0.056	0.050	0.047	0.052	0.040	0.066	0.064
	1500	0.048	0.054	0.049	0.059	0.046	0.036	0.071	0.070
	1750	0.044	0.062	0.050	0.061	0.053	0.040	0.070	0.054
	2000	0.044	0.047	0.052	0.063	0.055	0.037	0.054	0.064
	2250	0.042	0.041	0.049	0.054	0.064	0.039	0.054	0.048
	2500	0.042	0.045	0.048	0.051	0.067	0.042	0.050	0.048
	2750	0.043	0.046	0.058	0.057	0.067	0.041	0.037	0.035
	3000	0.045	0.048	0.059	0.068	0.064	0.044	0.036	0.039
	3500	0.055	0.031	0.050	0.062	0.068	0.025	0.027	0.040
	4000	0.069	0.032	0.051	0.061	0.067	0.033	0.029	0.048

Table G.4 MLP F-test results *F*-value for relationship between activation and proportion of correct pixels for class independent thematic uncertainty (degrees of freedom = 8).

		Nodes							
		5	**10**	**15**	**20**	**25**	**30**	**35**	**40**
Iterations	**250**	55.0	49.2	49.9	88.170	50.4	20.4	41.0	13.0
	500	38.9	42.7	42.4	54.192	37.4	23.0	24.6	12.4
	750	36.8	95.2	32.9	49.998	36.9	37.6	36.7	19.9
	1000	36.2	162.7	38.7	45.984	45.1	33.3	38.8	23.9
	1250	33.6	147.1	37.7	42.933	52.4	27.3	33.0	15.4
	1500	32.4	143.2	29.4	41.913	40.6	32.7	36.2	22.0
	1750	31.5	108.6	44.4	53.684	48.9	29.6	43.7	17.0
	2000	27.4	113.8	41.1	54.745	65.6	27.9	48.2	13.0
	2250	26.6	106.7	34.7	45.054	63.0	27.8	37.8	11.5
	2500	25.3	163.0	53.1	42.193	65.8	17.3	51.4	19.0
	2750	26.4	124.9	36.9	26.725	74.6	18.4	44.1	20.6
	3000	24.6	93.6	72.1	30.413	55.2	18.7	33.3	20.1
	3500	25.4	39.2	30.3	69.197	34.8	37.8	42.8	31.2
	4000	24.8	76.2	28.8	52.306	36.1	34.7	29.7	15.4

Table G.5 MLP F-test results p for relationship between activation and proportion of correct pixels (degrees of freedom = 8).

		Nodes							
		5	10	15	20	25	30	35	40
Iterations	250	<0.001	<0.001	<0.001	<0.001	<0.001	0.002	<0.001	0.007
	500	<0.001	<0.001	<0.001	<0.001	<0.001	0.001	0.001	0.008
	750	<0.001	<0.001	<0.001	<0.001	<0.001	<0.001	<0.001	0.002
	1000	<0.001	<0.001	<0.001	<0.001	<0.001	<0.001	<0.001	0.001
	1250	<0.001	<0.001	<0.001	<0.001	<0.001	<0.001	<0.001	0.004
	1500	<0.001	<0.001	<0.001	<0.001	<0.001	<0.001	<0.001	0.002
	1750	<0.001	<0.001	<0.001	<0.001	<0.001	<0.001	<0.001	0.003
	2000	<0.001	<0.001	<0.001	<0.001	<0.001	<0.001	<0.001	0.007
	2250	<0.001	<0.001	<0.001	<0.001	<0.001	<0.001	<0.001	0.009
	2500	0.001	<0.001	<0.001	<0.001	<0.001	0.003	<0.001	0.002
	2750	<0.001	<0.001	<0.001	<0.001	<0.001	0.003	<0.001	0.002
	3000	0.001	<0.001	<0.001	<0.001	<0.001	0.003	<0.001	0.002
	3500	0.001	<0.001	<0.001	<0.001	<0.001	<0.001	<0.001	<0.001
	4000	0.001	<0.001	<0.001	<0.001	<0.001	<0.001	<0.001	0.004

Table G.6 MLP F-test results *F*-value for relationship between average activation and proportion of correct pixels for class specific thematic uncertainty (degrees of freedom = 6).

		Nodes							
		5	10	15	20	25	30	35	40
Iterations	250	143.4	249.5	74.3	68.8	53.0	70.7	37.2	82.6
	500	160.0	168.3	114.1	83.8	90.5	145.4	35.1	59.3
	750	170.2	115.4	113.0	140.5	107.1	146.9	54.8	73.2
	1000	190.5	109.8	145.8	148.2	105.1	153.3	77.6	66.2
	1250	188.1	96.1	140.5	148.2	118.7	199.6	73.6	94.4
	1500	161.2	109.9	154.7	93.3	148.4	230.3	62.2	77.5
	1750	192.8	79.7	141.5	83.8	109.1	181.4	61.7	127.0
	2000	187.1	136.7	131.7	81.0	98.6	202.3	105.6	93.3
	2250	215.5	190.3	143.7	108.5	76.4	176.5	102.9	155.9
	2500	217.2	155.3	144.7	123.0	70.4	140.1	124.0	149.5
	2750	200.7	152.6	102.0	102.8	71.3	145.9	217.4	275.0
	3000	186.7	147.2	87.1	72.7	76.8	128.0	249.4	222.8
	3500	130.3	367.8	121.6	98.6	65.6	378.1	409.9	183.0
	4000	85.6	324.9	112.0	92.0	64.2	207.8	360.0	109.2

Table G.7 MLP F-test results *p* for relationship between activation and proportion of correct pixels for class specific thematic uncertainty (degrees of freedom = 6).

		Nodes							
		5	**10**	**15**	**20**	**25**	**30**	**35**	**40**
Iterations	**250**	<0.001	<0.001	<0.001	<0.001	<0.001	<0.001	<0.001	<0.001
	500	<0.001	<0.001	<0.001	<0.001	<0.001	<0.001	0.001	<0.001
	750	<0.001	<0.001	<0.001	<0.001	<0.001	<0.001	<0.001	<0.001
	1000	<0.001	<0.001	<0.001	<0.001	<0.001	<0.001	<0.001	<0.001
	1250	<0.001	<0.001	<0.001	<0.001	<0.001	<0.001	<0.001	<0.001
	1500	<0.001	<0.001	<0.001	<0.001	<0.001	<0.001	<0.001	<0.001
	1750	<0.001	<0.001	<0.001	<0.001	<0.001	<0.001	<0.001	<0.001
	2000	<0.001	<0.001	<0.001	<0.001	<0.001	<0.001	<0.001	<0.001
	2250	<0.001	<0.001	<0.001	<0.001	<0.001	<0.001	<0.001	<0.001
	2500	<0.001	<0.001	<0.001	<0.001	<0.001	<0.001	<0.001	<0.001
	2750	<0.001	<0.001	<0.001	<0.001	<0.001	<0.001	<0.001	<0.001
	3000	<0.001	<0.001	<0.001	<0.001	<0.001	<0.001	<0.001	<0.001
	3500	<0.001	<0.001	<0.001	<0.001	<0.001	<0.001	<0.001	<0.001
	4000	<0.001	<0.001	<0.001	<0.001	<0.001	<0.001	<0.001	<0.001

Table G.8 MLP Normalised entropy.

		Nodes							
		5	**10**	**15**	**20**	**25**	**30**	**35**	**40**
Iterations	**250**	0.239	0.204	0.158	0.126	0.139	0.121	0.123	0.111
	500	0.200	0.188	0.145	0.117	0.120	0.111	0.096	0.101
	750	0.200	0.196	0.141	0.112	0.112	0.112	0.096	0.089
	1000	0.196	0.196	0.140	0.109	0.111	0.107	0.091	0.084
	1250	0.196	0.190	0.140	0.107	0.110	0.105	0.090	0.083
	1500	0.197	0.184	0.142	0.109	0.109	0.104	0.087	0.082
	1750	0.192	0.182	0.143	0.110	0.104	0.100	0.090	0.079
	2000	0.190	0.183	0.142	0.111	0.103	0.096	0.090	0.081
	2250	0.190	0.173	0.142	0.112	0.101	0.094	0.089	0.078
	2500	0.189	0.164	0.147	0.113	0.101	0.095	0.088	0.077
	2750	0.188	0.166	0.143	0.113	0.101	0.093	0.092	0.076
	3000	0.185	0.161	0.147	0.114	0.099	0.093	0.091	0.077
	3500	0.188	0.144	0.132	0.109	0.104	0.100	0.103	0.075
	4000	0.190	0.149	0.128	0.111	0.106	0.098	0.100	0.075

Table G.9 Statistics of regressions of averaged thematic accuracy and thematic uncertainty variables as a function of MLP network variables.

Regression	Independent variable	Dependent variable	DF	R^2	F	p
Linear	P_o	No. nodes	6	0.323	4.3	0.082
Polynomial	P_o	No. nodes	5	0.866	23.7	0.003
Log-linear	P_o	No. nodes	6	0.609	11.9	0.014
Linear	Class independent RMSE	No. nodes	6	0.224	3.0	0.133
Polynomial	Class independent RMSE	No. nodes	5	0.397	3.3	0.122
Log-linear	Class independent RMSE	No. nodes	6	0.016	1.1	0.332
Linear	Class specific RMSE	No. nodes	6	0.064	1.5	0.269
Polynomial	Class specific RMSE	No. nodes	5	0.000	0.7	0.541
Log-linear	Class specific RMSE	No. nodes	6	0.095	1.7	0.236
Linear	Entropy	No. nodes	6	0.882	53.1	<0.001
Polynomial	Entropy	No. nodes	5	0.966	100.0	<0.001
Log-linear	Entropy	No. nodes	6	0.960	168.3	<0.001
Linear	P_o	Iterations	12	0.691	30.1	<0.001
Polynomial	P_o	Iterations	11	0.919	74.9	<0.001
Log-linear	P_o	Iterations	12	0.949	243.8	<0.001
Linear	Class independent RMSE	Iterations	12	0.077	2.1	0.175
Polynomial	Class independent RMSE	Iterations	11	0.324	4.1	0.046
Log-linear	Class independent RMSE	Iterations	12	0.000	0.5	0.503
Linear	Class specific RMSE	Iterations	12	0.703	31.8	<0.001
Polynomial	Class specific RMSE	Iterations	11	0.878	47.9	<0.001
Log-linear	Class specific RMSE	Iterations	12	0.922	155.5	<0.001
Linear	Entropy	Iterations	12	0.637	23.8	<0.001
Polynomial	Entropy	Iterations	11	0.826	31.9	<0.001
Log-linear	Entropy	Iterations	12	0.910	131.9	<0.001

Table G.10 Statistics of regressions between MLP thematic accuracy and thematic uncertainty variables.

Regression	Independent variable	Dependent variable	DF	R^2	F	p
Linear	Class independent RMSE	P_o	110	0.012	2.4	0.126
Linear	P_o	Class specific RMSE	110	0.000	0.0	0.949
Linear	Entropy	P_o	110	0.579	153.9	<0.001
Linear	Entropy	Class independent RMSE	110	0.145	19.8	<0.001
Linear	Entropy	Class specific RMSE	110	0.015	2.7	0.103
Linear	Class independent RMSE	Class specific RMSE	110	0.000	0.1	0.743

Appendix H PNN thematic uncertainty results

Table H.1 PNN thematic accuracy and uncertainty measures as a function of *h*.

h	P_o	Entropy	Class independent thematic uncertainty RMSE	Class specific thematic uncertainty RMSE
0.005	0.758	0.021	0.215	0.366
0.01	0.796	0.069	0.131	0.268
0.02	0.827	0.134	0.077	0.063
0.03	0.821	0.171	0.049	0.121
0.04	0.804	0.198	0.043	0.178
0.05	0.800	0.223	0.057	0.378
0.06	0.786	0.246	0.039	0.399
0.07	0.766	0.269	0.034	0.397
0.08	0.762	0.290	0.034	0.420
0.09	0.756	0.310	0.031	0.529
0.1	0.751	0.329	0.026	0.541
0.11	0.749	0.347	0.019	0.560
0.12	0.743	0.364	0.020	0.708
0.13	0.738	0.381	0.026	0.708
0.14	0.737	0.397	0.035	0.708
0.15	0.737	0.413	0.036	0.708
0.16	0.734	0.429	0.047	0.709
0.17	0.735	0.443	0.059	0.710
0.18	0.732	0.458	0.074	0.711
0.19	0.728	0.472	0.076	0.711
0.2	0.721	0.485	0.081	0.712

Table H.2 PNN *F*-test results for relationship between activation and proportion of correct pixels (degrees of freedom = 8).

h	F-value	p
0.005	9.71	0.014
0.01	28.37	<0.001
0.02	98.60	<0.001
0.03	250.39	<0.001
0.04	343.25	<0.001
0.05	200.10	<0.001
0.06	446.07	<0.001
0.07	568.85	<0.001
0.08	587.81	<0.001
0.09	679.04	<0.001
0.1	999.38	<0.001
0.11	1960.52	<0.001
0.12	1757.39	<0.001
0.13	1057.73	<0.001
0.14	623.50	<0.001
0.15	571.10	<0.001
0.16	356.24	<0.001
0.17	226.59	<0.001
0.18	145.68	<0.001
0.19	141.30	<0.001
0.2	125.13	<0.001

Appendix I Program to combine misregistration and thematic uncertainty datasets

IDL (Interactive Data Language) program to combine misregistration and thematic uncertainty datasets.

```
Pro combine_uncertainty
;*********************************
;**** IDL program file to merge geometric and thematic uncertainty layers
;*********************************


;*********************************
;** Defining acceleration values for each of the
;** error points derived from the Coventry data
;*********************************
dist_err_orig = $
[0.770,0.893,2.219,1.381,1.798,0.567,2.656,0.649,0.466,0.519,0.594,0.440,1.557, $
1.854,0.954,1.648,0.860,1.301,1.712,1.848,0.511,1.555,0.390,1.414,1.346,2.046 $
1.074,1.201,1.605,0.719,1.694,0.889,1.408,2.148,0.611,1.815,1.397,1.139,1.692, $
1.102,2.338,1.098,1.766,0.446,0.923,1.558,1.054,2.138,1.398,0.884,1.643,0.861, $
0.845,1.458,0.847,2.178]

;*********************************
;** The following define the proportion of each pixel that falls
;** within a specified distance
;** For example matrix 'proportion_per_pix1_0' defines proportion
;** of pixel within 0.5 and 1 pixels of the centre of the central pixel
;*********************************
proportion_per_pix0_5 = $
[0,0,0,0,0,0,0,0,0,0,0,0,0,0,0,0,0,0,0,0,0,0,0,0,0,0,0,0,0,0,0,0,0,0,0,0,0,0,0,0,1, $
0,0,0,0,0,0,0,0,0,0,0,0,0,0,0,0,0,0,0,0,0,0,0,0,0,0,0,0,0,0,0,0,0,0,0,0,0,0,0,0]

proportion_per_pix1_0  = $
[0,0,0,0,0,0,0,0,0,0,0,0,0,0,0,0,0,0,0,0,0,0,0,0,0,0,0,0,0,0,0.035884243,0.208003265, $
0.035884243,0,0,0,0,0,0,0.208003265,0.024449967,0.208003265,0,0,0,0,0,0, $
0.035884243,0.208003265,0.035884243,0,0,0,0,0,0,0,0,0,0,0,0,0,0,0,0,0,0,0,0,0,0,0,0, $
0,0,0,0,0,0]

proportion_per_pix1_5  = $
[0,0,0,0,0,0,0,0,0,0,0,0,0,0,0,0,0,0,0,0,0,0,0,0,0,0,0,0,0,0,0.118822935,0.131177065, $
0.118822935,0,0,0,0,0,0,0.131177065,0,0.131177065,0,0,0,0,0,0,0.118822935, $
0.131177065, 0.118822935,0,0,0,0,0,0,0,0,0,0,0,0,0,0,0,0,0,0,0,0,0,0,0,0,0,0,0,0,0,0]
```

```
proportion_per_pix2_0 = $
[0,0,0,0,0,0,0,0,0,0,0,0,0,0,0,0,0,0,0.059332641,0.066442971,0.059332641,0,0,0, $
0,0,0.059332641,0.060977071,0.003914676,0.060977071,0.059332641,0,0,0,0, $
0.066442971,0.003914676,0,0.003914676,0.066442971,0,0,0,0,0.059332641, $
0.060977071,0.003914676,0.060977071,0.059332641,0,0,0,0,0,0.059332641, $
0.066442971,0.059332641,0,0,0,0,0,0,0,0,0,0,0,0,0,0,0,0,0]

proportion_per_pix2_5 = $
[0,0,0,0,0,0,0,0,0,0,0,0,0,0,0,0,0.011882853,0.096502836,0.043809074, $
0.096502836,0.011882853,0,0,0,0,0.096502836,0.001302402,0,0.001302402, $
0.096502836,0,0,0,0,0.043809074,0,0,0,0.043809074,0,0,0,0,0.096502836, $
0.001302402,0,0.001302402,0.096502836,0,0,0,0,0.011882853,0.096502836, $
0.043809074,0.096502836,0.011882853,0,0,0,0,0,0,0,0,0,0,0,0,0,0,0,0]

proportion_per_pix3_0 = $
[0,0,0,0,0,0,0,0,0.001216927,0.047801189,0.037273298,0.047801189,0.001216927, $
0,0,0,0.001216927,0.042663598,0.035374303,0.001278264,0.035374303, $
0.042663598,0.001216927,0,0,0.047801189,0.035374303,0,0,0,0.035374303, $
0.047801189,0,0,0.037273298,0.001278264,0,0,0,0.001278264,0.037273298,0, $
0,0.047801189,0.035374303,0,0,0,0.035374303,0.047801189,0,0,0.001216927, $
0.042663598,0.035374303,0.001278264,0.035374303,0.042663598,0.001216927, $
0,0,0,0.001216927,0.047801189,0.037273298,0.047801189,0.001216927,0,0,0,0, $
0,0,0,0,0]

proportion_per_pix3_5 = $
[0,0,0,0,0,0,0,0,0.039995532,0.061517842,0.029200871,0.061517842,0.039995532, $
0,0,0,0.039995532,0.01777238,0,0,0,0.01777238,0.039995532,0,0,0.061517842,0,0, $
0,0,0,0.061517842,0,0,0.029200871,0,0,0,0,0,0.029200871,0,0,0.061517842,0,0,0,0, $
0,0.061517842,0,0,0.039995532,0.01777238,0,0,0,0.01777238,0.039995532,0,0,0, $
0.039995532,0.061517842,0.029200871,0.061517842,0.039995532,0,0,0,0,0,0,0,0,0]

proportion_per_pix4_0 = $
[0,0.004613213,0.0348964,0.023634415,0.0348964,0.004613213,0,0,0.010043429, $
0.052938433,0.015396424,0.000572984,0.015396424,0.052938433,0.010043429, $
0,0.004613213,0.052938433,6.02E-05,0,0,0,6.02E-05,0.052938433,0.004613213, $
0.0348964,0.015396424,0,0,0,0,0,0.015396424,0.0348964,0.023634415, $
0.000572984,0,0,0,0,0,0.000572984,0.023634415,0.0348964,0.015396424,0, $
0,0,0,0,0.015396424,0.0348964,0.004613213,0.052938433,6.02E-05,0,0,0, $
6.02E-05,0.052938433,0.004613213,0,0.010043429,0.052938433,0.015396424, $
0.000572984,0.015396424,0.052938433,0.010043429,0,0,0.004613213,0.0348964, $
0.023634415,0.0348964,0.004613213,0]

proportion_per_pix4_5 = $
[0.003659723,0.042061062,0.046134257,0.022406146,0.046134257,0.042061062, $
0.003659723,0.003659723,0.02602581,0.00892898,0,0,0,0.00892898,0.02602581, $
0.003659723,0.042061062,0.00892898,0,0,0,0,0,0.00892898,0.042061062, $
0.046134257,0,0,0,0,0,0,0,0.046134257,0.022406146,0,0,0,0,0,0,0,0.022406146, $
0.046134257,0,0,0,0,0,0,0,0.046134257,0.042061062,0.00892898,0,0,0,0,0, $
0.00892898,0.042061062,0.003659723,0.02602581,0.00892898,0,0,0,0.00892898, $
0.02602581,0.003659723,0.003659723,0.042061062,0.046134257,0.022406146, $
0.046134257,0.042061062,0.003659723]
```

```
;**********************************
;** Defining no. variables within different data sets
;**********************************
points_dist_error = size(dist_err_orig)
cols = long(1521)
rows = long(1521)

no_points = long(cols*rows)

standard_multiplier = DOUBLE(1)


;**********************************
;** The following section gets file names for input data
;**********************************

;**********************************
;** Obtaining file names of files containing angular acceleration data
;** modified by equation linking with geometric error and multiplied for
;** height AGL to normalise to 900 m
;**********************************
file = DIALOG_PICKFILE(/read, GET_PATH = path1, $
path = 'C:\ainsdale\processing\', $
Title = 'Select ASCII acceleration file ', $
FILTER = ["*.asc"], /MUST_EXIST)

;**********************************
;** Obtaining file names of files containing thematic uncertainty data
;**********************************
file_them = DIALOG_PICKFILE(/read, path = path1, $
Title = 'Select ASCII classification file', $
FILTER = ["*.asc"], /MUST_EXIST)

;**********************************
;** Obtaining file names of files containing geometric error data
;**********************************
file_geo          = DIALOG_PICKFILE(/read, path = path1, $
Title = 'Select ASCII geometric error file ', $
FILTER = ["*.asc"], /MUST_EXIST)

accel_array = DBLARR(cols, rows)
multiplied_array = DBLARR(cols, rows,77)
err_freq = DBLARR(cols, rows,9)

line1 = ''
line2 = ''
line3 = ''
line4 = ''
```

```
;*********************************
;**** Import acceleration  data
;*********************************
test = STRARR(no_points)
GET_LUN, lun
OPENR, lun, file
READF, lun, line1
READF, lun, line2
READF, lun, line3
READF, lun, line4
READF, lun, test
FREE_LUN, lun

FOR    yminus = 0, rows-1 DO BEGIN
FOR x = 0, cols-1 DO BEGIN

line = strsplit(test((yminus)*cols+x), ' ', /EXTRACT)

accel_array(x, yminus) = DOUBLE(line(2))/1000

ENDFOR
ENDFOR

PRINT, g, 'Acceleration data imported'
multiplier = (accel_array * slope + intercept)/standard_multiplier
;Loop to process every value in acceleration array
FOR x = 1, cols DO BEGIN
FOR    y = 1, rows DO BEGIN

multiplied_dist_err = dist_err_orig * multiplier(x-1, y-1)

;***********************************************************
;***** Loop to estimate frequency of errors as function of distance
;***********************************************************

FOR a = 1, points_dist_error(1) DO BEGIN

IF multiplied_dist_err(a-1) GE 0 AND multiplied_dist_err(a-1) LT 0.5 THEN $
err_freq(x-1, y-1,0) = err_freq(x-1, y-1,0)+1
IF multiplied_dist_err(a-1) GE 0.5 AND multiplied_dist_err(a-1) LT 1 THEN $
err_freq(x-1, y-1,1) = err_freq(x-1, y-1,1)+1
IF multiplied_dist_err(a-1) GE 1 AND multiplied_dist_err(a-1) LT 1.5 THEN $
err_freq(x-1, y-1,2) = err_freq(x-1, y-1,2)+1
IF multiplied_dist_err(a-1) GE 1.5 AND multiplied_dist_err(a-1) LT 2 THEN $
err_freq(x-1, y-1,3) = err_freq(x-1, y-1,3)+1
IF multiplied_dist_err(a-1) GE 2 AND multiplied_dist_err(a-1) LT 2.5 THEN $
err_freq(x-1, y-1,4) = err_freq(x-1, y-1,4)+1
IF multiplied_dist_err(a-1) GE 2.5 AND multiplied_dist_err(a-1) LT 3 THEN $
err_freq(x-1, y-1,5) = err_freq(x-1, y-1,5)+1
IF multiplied_dist_err(a-1) GE 3 AND multiplied_dist_err(a-1) LT 3.5 THEN $
err_freq(x-1, y-1,6) = err_freq(x-1, y-1,6)+1
IF multiplied_dist_err(a-1) GE 3.5 AND multiplied_dist_err(a-1) LT 4 THEN $
err_freq(x-1, y-1,7) = err_freq(x-1, y-1,7)+1
```

```
IF multiplied_dist_err(a-1) GE 4  THEN err_freq(x-1, y-1,8) = $
err_freq(x-1, y-1,8)+1

ENDFOR
ENDFOR
ENDFOR

FOR x = 1, cols DO BEGIN
FOR     y = 1, rows DO BEGIN
FOR  a = 1, 77 DO BEGIN

;*************************************************************
;***** Calculating per-pixel error frequencies from acceleration data
;*************************************************************

multiplied_array(x-1, y-1,a-1) = $
((err_freq(x-1, y-1,0)*proportion_per_pix0_5(a-1)) + $
(err_freq(x-1, y-1,1)*proportion_per_pix1_0(a-1)) + $
(err_freq(x-1, y-1,2)*proportion_per_pix1_5(a-1)) + $
(err_freq(x-1, y-1,3)*proportion_per_pix2_0(a-1)) + $
(err_freq(x-1, y-1,4)*proportion_per_pix2_5(a-1)) + $
(err_freq(x-1, y-1,5)*proportion_per_pix3_0(a-1)) + $
(err_freq(x-1, y-1,6)*proportion_per_pix3_5(a-1)) + $
(err_freq(x-1, y-1,7)*proportion_per_pix4_0(a-1)) + $
(err_freq(x-1, y-1,8)*proportion_per_pix4_5(a-1)))/points_dist_error(1)

ENDFOR
ENDFOR
ENDFOR

accel_array = LONG(0)
err_freq = LONG(0)
PRINT, g, 'Finished calculating geometric error probabilities from acceleration data'

;*************************************************************
;End of calculating geometric error uncertainty filter
;*************************************************************

line1 = ''
line2 = ''
line3 = ''
line4 = ''

;*********************************
; ***** Import geometric error  data
;*********************************

geo_error_array = DBLARR(cols, rows,154)
test1 = STRARR(no_points)

GET_LUN, lun
OPENR, lun, file_geo
READF, lun, line1
```

```
READF, lun, line2
READF, lun, line3
READF, lun, line4
READF, lun, test
FREE_LUN, lun

FOR    yminus = 0, rows-1 DO BEGIN
FOR x = 0, cols-1 DO BEGIN

line = strsplit(test((yminus)*cols+x), ' ', /EXTRACT)
FOR v = 0, 153 DO BEGIN

geo_error_array(x, yminus,v ) = DOUBLE(line(v+2))

ENDFOR
ENDFOR
ENDFOR

PRINT, g, 'Geometric error vector data imported'

;*********************************
;***** Import thematic uncertainty data
;*********************************

them_error_array = DBLARR(cols, rows,8)
test = STRARR(no_points)

GET_LUN, lun
OPENR, lun, file_them
READF, lun, line1
READF, lun, line2
READF, lun, line3
READF, lun, line4
READF, lun, test
FREE_LUN, lun

FOR    yminus = 0, rows-1 DO BEGIN
FOR x = 0, cols-1 DO BEGIN

line = strsplit(test((yminus)*cols+x), ' ', /EXTRACT)
FOR cla = 0, 7 DO BEGIN

them_error_array(x, yminus,cla ) = DOUBLE(line(cla+2))

ENDFOR
ENDFOR
ENDFOR

PRINT, g, 'Classification data imported'
```

```
;*********************************************
;******** Defining x and y positions within matrix
;*********************************************
x_filter_pos = DBLARR(77)
x_filter_pos = [ $
-3,-2,-1,0,1,2,3, $
-4,-3,-2,-1,0,1,2,3,4, $
-4,-3,-2,-1,0,1,2,3,4, $
-4,-3,-2,-1,0,1,2,3,4, $
-4,-3,-2,-1,0,1,2,3,4, $
-4,-3,-2,-1,0,1,2,3,4, $
-4,-3,-2,-1,0,1,2,3,4, $
-4,-3,-2,-1,0,1,2,3,4, $
-3,-2,-1,0,1,2,3]

y_filter_pos = DBLARR(77)
y_filter_pos = [ $
4,4,4,4,4,4,4, $
3,3,3,3,3,3,3,3,3, $
2,2,2,2,2,2,2,2,2, $
1,1,1,1,1,1,1,1,1, $
0,0,0,0,0,0,0,0,0, $
-1,-1,-1,-1,-1,-1,-1,-1,-1, $
-2,-2,-2,-2,-2,-2,-2,-2,-2, $
-3,-3,-3,-3,-3,-3,-3,-3,-3, $
-4,-4,-4,-4,-4,-4,-4]

comb_uncer_array = DBLARR(cols, rows,8)

;*****************************************************************
;Final processing for combined data
;*****************************************************************
FOR    yminus = 0, rows-1 DO BEGIN
FOR x = 0, cols-1 DO BEGIN

FOR filter_no = 0, 76 DO BEGIN


;********************************
;***** Calculating geometric error
;***** Orthometric error is defined in terms of error from
;*****  actual pixel position to error position.
;*****
;***** Position in matrix is defined as from
;*****  error position to actual position
;*****
;***** To apply the error have to apply from error position
;***** to actual position and so orthometric error is negative
;********************************

x_up = DOUBLE(CEIL(x_filter_pos(filter_no) - $
geo_error_array(x, yminus, filter_no*2)))
```

```
y_up = DOUBLE(CEIL(y_filter_pos(filter_no) - $
geo_error_array(x, yminus, filter_no*2+1)))

x_offset = DOUBLE(x_filter_pos(filter_no) - $
geo_error_array(x, yminus, filter_no*2))

y_offset = DOUBLE(y_filter_pos(filter_no) - $
geo_error_array(x, yminus, filter_no*2+1))

;*****************************************************************
;** Repositioning to account for geometric error that is not an integer.
;** Positions as follows
;**      1       2
;**      4       3
;*****************************************************************

;*********************************
;***** Calculating proportion of thematic value applied to each pixel.
;*********************************

proportion1 = ABS((x_up - x_offset) * (y_offset - y_up + 1))
proportion2 = ABS((x_offset - x_up + 1) * (y_offset - y_up + 1))
proportion3 = ABS((x_offset - x_up + 1) * (y_up - y_offset))
proportion4 = ABS((x_up - x_offset) * (y_up - y_offset))


IF x + x_up LT cols - 2 AND x + x_up GT 2 AND yminus - y_up LT rows - 2 $
AND yminus - y_up GT 2 THEN BEGIN
FOR class_no = 0, 7 DO BEGIN

comb_uncer_array(x + x_up-1, yminus - y_up, class_no) = $
comb_uncer_array(x + x_up-1, yminus - y_up, class_no) + $
(proportion1 * them_error_array(x, yminus,class_no ) * $
multiplied_array(x, yminus,filter_no))

comb_uncer_array(x + x_up, yminus - y_up, class_no) = $
comb_uncer_array(x + x_up, yminus - y_up, class_no) + $
(proportion2 * them_error_array(x, yminus,class_no ) * $
multiplied_array(x, yminus,filter_no))

comb_uncer_array(x + x_up, yminus - y_up + 1, class_no) = $
comb_uncer_array(x + x_up, yminus - y_up + 1, class_no) + $
(proportion3 * them_error_array(x, yminus,class_no ) * $
multiplied_array(x, yminus,filter_no))

comb_uncer_array(x + x_up-1, yminus - y_up + 1, class_no) = $
comb_uncer_array(x + x_up-1, yminus - y_up + 1, class_no) + $
(proportion4 * them_error_array(x, yminus,class_no ) * $
multiplied_array(x, yminus,filter_no))

ENDFOR
ENDIF
ENDFOR
```

```
ENDFOR
ENDFOR

PRINT, g, 'Finished processing combination'

them_error_array = LONG(0)

;*****************************
;** Saving output data
;*****************************

save_path = path1 + 'combined_'+ g_no +'.asc'
save_path = STRJOIN((STRSPLIT(save_path, ' ', /EXTRACT)))
get_lun, lun
openw,  lun, save_path, WIDTH = cols*100
printf, lun, comb_uncer_array
FREE_LUN, lun

comb_uncer_array = LONG(0)


END
```

Appendix J Change detection model results using synthetic data

Table J.1 No uncertainty model two-class problem P_0 using synthetic data.

		Thematic error				
Change distance (m)	Fuzzy boundary width (m)	5	10	20	30	40
0	0	0.897	0.813	0.675	0.575	0.518
0	5	0.894	0.811	0.674	0.575	0.518
0	10	0.890	0.807	0.671	0.573	0.517
0	15	0.886	0.804	0.669	0.572	0.518
0	20	0.882	0.801	0.667	0.571	0.517
5	0	0.896	0.812	0.675	0.575	0.519
5	5	0.890	0.807	0.671	0.574	0.518
5	10	0.874	0.796	0.665	0.571	0.517
5	15	0.875	0.796	0.664	0.570	0.517
5	20	0.874	0.795	0.663	0.570	0.516
10	0	0.898	0.814	0.676	0.576	0.519
10	5	0.892	0.809	0.672	0.574	0.518
10	10	0.885	0.804	0.668	0.573	0.517
10	15	0.881	0.800	0.665	0.570	0.516
10	20	0.861	0.784	0.658	0.568	0.516
15	0	0.898	0.814	0.676	0.576	0.519
15	5	0.893	0.810	0.672	0.574	0.518
15	10	0.886	0.805	0.670	0.573	0.517
15	15	0.881	0.800	0.666	0.571	0.517
15	20	0.874	0.794	0.663	0.568	0.515
20	0	0.898	0.814	0.676	0.576	0.519
20	5	0.893	0.810	0.673	0.575	0.519
20	10	0.887	0.805	0.670	0.573	0.518
20	15	0.881	0.800	0.666	0.571	0.517
20	20	0.876	0.795	0.662	0.567	0.514
40	0	0.899	0.815	0.677	0.576	0.519
40	5	0.894	0.810	0.673	0.575	0.518
40	10	0.890	0.808	0.671	0.573	0.517
40	15	0.886	0.804	0.668	0.572	0.517
40	20	0.881	0.799	0.665	0.570	0.516

Table J.2 **Misregistration model two-class problem P_0 using synthetic data.**

Change distance (m)	Fuzzy boundary width (m)	Thematic error 5	10	20	30	40
0	0	0.997	0.998	0.999	0.998	0.998
0	5	0.996	0.997	0.999	0.999	0.998
0	10	0.996	0.997	0.999	0.999	0.998
0	15	0.999	0.999	0.999	0.999	0.998
0	20	0.999	1.000	0.999	0.999	0.997
5	0	0.984	0.981	0.971	0.961	0.955
5	5	0.982	0.978	0.969	0.960	0.956
5	10	0.965	0.967	0.971	0.973	0.973
5	15	0.978	0.985	0.993	0.997	0.997
5	20	0.990	0.993	0.997	0.997	0.997
10	0	0.988	0.984	0.966	0.934	0.916
10	5	0.986	0.981	0.963	0.933	0.917
10	10	0.978	0.972	0.950	0.925	0.913
10	15	0.982	0.975	0.952	0.930	0.923
10	20	0.952	0.950	0.949	0.948	0.947
15	0	0.989	0.985	0.958	0.907	0.880
15	5	0.987	0.983	0.957	0.907	0.882
15	10	0.979	0.974	0.946	0.901	0.879
15	15	0.981	0.975	0.945	0.906	0.891
15	20	0.975	0.965	0.934	0.899	0.888
20	0	0.989	0.985	0.951	0.882	0.847
20	5	0.986	0.982	0.950	0.883	0.850
20	10	0.980	0.974	0.939	0.877	0.849
20	15	0.982	0.976	0.940	0.883	0.861
20	20	0.977	0.967	0.927	0.877	0.860
40	0	0.990	0.986	0.928	0.804	0.743
40	5	0.988	0.983	0.928	0.808	0.751
40	10	0.984	0.977	0.921	0.810	0.757
40	15	0.986	0.979	0.924	0.821	0.774
40	20	0.981	0.972	0.916	0.822	0.780

Table J.3 Thematic model two-class problem P_0 using synthetic data.

		Thematic error				
Change distance (m)	Fuzzy boundary width (m)	5	10	20	30	40
0	0	0.911	0.837	0.716	0.629	0.580
0	5	0.914	0.841	0.720	0.635	0.585
0	10	0.917	0.845	0.726	0.641	0.592
0	15	0.920	0.849	0.731	0.647	0.599
0	20	0.922	0.852	0.736	0.653	0.606
5	0	0.906	0.832	0.710	0.622	0.571
5	5	0.898	0.825	0.705	0.620	0.570
5	10	0.892	0.823	0.707	0.625	0.579
5	15	0.910	0.840	0.725	0.643	0.597
5	20	0.915	0.846	0.731	0.650	0.603
10	0	0.908	0.833	0.709	0.619	0.566
10	5	0.901	0.827	0.705	0.617	0.566
10	10	0.890	0.818	0.698	0.614	0.564
10	15	0.883	0.812	0.695	0.612	0.564
10	20	0.875	0.808	0.698	0.620	0.576
15	0	0.907	0.832	0.707	0.616	0.561
15	5	0.901	0.827	0.703	0.614	0.561
15	10	0.892	0.819	0.699	0.612	0.560
15	15	0.887	0.816	0.697	0.612	0.563
15	20	0.874	0.805	0.689	0.606	0.558
20	0	0.907	0.831	0.705	0.612	0.556
20	5	0.901	0.826	0.702	0.612	0.557
20	10	0.893	0.820	0.697	0.609	0.555
20	15	0.887	0.816	0.695	0.609	0.557
20	20	0.878	0.807	0.689	0.604	0.554
40	0	0.907	0.829	0.699	0.602	0.541
40	5	0.901	0.824	0.696	0.602	0.542
40	10	0.895	0.820	0.693	0.600	0.542
40	15	0.892	0.817	0.692	0.602	0.545
40	20	0.884	0.811	0.688	0.599	0.545

Table J.4 **Combined model two-class problem P_0 using synthetic data.**

Change distance (m)	Fuzzy boundary width (m)	Thematic error 5	10	20	30	40
0	0	0.999	0.999	1.000	1.000	1.000
0	5	1.000	1.000	1.000	1.000	1.000
0	10	1.000	1.000	1.000	1.000	1.000
0	15	1.000	1.000	1.000	1.000	1.000
0	20	1.000	1.000	1.000	1.000	1.000
5	0	0.982	0.979	0.971	0.962	0.957
5	5	0.974	0.971	0.964	0.959	0.958
5	10	0.973	0.974	0.975	0.975	0.975
5	15	1.000	1.000	1.000	1.000	1.000
5	20	1.000	1.000	1.000	1.000	1.000
10	0	0.986	0.982	0.967	0.940	0.920
10	5	0.981	0.976	0.959	0.934	0.921
10	10	0.968	0.958	0.936	0.920	0.914
10	15	0.959	0.944	0.928	0.925	0.924
10	20	0.949	0.949	0.949	0.949	0.949
15	0	0.986	0.983	0.963	0.918	0.885
15	5	0.983	0.977	0.955	0.913	0.887
15	10	0.971	0.962	0.934	0.899	0.882
15	15	0.971	0.957	0.925	0.899	0.892
15	20	0.952	0.934	0.900	0.890	0.889
20	0	0.986	0.983	0.958	0.897	0.853
20	5	0.983	0.978	0.950	0.893	0.856
20	10	0.972	0.963	0.930	0.881	0.853
20	15	0.972	0.959	0.922	0.881	0.864
20	20	0.957	0.941	0.901	0.871	0.861
40	0	0.988	0.984	0.942	0.832	0.754
40	5	0.984	0.980	0.936	0.831	0.761
40	10	0.976	0.968	0.922	0.826	0.765
40	15	0.977	0.966	0.917	0.831	0.781
40	20	0.965	0.951	0.901	0.828	0.786

Table J.5 **No uncertainty and Thematic models four-class problem P_0 using synthetic data.**

		Thematic error				
Change distance (m)	Fuzzy boundary width (m)	5	10	20	30	40
0	0	0.894	0.803	0.634	0.485	0.357
0	5	0.890	0.798	0.631	0.483	0.356
0	10	0.883	0.793	0.626	0.480	0.354
0	15	0.878	0.788	0.621	0.476	0.350
0	20	0.872	0.782	0.617	0.472	0.348
5	0	0.893	0.802	0.634	0.486	0.358
5	5	0.887	0.796	0.629	0.482	0.355
5	10	0.882	0.792	0.626	0.480	0.354
5	15	0.877	0.787	0.621	0.475	0.350
5	20	0.870	0.781	0.616	0.473	0.348
10	0	0.895	0.803	0.635	0.486	0.358
10	5	0.889	0.797	0.630	0.483	0.355
10	10	0.883	0.793	0.626	0.480	0.354
10	15	0.877	0.787	0.621	0.476	0.350
10	20	0.869	0.780	0.617	0.473	0.348
15	0	0.895	0.804	0.635	0.486	0.358
15	5	0.890	0.798	0.631	0.483	0.355
15	10	0.883	0.794	0.627	0.481	0.355
15	15	0.878	0.788	0.622	0.477	0.351
15	20	0.871	0.781	0.618	0.473	0.349
20	0	0.895	0.804	0.635	0.486	0.358
20	5	0.890	0.799	0.631	0.484	0.356
20	10	0.884	0.794	0.628	0.481	0.355
20	15	0.878	0.788	0.622	0.476	0.351
20	20	0.872	0.783	0.618	0.473	0.348
40	0	0.896	0.805	0.636	0.487	0.358
40	5	0.891	0.799	0.632	0.483	0.356
40	10	0.887	0.796	0.628	0.482	0.355
40	15	0.883	0.792	0.625	0.478	0.352
40	20	0.877	0.787	0.622	0.476	0.350

Table J.6 **Misregistration model four-class problem P_0 using synthetic data.**

		Thematic error				
Change distance (m)	Fuzzy boundary width (m)	5	10	20	30	40
0	0	0.990	0.989	0.980	0.903	0.633
0	5	0.987	0.987	0.979	0.901	0.628
0	10	0.983	0.982	0.973	0.893	0.620
0	15	0.984	0.983	0.971	0.887	0.613
0	20	0.981	0.978	0.963	0.877	0.606
5	0	0.987	0.987	0.979	0.902	0.631
5	5	0.986	0.985	0.977	0.898	0.627
5	10	0.983	0.982	0.973	0.892	0.621
5	15	0.984	0.982	0.970	0.885	0.613
5	20	0.979	0.976	0.960	0.874	0.604
10	0	0.990	0.990	0.982	0.904	0.632
10	5	0.988	0.987	0.979	0.901	0.630
10	10	0.984	0.983	0.973	0.893	0.622
10	15	0.985	0.983	0.971	0.886	0.611
10	20	0.981	0.977	0.961	0.873	0.603
15	0	0.990	0.990	0.982	0.905	0.633
15	5	0.988	0.988	0.980	0.901	0.629
15	10	0.985	0.984	0.974	0.895	0.623
15	15	0.985	0.983	0.971	0.887	0.613
15	20	0.981	0.977	0.962	0.874	0.601
20	0	0.990	0.990	0.981	0.904	0.632
20	5	0.988	0.987	0.980	0.902	0.630
20	10	0.984	0.984	0.975	0.895	0.623
20	15	0.985	0.983	0.971	0.888	0.613
20	20	0.982	0.979	0.964	0.875	0.603
40	0	0.992	0.991	0.983	0.905	0.633
40	5	0.989	0.989	0.981	0.903	0.631
40	10	0.987	0.986	0.977	0.898	0.625
40	15	0.988	0.987	0.976	0.893	0.619
40	20	0.984	0.982	0.968	0.883	0.613

Table J.7 Combined model four-class problem P_o using synthetic data.

		Thematic error				
Change distance (m)	Fuzzy boundary width (m)	5	10	20	30	40
0	0	0.990	0.989	0.987	0.978	0.921
0	5	0.988	0.988	0.987	0.977	0.916
0	10	0.985	0.984	0.982	0.969	0.903
0	15	0.986	0.984	0.978	0.959	0.885
0	20	0.985	0.982	0.972	0.946	0.869
5	0	0.988	0.987	0.986	0.977	0.919
5	5	0.987	0.986	0.985	0.976	0.914
5	10	0.985	0.984	0.982	0.968	0.900
5	15	0.987	0.986	0.978	0.958	0.883
5	20	0.983	0.980	0.968	0.943	0.868
10	0	0.990	0.990	0.988	0.980	0.921
10	5	0.989	0.988	0.988	0.978	0.916
10	10	0.985	0.984	0.981	0.967	0.900
10	15	0.988	0.986	0.979	0.957	0.881
10	20	0.984	0.982	0.970	0.941	0.861
15	0	0.990	0.990	0.989	0.980	0.922
15	5	0.990	0.989	0.988	0.978	0.916
15	10	0.986	0.986	0.982	0.969	0.903
15	15	0.987	0.986	0.979	0.958	0.883
15	20	0.984	0.981	0.971	0.942	0.858
20	0	0.990	0.990	0.989	0.979	0.921
20	5	0.989	0.989	0.988	0.978	0.918
20	10	0.986	0.985	0.983	0.969	0.903
20	15	0.987	0.986	0.979	0.958	0.884
20	20	0.986	0.983	0.972	0.944	0.862
40	0	0.991	0.991	0.990	0.981	0.923
40	5	0.990	0.990	0.989	0.980	0.919
40	10	0.988	0.987	0.985	0.972	0.908
40	15	0.991	0.989	0.984	0.966	0.894
40	20	0.987	0.985	0.977	0.954	0.879

Table J.8 No uncertainty model thematic change vector RMSE using synthetic data.

Change distance (m)	Fuzzy boundary width (m)	Thematic error 5	10	20	30	40
0	0	0.323	0.433	0.571	0.652	0.695
0	5	0.328	0.437	0.572	0.652	0.694
0	10	0.336	0.442	0.575	0.654	0.695
0	15	0.343	0.446	0.577	0.655	0.695
0	20	0.350	0.451	0.579	0.656	0.696
5	0	0.328	0.439	0.580	0.666	0.716
5	5	0.329	0.439	0.577	0.662	0.710
5	10	0.337	0.443	0.578	0.659	0.704
5	15	0.345	0.448	0.579	0.658	0.701
5	20	0.352	0.452	0.581	0.659	0.701
10	0	0.325	0.439	0.585	0.677	0.737
10	5	0.328	0.441	0.583	0.674	0.731
10	10	0.335	0.443	0.583	0.669	0.723
10	15	0.344	0.447	0.582	0.666	0.716
10	20	0.355	0.454	0.584	0.664	0.711
15	0	0.325	0.441	0.591	0.689	0.756
15	5	0.327	0.441	0.589	0.684	0.749
15	10	0.334	0.444	0.588	0.680	0.741
15	15	0.342	0.448	0.586	0.676	0.733
15	20	0.352	0.453	0.587	0.673	0.727
20	0	0.326	0.442	0.597	0.699	0.773
20	5	0.328	0.443	0.594	0.695	0.766
20	10	0.335	0.446	0.593	0.691	0.758
20	15	0.342	0.449	0.591	0.686	0.749
20	20	0.349	0.453	0.591	0.682	0.742
40	0	0.327	0.448	0.614	0.732	0.825
40	5	0.328	0.448	0.611	0.728	0.817
40	10	0.333	0.450	0.608	0.722	0.807
40	15	0.338	0.451	0.605	0.716	0.797
40	20	0.344	0.454	0.603	0.710	0.788

Table J.9 **Misregistration model thematic change vector RMSE using synthetic data.**

Change distance (m)	Fuzzy boundary width (m)	Thematic error				
		5	10	20	30	40
0	0	0.093	0.115	0.142	0.160	0.168
0	5	0.098	0.118	0.142	0.159	0.168
0	10	0.100	0.120	0.144	0.160	0.168
0	15	0.093	0.114	0.142	0.159	0.168
0	20	0.091	0.113	0.142	0.159	0.167
5	0	0.137	0.158	0.194	0.225	0.252
5	5	0.106	0.132	0.168	0.200	0.228
5	10	0.102	0.124	0.155	0.182	0.204
5	15	0.103	0.122	0.150	0.173	0.189
5	20	0.102	0.122	0.150	0.173	0.189
10	0	0.129	0.157	0.207	0.256	0.304
10	5	0.103	0.135	0.185	0.234	0.282
10	10	0.099	0.126	0.172	0.216	0.260
10	15	0.105	0.125	0.163	0.201	0.240
10	20	0.116	0.132	0.164	0.196	0.228
15	0	0.129	0.161	0.222	0.283	0.346
15	5	0.102	0.139	0.201	0.264	0.328
15	10	0.101	0.132	0.190	0.248	0.307
15	15	0.103	0.128	0.180	0.233	0.286
15	20	0.110	0.131	0.175	0.223	0.271
20	0	0.131	0.166	0.236	0.309	0.383
20	5	0.106	0.145	0.217	0.290	0.364
20	10	0.103	0.139	0.207	0.276	0.345
20	15	0.104	0.133	0.196	0.262	0.326
20	20	0.107	0.133	0.190	0.252	0.311
40	0	0.131	0.177	0.275	0.376	0.477
40	5	0.110	0.161	0.260	0.361	0.460
40	10	0.105	0.152	0.248	0.346	0.442
40	15	0.104	0.147	0.237	0.330	0.422
40	20	0.106	0.145	0.230	0.319	0.406

Table J.10 Thematic model thematic change vector RMSE using synthetic data.

		Thematic error				
Change distance (m)	Fuzzy boundary width (m)	5	10	20	30	40
0	0	0.253	0.324	0.415	0.471	0.502
0	5	0.250	0.321	0.412	0.467	0.498
0	10	0.247	0.318	0.409	0.464	0.494
0	15	0.246	0.316	0.406	0.460	0.490
0	20	0.245	0.314	0.403	0.456	0.486
5	0	0.267	0.338	0.432	0.491	0.528
5	5	0.256	0.328	0.422	0.481	0.516
5	10	0.250	0.322	0.414	0.472	0.506
5	15	0.247	0.318	0.410	0.466	0.498
5	20	0.247	0.316	0.406	0.462	0.493
10	0	0.266	0.340	0.438	0.503	0.546
10	5	0.258	0.332	0.430	0.494	0.536
10	10	0.253	0.326	0.423	0.485	0.525
10	15	0.250	0.322	0.417	0.477	0.515
10	20	0.249	0.319	0.412	0.471	0.506
15	0	0.269	0.344	0.446	0.515	0.565
15	5	0.260	0.335	0.437	0.506	0.554
15	10	0.255	0.330	0.431	0.497	0.543
15	15	0.253	0.326	0.425	0.489	0.533
15	20	0.251	0.323	0.420	0.483	0.523
20	0	0.270	0.346	0.453	0.526	0.581
20	5	0.263	0.340	0.445	0.517	0.571
20	10	0.259	0.335	0.439	0.509	0.559
20	15	0.256	0.331	0.433	0.501	0.549
20	20	0.254	0.328	0.427	0.494	0.539
40	0	0.279	0.359	0.475	0.561	0.629
40	5	0.272	0.353	0.468	0.552	0.619
40	10	0.266	0.347	0.460	0.543	0.607
40	15	0.263	0.342	0.454	0.534	0.596
40	20	0.261	0.339	0.448	0.526	0.585

Table J.11 Combined model thematic change vector RMSE using synthetic data.

		Thematic error				
Change distance (m)	Fuzzy boundary width (m)	5	10	20	30	40
0	0	0.077	0.090	0.107	0.117	0.122
0	5	0.077	0.089	0.105	0.116	0.121
0	10	0.072	0.085	0.102	0.114	0.120
0	15	0.067	0.081	0.100	0.112	0.118
0	20	0.064	0.080	0.099	0.111	0.117
5	0	0.136	0.149	0.172	0.193	0.213
5	5	0.102	0.119	0.143	0.166	0.185
5	10	0.081	0.099	0.123	0.144	0.160
5	15	0.073	0.090	0.113	0.132	0.146
5	20	0.070	0.087	0.110	0.128	0.141
10	0	0.133	0.153	0.187	0.221	0.255
10	5	0.105	0.128	0.164	0.199	0.233
10	10	0.090	0.113	0.148	0.182	0.213
10	15	0.081	0.102	0.137	0.167	0.195
10	20	0.077	0.097	0.129	0.157	0.181
15	0	0.139	0.161	0.204	0.247	0.291
15	5	0.111	0.137	0.182	0.227	0.272
15	10	0.098	0.124	0.169	0.211	0.253
15	15	0.091	0.116	0.159	0.200	0.238
15	20	0.085	0.110	0.151	0.189	0.224
20	0	0.143	0.169	0.219	0.270	0.322
20	5	0.118	0.147	0.199	0.251	0.303
20	10	0.106	0.135	0.187	0.238	0.287
20	15	0.098	0.127	0.178	0.226	0.271
20	20	0.093	0.121	0.170	0.216	0.258
40	0	0.155	0.190	0.260	0.331	0.401
40	5	0.135	0.173	0.244	0.315	0.385
40	10	0.123	0.161	0.232	0.301	0.369
40	15	0.116	0.153	0.222	0.289	0.353
40	20	0.112	0.147	0.213	0.278	0.339

Table J.12 No uncertainty model thematic change vector RMSE for areas of change using synthetic data.

		Thematic error				
Change distance (m)	Fuzzy boundary width (m)	5	10	20	30	40
5	0	0.549	0.624	0.774	0.904	1.049
5	5	0.498	0.568	0.669	0.767	0.859
5	10	0.490	0.551	0.636	0.708	0.763
5	15	0.484	0.541	0.625	0.692	0.732
5	20	0.483	0.541	0.627	0.686	0.724
10	0	0.429	0.537	0.715	0.877	1.046
10	5	0.440	0.531	0.674	0.803	0.929
10	10	0.444	0.521	0.645	0.749	0.844
10	15	0.455	0.521	0.630	0.716	0.791
10	20	0.469	0.532	0.629	0.702	0.761
15	0	0.397	0.516	0.709	0.879	1.050
15	5	0.406	0.508	0.674	0.820	0.966
15	10	0.419	0.507	0.654	0.775	0.890
15	15	0.430	0.510	0.638	0.745	0.839
15	20	0.445	0.518	0.632	0.725	0.803
20	0	0.382	0.503	0.705	0.879	1.053
20	5	0.393	0.503	0.681	0.836	0.985
20	10	0.405	0.504	0.663	0.800	0.924
20	15	0.417	0.504	0.647	0.768	0.873
20	20	0.428	0.509	0.639	0.747	0.838
40	0	0.355	0.489	0.702	0.885	1.057
40	5	0.364	0.490	0.688	0.861	1.021
40	10	0.375	0.490	0.676	0.836	0.982
40	15	0.383	0.490	0.662	0.814	0.947
40	20	0.395	0.496	0.656	0.797	0.920

Table J.13 Misregistration model thematic change vector RMSE for areas of change using synthetic data.

		Thematic error				
Change distance (m)	Fuzzy boundary width (m)	5	10	20	30	40
5	0	0.456	0.499	0.602	0.720	0.849
5	5	0.257	0.290	0.350	0.439	0.542
5	10	0.204	0.214	0.242	0.293	0.359
5	15	0.186	0.188	0.198	0.230	0.271
5	20	0.167	0.174	0.189	0.218	0.253
10	0	0.300	0.363	0.500	0.656	0.823
10	5	0.205	0.257	0.366	0.498	0.642
10	10	0.171	0.202	0.282	0.387	0.503
10	15	0.176	0.186	0.234	0.312	0.407
10	20	0.192	0.195	0.224	0.281	0.353
15	0	0.254	0.322	0.472	0.639	0.817
15	5	0.181	0.243	0.376	0.529	0.693
15	10	0.164	0.206	0.315	0.443	0.581
15	15	0.160	0.185	0.270	0.378	0.495
15	20	0.170	0.183	0.246	0.337	0.436
20	0	0.233	0.303	0.462	0.637	0.820
20	5	0.176	0.243	0.388	0.550	0.718
20	10	0.162	0.212	0.339	0.481	0.629
20	15	0.155	0.191	0.298	0.424	0.554
20	20	0.157	0.184	0.273	0.388	0.502
40	0	0.189	0.268	0.445	0.631	0.819
40	5	0.159	0.238	0.408	0.586	0.766
40	10	0.145	0.216	0.375	0.543	0.712
40	15	0.140	0.201	0.348	0.505	0.663
40	20	0.143	0.195	0.329	0.477	0.625

Table J.14 Thematic model thematic change vector RMSE for areas of change using synthetic data.

		Thematic error				
Change distance (m)	Fuzzy boundary width (m)	5	10	20	30	40
5	0	0.518	0.570	0.678	0.772	0.874
5	5	0.358	0.412	0.497	0.572	0.643
5	10	0.293	0.345	0.419	0.477	0.525
5	15	0.268	0.317	0.388	0.441	0.477
5	20	0.259	0.307	0.376	0.425	0.457
10	0	0.404	0.479	0.610	0.727	0.846
10	5	0.338	0.409	0.521	0.621	0.716
10	10	0.294	0.361	0.462	0.546	0.621
10	15	0.273	0.333	0.427	0.498	0.558
10	20	0.264	0.320	0.405	0.468	0.517
15	0	0.376	0.460	0.599	0.724	0.845
15	5	0.326	0.405	0.534	0.645	0.751
15	10	0.296	0.370	0.487	0.582	0.670
15	15	0.280	0.348	0.456	0.541	0.615
15	20	0.271	0.335	0.434	0.511	0.573
20	0	0.357	0.443	0.591	0.720	0.844
20	5	0.326	0.408	0.544	0.660	0.771
20	10	0.300	0.379	0.505	0.609	0.704
20	15	0.286	0.360	0.476	0.571	0.653
20	20	0.277	0.347	0.456	0.542	0.613
40	0	0.338	0.432	0.586	0.719	0.843
40	5	0.321	0.413	0.560	0.687	0.805
40	10	0.304	0.394	0.535	0.654	0.763
40	15	0.294	0.380	0.514	0.628	0.729
40	20	0.288	0.370	0.498	0.605	0.699

Table J.15 Combined model thematic change vector RMSE for areas of change using synthetic data.

		Thematic error				
Change distance (m)	Fuzzy boundary width (m)	5	10	20	30	40
5	0	0.503	0.535	0.608	0.689	0.776
5	5	0.281	0.308	0.355	0.417	0.484
5	10	0.163	0.184	0.221	0.265	0.312
5	15	0.117	0.133	0.163	0.197	0.230
5	20	0.099	0.115	0.141	0.170	0.198
10	0	0.354	0.403	0.500	0.608	0.721
10	5	0.241	0.285	0.367	0.459	0.557
10	10	0.172	0.209	0.280	0.356	0.435
10	15	0.132	0.164	0.225	0.288	0.353
10	20	0.115	0.141	0.192	0.244	0.297
15	0	0.312	0.365	0.471	0.587	0.707
15	5	0.228	0.278	0.376	0.482	0.593
15	10	0.178	0.223	0.310	0.402	0.496
15	15	0.151	0.190	0.268	0.348	0.428
15	20	0.130	0.166	0.236	0.307	0.376
20	0	0.292	0.345	0.458	0.579	0.705
20	5	0.226	0.279	0.385	0.498	0.613
20	10	0.185	0.235	0.333	0.434	0.536
20	15	0.159	0.205	0.295	0.386	0.475
20	20	0.143	0.185	0.267	0.350	0.429
40	0	0.253	0.314	0.439	0.567	0.696
40	5	0.219	0.280	0.401	0.525	0.649
40	10	0.192	0.251	0.368	0.485	0.602
40	15	0.176	0.232	0.343	0.454	0.563
40	20	0.165	0.218	0.323	0.427	0.530

References

Agumya, A. and Hunter, G.J. (2002) Responding to the consequences of uncertainty in geographical data. *International Journal of Geographical Information Science*, **16**, 405-417.

Ahlqvist, O., Keukelaar, J. and Oukbir, K. (2003) Rough and fuzzy geographical data integration. *International Journal of Remote Sensing*, **17**, 223-234.

Aires, F., Prigent, C. and Rossow, W.B. (2004) Neural network uncertainty assessment using Bayesian statistics: A remote sensing application. *Neural Computation*, **16**, 2415-2458.

ANGEL (2000) http://www.gfz-potsdam.de/pb1/pg3/aero/equipment/WebPage-Astech-Z-Surveyor.pdf *Airborne Navigation and Gravity Ensemble & Laboratory, the Ashtech Z-Surveyor*, accessed 16/04/04.

Applanix (2004) http://www.applanix.com/media/downloads/products/specs/POSAV_OEM_Specifications_2004.pdf *Applanix POS AV Specifications*, accessed 10/12/04

Arbia, G., Griffith, D. and Haining, R. (1998) Error propagation modelling in raster GIS: overlay operations. *International Journal of Geographic Information Science*, **12**, 145-167.

Arnot, C., Fisher, P.F., Wadsworth, R. and Wellens, J. (2004) Landscape metrics with ecotones: pattern under uncertainty. *Landscape Ecology*, **19**, 181-195.

Arora, M.K. and Foody, G.M. (1997) Log-Linear modelling for the evaluation of the variables affecting the accuracy of probabilistic, fuzzy and neural network classifications. *International Journal of Remote Sensing*, **18**, 785-798.

Arzandeh, S. and Wang, J.F. (2003) Monitoring the change of Phragmites distribution using satellite data. *Canadian Journal of Remote Sensing*, **29**, 24-35.

Ashish, D., Hoogenboom, G. and McClendon, R.W. (2004) Land-use classification of gray-scale aerial images using probabilistic neural networks. *Transactions of the American Society of Agricultural Engineers*, **47**, 1813-1819.

Ashkenazi, V., Dumville, M., Bingley, R. and Dodson, A. (1999) *The Use of Remote Sensing in Climate Change (Report 3)*. R&D Technical Report E82, Environment Agency, Bristol, pp85.

Atkinson, P.M. and Foody, G.M. (2002) Uncertainty in remote sensing and GIS: Fundamentals. In Foody, G.M. and Atkinson, P.M. (Eds) *Uncertainty in Remote Sensing and GIS*. Wily, Chichester, 1-18.

Atkinson, P.M. and Tatnall, A.R.L. (1997) Neural networks in remote sensing. *International Journal of Remote Sensing*, **18**, 699-709.

Augusteijn, M.F. and Folkert, B.A. (2002) Neural network classification and novelty detection. *International Journal of Remote Sensing*, **23**, 2891-2902.

Barber, G.M. (1988) *Elementary Statistics for Geographers*. The Guildford Press, New York, pp513.

Bastin, L. (1997) Comparison of fuzzy c-means classification, linear mixture modelling and MLC probabilities as tools for unmixing coarse pixels. *International Journal of Remote Sensing*, **18**, 3629-3648.

BEI (2005) http://www.willburger.de/produkte/neigunggier/datasheets/mmq50.pdf *BEI Technologies, Inc. MMQ50 IMU*, accessed 17/03/05.

Benediktsson, J.A., Swain, P.H. and Ersoy, O.K. (1990) Neural network approaches versus statistical methods in classification of multisource remote sensing data. *IEEE Transactions on Geoscience and Remote Sensing*, **28**, 540-551.

Benediktsson, J.A., Swain, P.H. and Ersoy, O.K. (1993) Conjugate-gradient neural networks in classification of multisource and very-high-dimensional remote sensing data. *International Journal of Remote Sensing*, **14**, 2883-2903.

Bishop, C.M. (1995) *Neural Networks for Pattern Recognition*. Oxford University Press, Oxford, pp504.

Boardman, J. W. (1999) Precision geocoding of low-altitude AVIRIS data: Lessons learned in 1998. In Green, R.O. (Ed) *Summaries of the Eighth Annual JPL Airborne Geoscience Workshop, JPL, Pasadena, California, 9th- 11th February 1999, JPL Publication 99-17*, 63-68.

Brown, D.G. (1998) Classification and boundary vagueness in mapping presettlement forest types. *International Journal of Geographical Information Science*, **12**, 105-129.

Brown, D.G. and Arbogast, A.F. (1999) Digital photogrammetric change analysis as applied to active coastal dunes in Michigan. *Photogrammetric Engineering and Remote Sensing*, **65**, 467-474.

Brown, K., Hambidge, C. and Matthews, A. (2003a) *The Development of Remote Sensing Techniques for Marine SAC Monitoring: Project PM_0020*. Environment Agency, Bath, pp112.

Brown, K., Duncan, A., O'Dwyer, C., Davison, B. Hogarth, P., Butler, D. and Sampson, E. (2003b) Integrated airborne data collection by the Environment Agency. In *Proceedings Annual Conference of the Remote Sensing and Photogrammetry Society, Nottingham, 10th-12th September 2003.*

Bruzzone, L., Cossu, R. and Vernazza, G. (2004) Detection of land-cover transitions by combining multidate classifiers. *Pattern Recognition Letters*, **25**, 1491-1500.

Bruzzone, L and Prieto, DF (2000) Automatic analysis of the difference image for unsupervised change detection. *IEEE Transactions on Geoscience and Remote Sensing*, **38**, 1171-1182.

Burnside, C.D. (1985) *Mapping from Aerial Photographs* (2nd Edition). Collins Professional and Technical Books, London, pp348.

Campbell, J.B. (1981) Spatial correlation effects upon accuracy of supervised classification of land cover. *Photogrammetric Engineering and Remote Sensing*, **47**, 355-363.

Campbell, J.B. (2002) *Introduction to Remote Sensing* (3rd Edition). Guildford Publications, New York, pp621.

Carmel, Y. and Dean, D.J. (2004) Performance of a spatio-temporal error model for raster datasets under complex error patterns. *International Journal of Remote Sensing*, **25**, 5283-5296.

Carmel, Y., Dean, D.J. and Flather, C.H. (2001) Combining location and classification error sources for estimating multi-temporal database accuracy. *Photogrammetric Engineering and Remote Sensing*, **67**, 865-872.

Chen, J., Gong, P., He, C.Y., Pu, R.L. and Shi, P.J. (2003a) Land-use/land-cover change detection using improved change-vector analysis. *Photogrammetric Engineering and Remote Sensing*, **69**, 369-379.

Chen, H-M., Varshney, P.K. and Arora, M.J. (2003b) Performance of mutual information similarity measure for registration of multitemporal remote sensing images. *IEEE Transactions on Geoscience and Remote Sensing*, **41**, 2445-2454.

Cheng, T. (2002) Fuzzy objects: their changes and uncertainties. *Photogrammetric Engineering and Remote Sensing*, **68**, 41-49

Cheng, T. and Molenaar, M. (1999) Objects with fuzzy spatial extent. *Photogrammetric Engineering and Remote Sensing*, **65**, 797-801.

Cloud Cap Technology (2005) http://cloudcaptech.com/crista_imu.htm *Crista Inertial Measurement Unit*, accessed 17/03/05.

Cohen, J. (1960) A coefficient of agreement for nominal scales. *Educational and Psychological Measurement*, **20**, 37-46.

Comber, A., Fisher, P. and Wadsworth, R. (2004) Assessment of a semantic statistical approach to detecting land cover change using inconsistent data sets. *Photogrammetric Engineering and Remote Sensing*, **70**, 931-938.

Congalton, R.G. (1988) A comparison of sampling schemes used in generating error matrices for assessing the accuracy of maps generated from remotely sensed data. *Photogrammetric Engineering and Remote Sensing*, **54**, 593-600.

Congalton, R.G. (1991) A review of assessing the accuracy of classifications of remotely sensed data. *Remote Sensing of Environment*, **37**, 35-46.

Coppin, P., Jonckheere, I., Nackaerts, K., Muys, B. and Lambin, I. (2004) Digital change detection methods in ecosystem monitoring: a review. *International Journal of Remote Sensing*, **25**, 1565-1596.

Crosetto, M., Ruiz, J.A.M. and Crippa, B. (2001) Uncertainty propagation in models driven by remotely sensed data. *Remote Sensing of Environment*, **76**, 373-385.

Crosetto, M. and Tarantola, S. (2001) Uncertainty and sensitivity analysis: tools for GIS-based model implementation. *International Journal of Geographical Information Sciences*, **15**, 415-437.

Dai, X. and Khorram, S. (1998) The effects of image misregistration on the accuracy of remotely sensed change detection. *IEEE Transactions on Geoscience and Remote Sensing*, **36**, 1566-1577.

De Bruin, S. (2000) Querying probabilistic land cover data using fuzzy set theory. *International Journal of Geographical Information Sciences*, **14**, 359-372.

De Bruin, S. and Gorte, B.G.H. (2000) Probabilistic image classification using geological map units applied to land-cover change detection. *International Journal of Remote Sensing*, **21**, 2389-2402.

Dewidar, K.M. (2004) Detection of land use land cover changes for the northern part of the Nile delta (Burullus region), Egypt. *International Journal of Remote Sensing*, **25**, 4079-4089.

De Zeeuw, C.J., Bregt, A.K., Sonneveld, M.P.W. and Van den Brink, J.A.T. (1999) Geo-information for monitoring land use: from map overlay to object-structured noise reduction. In *Proceedings of 10th International Workshop on Database and Expert Systems Applications, 1st-3rd September 1999, Florence, Italy*, 419-425.

Digital Globe (2005) http://www.digitalglobe.com/product/basic_imagery.shtml *Digital Globe imagery*, accessed 05/03/05.

Donoghue, D.N.M (2002) Remote sensing: environmental change. *Progress in Physical Geography*, **26**, 144-151.

Donoghue, D.N.M., Reid Thomas, D.C. and Zong, Y. (1994) Mapping and monitoring the intertidal zone of the east coast of England using remote sensing techniques and a coastal monitoring GIS. *Marine Technology Society Journal*, **28**, 19-29.

Donoghue, D.N.M and Shennan, I. (1987) A preliminary assessment of Landsat TM imagery for mapping vegetation and sediment distribution in the Wash estuary. *International Journal of Remote Sensing*, **8**, 1101-1108.

Ediriwickrema, J. and Khorram, S. (1997) Hierarchical maximum-likelihood classification for improved accuracies. *IEEE Transactions on Geoscience and Remote Sensing*, **35**, 810-816.

Edwards, G. and Lowell, K.E. (1996) Modelling uncertainty in photointerpreted boundaries. *Photogrammetric Engineering and Remote Sensing*, **62**, 337-391.

EEC (1992) http://www.ecnc.nl/doc/europe/legislat/habidire.html *Directive 92/43/EEC Conservation of Natural Habitats and of Wild Fauna and Flora,* accessed 07/11/01.

English Nature (2005) http://www.english-nature.org.uk/ *English Nature*, accessed 18/01/05.

Environment Agency (2005) http://www.environment-agency.gov.uk/ *Environment Agency*, accessed 18/01/05.

Erbek, F.S., Ozkan, C. and Taberner, M. (2004) Comparison of maximum likelihood classification method with supervised artificial neural network algorithms for land use activities. *International Journal of Remote Sensing*, **25**, 1733-1748.

ERDAS (2001) *ERDAS Imagine 8.5 Field Guide*. ERDAS Inc., Atlanta, Georgia, pp656.

ESA (2005) http://www.esa.int/esaNA/GGGMX650NDC_index_0.html *European Space Agency - Navigation*, accessed 5/03/05.

Fisher, P. (1997) The pixel: a snare and a delusion. *International Journal of Remote Sensing*, **18**, 679-685.

Fontana, D., Collier, P. and Pearson, A. (1997) The development of a GIS for inter-tidal area using CIR photography and CASI data. *Proceedings of the Third International Airborne Remote Sensing Conference, 7th-10th July 1997, Copenhagen, Denmark.* I-363-370.

Foody, G.M. (1992) On the compensation for chance agreement in image classification accuracy assessment. *Photogrammetric Engineering and Remote Sensing*, **58,** 1459-1460.

Foody, G.M. (1997) Fully fuzzy supervised classification of land cover from remotely sensed imagery with an artificial neural network. *Neural Computing and Applications*, **5**, 238-247.

Foody, G.M. (1999) The continuum of classification fuzziness in thematic mapping. *Photogrammetric Engineering and Remote Sensing*, **65**, 443-451.

Foody, G.M. (2000) Mapping land cover from remotely sensed data with a softened feedforward neural network classification. *Journal of Intelligent and Robotic Systems*, **29**, 433-449.

Foody, G.M. (2002) Status of land cover classification accuracy assessment. *Remote Sensing of Environment*, **80**, 185-201.

Foody, G.M. (2005) Local characterization of thematic classification accuracy spatially constrained confusion matrices. *International Journal of Remote Sensing*, **26**, 1217–1228.

Foody, G.M. and Arora, M.K. (1997) An evaluation of some factors affecting the accuracy of classification by an artificial neural network. *International Journal of Remote Sensing*, **18**, 799-810.

Foody, G.M. and Boyd, D.S. (1999) Detection of partial land cover change associated with the migration of inter-class transitional zones. *International Journal of Remote Sensing*, **20**, 2723-2740.

Foody, G.M., Campbell, N.A., Trodd, N.M. and Wood, T.F. (1992) Derivation and application of probabilistic measures of class membership from maximum-likelihood classification. *Photogrammetric Engineering and Remote Sensing*, **58**, 1335-1341.

Fortin, M.J., Olson, R.J., Ferson, S., Iverson, L., Hunsaker, C., Edwards, G., Levine, D., Butera, K. and Klemas, V. (2000) Issues related to the detection of boundaries. *Landscape Ecology*, **15**, 453-466.

Fowler, J. and Cohen, L. (1990) *Practical Statistics for Field Biology*. Wiley, Chichester, pp227.

Gahegan, M. and Ehlers, M. (2000) A framework for the modelling of uncertainty between remote sensing and geographic information systems. *ISPRS Journal of Photogrammetry and Remote Sensing*, **55**, 176-188.

Gong, P., Pu, R. and Chen, J. (1996) Mapping ecological land systems and classification uncertainties from digital elevation and forest-cover data using neural networks. *Photogrammetric Engineering and Remote Sensing*, **62**, 1249-1260.

Goodchild, M.F., Guoqing, S. and Shiren, Y. (1992) Development and test of an error model for categorical data. *International Journal of Geographical Information Sciences*, **6**, 87-104.

Grejner-Brzezinska, D.A., Da, R., Toth, C. (1998) GPS error modelling and OTF ambiguity resolution for high-accuracy GPS/INS integrated system. *Journal of Geodesy*, **72**, 626-638.

Gross, M.F., Hardisky, M.A., Klemas, V. and Wolf, P.L. (1987) Quantification of biomass of the marsh grass Spartina alterniflora Loisel using Landsat Thematic Mapper imagery. *Photogrammetric Engineering and Remote Sensing*, **53**, 1577-1583.

Gross, M.F., Klemas, V. and Levasseur, J.E. (1986) Remote sensing of Spartina anglica biomass in five French salt marshes. *International Journal of Remote Sensing*, 7, 657-664.

Guild, L.S., Cohen, W.B. and Kauffman, J.B. (2004) Detection of deforestation and land conversion in Rondonia, Brazil using change detection techniques. *International Journal of Remote Sensing*, **20**, 731-750.

Hagen, A. (2003) Fuzzy set approach to assessing similarity of categorical maps. *International Journal of Geographical Information Science*, **17**, 235-249.e

Hame, T., Heiler, I. and Miguel-Ayanz, J.S. (1998) An unsupervised change detection and recognition system for forestry. *International Journal of Remote Sensing*, **19**, 1079-1099.

Hart, S.J., Shaffer, R.E., Rose-Pehrsson, S.L. and McDonald, J.R. (2001) Using physics-based modeler outputs to train probabilistic neural networks for unexploded ordnance (UXO) classification in magnetometry surveys. *IEEE Transactions on Geoscience and Remote* Sensing, **39**, 797-804.

Heuvelink, G.B.M. (2002) Analysing uncertainty propagation in GIS: why is it not that simple. In Foody, G.M. and Atkinson, P.M. (Eds) *Uncertainty in Remote Sensing and GIS*. Wily, Chichester, 155-166.

Hobma, T.W. (1995) Merging SPOT for landscape-ecological studies, applied to a coastal dune environment. *Journal of Coastal Research*, **11**, 1003-1019.

Hong, S., Lee, M.H., Rios, J.A. and Speyer, J.L. (2002) Observability analysis of INS with a GPS multi-antenna system. *KMSE International Journal*, **16**,1367-1378.

Intermap (2005) http://www.intermap.com/ *Intermap Technologies*, accessed 18/01/05.

Itres (2000) *The CASI Manual: Volume 2 Standard Processing*. ITRES Research Limited, Calgary, pp672.

Itres (2005) http://www.itres.com/docs/casi2.html *ITRES instruments*, accessed 18/01/05.

Jansen, L.J.M. and Gregorio, A.D. (2002) Parametric land cover and land-use classifications as tools for environmental change detection. *Agriculture, Ecosystems and Environment*, **91**, 89-100.

Janssen, L.L.F. and van der Wel, F.J.M. (1994) Accuracy assessment of satellite derived land-cover data: A review. *Photogrammetric Engineering and Remote Sensing*, **60**, 419-426.

Johnson, R.D. and Kasischke, E.S. (1998) Change vector analysis: a technique for the multispectral monitoring of land cover and condition. *International Journal of Remote Sensing*, **19**, 411-426.

Kanellopoulos, I., Varfis, A., Wilkinson, G.G. and Megier, J. (1992) Land-cover discrimination in SPOT HRV imagery using an artificial neural network- a 20-class experiment. *International Journal of Remote Sensing*, **13**, 917-924.

Kanellopoulos, I. and Wilkinson, G.G. (1997) Strategies and best practice for neural network image classification. *International Journal of Remote Sensing*, **18**, 711-725.

Kavzoglu, T. and Mather, P.M. (1999) Pruning artificial neural networks: an example using land cover classification of multi-sensor images. *International Journal of Remote Sensing*, **20**, 2787-2803.

Kavzoglu, T. and Mather P.M. (2003) The use of backpropagating artificial neural networks in land cover classification. *International Journal of Remote Sensing*, **24**, 4907-4938.

Kruse, F. A., Boardman, J. W., Lefkoff, A. B., Young, J. M., Kierein-Young, K. S., Cocks, T. D., Jenssen, R. and Cocks, P. A. (2000) HyMap: an Australian hyperspectral sensor solving global problems – results from USA HyMap data acquisitions. In *Proceedings of the 10th Australasian Remote Sensing and Photogrammetry Conference, Adelaide, Australia, 21st-25th August 2000.*

Lambin, E.F. and Strahler, A.H. (1994) Change vector analysis in multitemporal space: a tool to detect change processes using high temporal-resolution satellite data. *Remote Sensing of Environment*, **48**, 231-244.

Lanter, D.P. and Veregin, H. (1992) A research paradigm for propagating error in layer-based GIS. *Photogrammetric Engineering and Remote Sensing*, **58**, 825-833.

Lee, C. and Landgrebe, D.A. (1993) Analyzing high-dimensional multispectral data. *IEEE Transactions on Geoscience and Remote Sensing*, **31**, 792-800.

Leick, A. (2004) *GPS Satellite Surveying: 3rd Edition.* Wiley, New Jersey, pp464.

Liu, W.G., Gopal, S., Woodcock, C.E. (2004) Uncertainty and confidence in land cover classification using a hybrid classifier approach. *Photogrammetric Engineering and Remote Sensing*, **70**, 963-971.

Liu, W.G. and Wu, E.Y. (2005) Comparison of non-linear mixture models: Sub-pixel classification. *Remote Sensing of Environment*, **94**, 145-154.

Lo, C-P. and Choi, J. (2004) A hybrid approach to urban land use/cover mapping using Landsat 7 Enhanced Thematic Mapper Plus (ETM+) images. *International Journal of Remote Sensing*, **25**, 2687-2700.

Lo, C-P. and Watson, L.J. (1998) The influence of geographic sampling methods on vegetation map accuracy evaluation in a swampy environment. *Photogrammetric Engineering and Remote Sensing*, **64**, 1189-1200.

Lu, D., Mausel, P., Brondizio, E., and Moran, E. (2004) Change detection techniques. *International Journal of Remote Sensing*, **25**, 2365-2407.

Lucieer, A. and Kraak, M.J. (2004) Interactive and visual fuzzy classification of remotely sensed imagery for exploration of uncertainty. *International Journal of Geographical Information Science*, **18**, 491-512.

Lunetta, R.S., Johnson, D.M., Lyon, J.G. and Crotwell, J. (2004) Impacts of image temporal frequency on land-cover change detection monitoring. *Remote Sensing of Environment*, **89**, 444-454.

Lyon, J.G., Yuan, D. Lunetta, R.S. and Elvidge, C.D. (1998) A change detection experiment using vegetation indices. *Photogrammetric Engineering and Remote Sensing*, **64**, 143-150.

Ma, Z. and Redmond, R.L. (1995) Tau coefficients for accuracy assessment of classification of remote sensing data. *Photogrammetric Engineering and Remote Sensing*, **61**, 435-439.

Mahapatra, A., Ramchandran, R. and Krishnan, R. (2004) Modelling the uncertainty in orientation of IRS-1C/1D with a rigorous photogrammetric model. *Photogrammetric Engineering and Remote Sensing*, **70**, 939-946.

Manslow, J.F. and Nixon, M.S. (2002) On the ambiguity induced by a remote sensor's PSF. In Foody, G.M. and Atkinson, P.M. (Eds) *Uncertainty in Remote Sensing and GIS*. Wily, Chichester, 37-57.

Mas, J-F. (1999) Monitoring land-cover changes: a comparison of change detection techniques. *International Journal of Remote Sensing*, **20,** 139-152.

Maselli, F. (2001) Extension of environmental parameters over the land surface by improved fuzzy classification of remotely sensed data. *International Journal of Remote Sensing*, **22,** 3597-3610.

Maselli, F., Conese, C. and Petkov, L. (1994) Use of probability entropy for the estimation and graphical representation of the accuracy of maximum likelihood classifications. *ISPRS Journal of Photogrammetry and Remote Sensing*, **49**, 13-20.

McIver, D.K. and Friedl, M.A. (2001) Estimating pixel-scale land cover classification confidence using non-parametric machine learning methods. *IEEE Transactions on Geoscience and Remote Sensing*, **39**, 1959-1968.

Mehner, H., Cutler, M., Fairbairn, D. and Thompson, G. (2004) Remote sensing of upland vegetation: the potential of high spatial resolution satellite sensors. *Global Ecology and Biogeography*, **13**, 359-369.

Melgani, F., Moser, G. and Serpico SB (2002) Unsupervised change-detection methods for remote-sensing images. *Optical Engineering*, **41,** 3288-3297.

Molenaar, M. and Cheng, T. (2000) Fuzzy spatial objects and their dynamics. *ISPRS Journal of Photogrammetry and Remote Sensing*, **55**, 164-175.

Mostafa, M. and Hutton, J. (2001) Direct positioning and orientation systems: How do they work? What is the attainable accuracy? In *Proceedings of The American Society of Photogrammetry and Remote Sensing Annual Meeting, St. Louis, MO, USA, 23rd - 27th April 2001.*

Mostafa, M., Hutton, J. and Reid, B. (2001) GPS/IMU products – the Applanix approach. *Proceedings of the 48th Photogrammetric Week, Stuttgart, Germany, September 24th – 28th 2001.*

Narumalani, S., Mishra, D.R. and Rothwell, R.G. (2004) Change detection and landscape metrics for inferring anthropogenic processes in the greater EFMO area. *Remote Sensing of Environment*, **91**, 478-489.

NASA (2002) http://geo.arc.nasa.gov/sge/landsat/lpsum.html *NASA Landsat Program Summary*, accessed 18/01/05.

NASA (2004) http://modis.gsfc.nasa.gov/about/specs.html *NASA MODIS Technical Specifications*, accessed 22/07/04.

Nelson, R.F. (1983) Detecting forest canopy change due to insect activity using Landsat MSS. *Photogrammetric Engineering and Remote Sensing*, **9**, 1303-1314.

NERC (2002) http://www.nerc.ac.uk/funding/earthobs/shacnew2.shtml *Natural Environment Research Council (NERC) SAR and Hyperspectral Airborne Campaign (SHAC)*, accessed 09/02/02.

Nordberg, M.L. and Evertson, J. (2003) Monitoring change in mountainous dry-heath vegetation at a regional scale using multitemporal Landsat TM data. *Ambio*, **32**, 502-509.

Novatel (1999) *MiLLennium® GPSCard™ and Enclosures*. Novatel Inc., Calgary, pp72.

Novatel (2005) http://www.novatel.ca/Documents/Papers/BDSseries.pdf *BDS Series IMU and GPS*, accessed 27/03/05

NSL (2001) *Comparative System Analysis*. National Centre for Environmental Data and Surveillance, Bath, pp56.

Optech (2002) www.optech.on.ca *Optech Airborne Laser Terrain Mappers*, accessed 27/10/02.

Paola, J.D. and Schowengerdt, R.A. (1995) A detailed comparison of backpropagation neural network and maximum-likelihood classifiers for urban land use classification. *IEEE Transactions on Geoscience and Remote Sensing*, **33**, 981-996.

Paola, J.D. and Schowengerdt, R.A. (1997) The effect of neural-network structure on a multispectral land-use/land-cover classification. *Photogrammetric Engineering and Remote Sensing*, **63**, 535-544.

Parr, T.W., Sier, A.R.J., Battarbee, R.W., Mackay, A. and Burgess, J. (2003) Detecting environmental change: science and society - perspectives on long-term research and monitoring in the 21st century. *Science of the Total Environment*, **310**, 1-8.

Parzen, E. (1962) On estimation of a probability density function and mode. *Annals of Mathematical Statistics*, **33**, 1065-1076.

Peddle, D.R., Foody, G.M., Zhang, A., Franklin, S.E. and Ledrew, E.F. (1994) Multi-source image classification II: an empirical comparison of evidential reasoning and neural network approaches. *Canadian Journal of Remote Sensing*, **20**, 396-407.

Pontius, R.G. (2000) Quantification error versus location error in comparison of categorical maps. *Photogrammetric Engineering and Remote Sensing*, **66**, 1011-1016.

Rabus, B., Eineder, M., Roth, A. and Bamler, R. (2003) The shuttle radar topography mission - a new class of digital elevation models acquired by spaceborne radar. *ISPRS Journal of Photogrammetry and Remote Sensing*, **57**, 241-262.

Raghu, P.P. and Yegnanarayana, B. (1998) Supervised texture classification using a probabilistic neural network and constraint satisfaction model. *IEEE Transactions on Neural Networks*, **9**, 516-522.

Richards, J.A. (2005) Analysis of remotely sensed data: The formative decades and the future. *IEEE Transactions on Geoscience and Remote Sensing*, **43**, 422-432.

Ricotta, C. (2004) Evaluating the classification accuracy of fuzzy thematic maps with a simple parametric measure. *International Journal of Remote Sensing*, **25**, 2169–2176.

Rodwell, J.S. (2000) *British Plant Communities. Volume 5 Maritime Communities and Vegetation of Open Habitats*. Cambridge University Press, Cambridge, 512 pp.

Roy, D.P. (2000) The impact of misregistration upon composited wide field of view satellite data and implications for change detection. *IEEE Transactions on Geoscience and Remote Sensing*, **38**, 2017-2032.

Schneider, M. (1999) Uncertainty management for spatial data in databases: fuzzy spatial data types. In *Proceedings of 6th International Symposium on Advances in Spatial Databases, Lecture Notes in Computer Sciences,* **1651**,330-351.

Schowengerdt, R.A. (1997) *Remote Sensing: Models and Methods for Image Processing.* Second Edition. Academic Press, San Diego, pp522.

Seeliger, U., Cordazzo, C.V., Oliveira, C.P.L. and Seeliger, M. (2000) Long-term changes of coastal foredunes in the southwestern Atlantic. *Journal of Coastal Research*, **16**, 1068-1072.

Serra, P., Pons, X. and Sauri, D. (2003) Post-classification change detection with data from different sensors: some accuracy considerations. *International Journal of Remote Sensing*, **24**, 3311-3340.

Shanmugan, S. Lucas, N., Phipps, P. Richards, A. and Barnsley, M. (2003) Assessment of remote sensing techniques for habitat mapping in castal dune ecosystems. *Journal of Coastal Research*, **19**, 64-75.

Shi, W.Z. and Ehlers, M. (1996) Determining uncertainties and their propagation in dynamic change detection based on classified remotely-sensed images. *International Journal of Remote Sensing*, **17**, 2729-2741.

Shi, W.Z. and Liu, K.F. (2004) Modeling fuzzy topological relations between uncertain objects in a GIS. *Photogrammetric Engineering and Remote Sensing*, **70**, 921-929.

Shi, W.Z., Yang, B.S. and Li, Q.Q. (2004) Modelling error propagation in vector-based overlay analysis. *ISPRS Journal of Photogrammetry & Remote Sensing*, **59**, 47-59.

Smith, G.M., Spencer, T., Murray, A.L. and French, J.R. (1998) Assessing seasonal vegetation change in coastal wetlands with airborne remote sensing: an outline methodology. *Mangroves and Salt Marshes*, **2**, 15-28.

Smits, P.C. and Annoni, A. (2000) Towards specification-driven change-detection. *IEEE Transactions on Geoscience and Remote Sensing*, **38**, 1484-1488.

Sohl, T.L., Gallant, A.L. and Loveland, T.R. (2004) The characteristics and interpretability of land surface change and implications for project design. *Photogrammetric Engineering and Remote Sensing*, **70**, 439-448.

Song, C.H. and Woodcock, C.E. (2003) Monitoring forest succession with multitemporal Landsat images: Factors of uncertainty. *IEEE Transactions on Geoscience and Remote Sensing*, **41**, 2557-2567.

Song, C.H., Woodcock, C.E., and Li, X.W. (2002) The spectral/temporal manifestation of forest succession in optical imagery - The potential of multitemporal imagery. *Remote Sensing of Environment*, **82**, 285-302.

Space Imaging (2005) http://www.spaceimaging.com *Space Imaging*, accessed 18/01/05.

Specht, D.F. (1990) Probabilistic neural networks. *Neural Networks*, **3**, 109-118.

Specim (2004) http://www.specim.fi/ *Specim*, accessed 14/07/04.

SPOT (2005) http://www.spotimage.fr/ *SPOT System*, accessed 18/01/05.

Stanislawski, L.V., Dewitt, B.A. and Shrestha, R.L. (1996) Estimating positional accuracy of data layers within a GIS through error propagation. *Photogrammetric Engineering and Remote Sensing*, **62**, 429-433.

Steele, B.M., Winne, J.C. and Redmond, R.L. (1998) Estimation and mapping of misclassification probabilities for thematic land cover maps. *Remote Sensing of Environment*, **66**, 192-202.

Stehman, S.V. (1992) Comparison of systematic and random sampling for estimating accuracy of maps generated from remote sensed data. *Photogrammetric Engineering and Remote Sensing*, **58**, 1343-1350.

Stehman, S.V. (1996) Estimating the Kappa coefficient and its variance under stratified random sampling. *Photogrammetric Engineering and Remote Sensing*, **62**, 401-407.

Stehman, S.V. (1999) Basic probability sampling designs for thematic accuracy assessment. *International Journal of Remote* Sensing, **20**, 2423-2441.

Stehman, S.V. (2000) Practical implications of design-based sampling inference for thematic map accuracy assessment. *Remote Sensing of Environment*, **72**, 35-45.

Stehman, S.V. (2001) Statistical rigor and practical utility in thematic map accuracy assessment. *Photogrammetric Engineering and Remote Sensing*, **67**, 727-734.

Sties, M., Kruger, S., Mercer, J.B. and Schnick, S. (2000) Comparison of digital elevation data from airborne laser and interferometric SAR systems. In *Proceedings ISPRS, Volume XXXIII, Amsterdam, 16th – 23rd July 2000.*

Storey, M. and Congalton, R.G. (1986) Accuracy assessment- a users perspective. *Photogrammetric Engineering and Remote Sensing*, **52**, 397-399.

Stow, D.A. (1999) Reducing the effects of misregistration on pixel-level change detection. *International Journal of Remote Sensing*, **20**, 2477-2483.

Stow, D.A. and Chen, D.M. (2002) Sensitivity of multitemporal NOAA AVHRR data of an urbanizing region to land-use/land-cover changes and misregistration. *Remote Sensing of Environment*, **80**, 297– 307.

Strawbridge, F., Haslett, S.K., Koh, A., Edwards, E. and Davies, C.F.C. (2000) The potential of aerial digital photography for saltmarsh monitoring. In Haslett, S.K. (Ed) *Bath Spa University College Occasional Papers in Geography*, **1**, 1-15.

Swain, P.H. (1978) Fundamentals of pattern recognition in remote sensing. In Swain, P.H. and Davis, S. (Eds) *Remote Sensing- The Quantitative Approach*, McGraw-Hill, New York, 136-187.

Thomson, A.G. (1995) Airborne radiometry and a sheep grazing experiment on dune grassland. *International Journal of Remote Sensing*, **16**, 981-988.

Thomson, A.G., Fuller, R.M., Sparks, T.H., Yates, M.G. and Eastwood, J.A. (1998) Ground and airborne radiometry over intertidal surfaces: waveband selection for cover classification. *International Journal of Remote Sensing*, **19**, 1189-1205.

Thomson, A.G., Fuller, R.M., Yates, M.G., Brown , S.L., Cox, R. and Wadsworth, R.A. (2003) The use of airborne remote sensing for extensive mapping of intertidal sediments and saltmarshes in eastern England. *International Journal of Remote Sensing*, **24**, 2717-2737.

Tian, B. and Azimi-Sadjadi, M.R. (2001) Comparison of two different PNN training approaches for satellite cloud data classification. *IEEE Transactions on Neural Networks*, **12**, 164-168.

Toth, C.K. (2002) Sensor integration in airborne mapping. *IEEE Transactions on Instrumentation and Measurement*, **51**, 1367-1373.

Townshend, J. R. G., Huang, C., Kalluri, S. N. V., Defries, R. S., Liang, S. and Yang, K. (2000) Beware of per-pixel characterization of land cover. *International Journal of Remote Sensing*, **21**, 839-843.

Townshend, J.R.G., Justice, C.O., Gurney, C. and McManus, J. (1992) The impact of misregistration on change detection, *IEEE Transactions on Geoscience and Remote Sensing*, **30**, 1054-1060.

Townshend, J.R.G. and Justice, C.O. (1995) Spatial variability of images and the monitoring of changes in the normalised difference vegetation index. *International Journal of Remote Sensing*, **16**, 2187-2195.

Trajan (2001) http://www.trajan-software.demon.co.uk/ *Trajan 6.0 Professional Neural Network Simulator* accessed 12/12/01.

Tresp, V. Hollatz, J. and Ahmad, S. (1997) Representing probabilistic rules with networks of Gaussian basis functions. *Machine Learning*, **27**, 173-200.

Trinity House (2005) http://www.trinityhouse.co.uk/aids_to_navigation/the_task/ satellite_navigation.html *Trinity House Marine Differential GPS*, accessed 24/03/05.

Tucker, C.J. (1979) Red and photographic infrared linear combinations for monitoring vegetation. *Remote Sensing of Environment*, **8**, 127-150.

Turk, G. (2002) Letter to the editor: Chance correction and map evaluation. *Remote Sensing of Environment*, **82**, 1-3.

USGS (2005) http://landsat.usgs.gov/faq.html *United States Geological Survey Landsat Project*, accessed 18/01/05.

Verbyla, D.L. and Boles, S.H. (2000) Bias in land cover change estimates due to misregistration. *International Journal of Remote Sensing*, **21**, 3553-3560.

Veregin, H. (1996) Error propagation through the buffer operation for probability surfaces. *Photogrammetric Engineering and Remote Sensing*, **62**, 419-428.

Wang, J.Q., Azimi-Sadjadi, M.R. and Reinke, D. (2004) A temporally adaptive classifier for multispectral imagery. *IEEE Transactions on Neural Networks.* **15**, 159-165.

Warren, A.J., Collins, M.J., Johnson, E.A. and Ehlers, P.F. (2002) Managing uncertainty in a geospatial model of biodiversity. In Foody, G.M. and Atkinson, P.M. (Eds) *Uncertainty in Remote Sensing and GIS.* Wily, Chichester, 167-185.

Waypoint (2001) *GrafNav/GrafNet, GrafNav Lite, GrafMov Operating Manual: Version 6.03.* Waypoint Consulting Inc., Calgary, Canada.

Wei, L.L. and Zhang, W.X. (2004) Probabilistic rough sets characterized by fuzzy sets. *International Journal of Uncertainty Fuzziness and Knowledge-Based Systems*, **12**, 47-60.

Wright, G.G. and Morrice, J.G. (1997) Landsat TM spectral information to enhance the land cover of Scotland 1988 dataset. *International Journal of Remote Sensing*, **18**, 3811-3834.

WS Atkins (2004) *Ainsdale Sand Dunes National Nature Reserve Environmental Impact Assessment of Options for Management of Seaward Areas.* WS Atkins, Warrington, pp171.

Yamamoto, T., Hanaizumi, H. and Chino, S. (2001) A change detection method for remotely sensed multispectral and multitemporal images using 3-D segmentation. *IEEE Transactions on Geoscience and Remote Sensing*. **39**, 976-985.

Yamano, H. and Tamura, M. (2004) Detection limits of coral reef bleaching by satellite remote sensing: Simulation and data analysis. *Remote Sensing of Environment*, **90**, 86-103.

Yang, X. and Lo, C.P. (2002) Using a time series of satellite imagery to detect land use and land cover changes in the Atlanta, Georgia metropolitan area. *International Journal of Remote Sensing*, **23**, 1775-1798.

Yool, S.R. (1998) Land cover classification in rugged areas using simulated moderate-resolution remote sensor data and an artificial neural network. *International Journal of Remote Sensing*, **19**, 85-96.

Yuan, M., Dickens-Micozzi, M. and Magsig, M.A. (2002) Analysis of tornado damage tracks from the 3 May tornado outbreak using multispectral satellite imagery. *Weather and Forecasting*, **17**, 382-398.

Zhan, X., Sohlberg, R.A., Townshend, J.R.G., DiMiceli, C., Eastman, J.C., Hansen, M.C. and DeFries, R.S. (2002) Detection of land cover changes using MODIS 250 m data. *Remote Sensing of Environment*, **83**, 336–350.

Zhang, J. and Foody, G.M. (2001) Fully-fuzzy supervised classification of sub-urban land cover from remotely sensed imagery: statistical and artificial neural network approaches. *International Journal of Remote Sensing*, **22**, 615-628.

Zhang, J. and Kirby, R.P. (1999) Alternative criteria for defining fuzzy boundaries based on fuzzy classification of aerial photographs and satellite images. *Photogrammetric Engineering and Remote Sensing*, **65**, 1379-1387.

Zhang, L.J., Liu, C.M., Davis, C.J., Solomon, D.S., Brann, T.B. and Caldwell, L.E. (2004) Fuzzy classification of ecological habitats from FIA data. *Forest Science*, **50**, 117-127.

Zhang, M., Ustin, S.L., Rejmankova, E. and Sanderson, E.W. (1997) Monitoring Pacific coast salt mashes using remote sensing. *Ecological Applications*, **7**, 1039-1053.

Zhou, W. (1999) Verification of the nonparametric characteristics of backpropagation neural networks for image classification. *IEEE Transactions on Geoscience and Remote Sensing*, **37**, 771-779.